2019

Multiscale Mathematical Modelling of Nonlinear Nanowire Resonators for Biological Applications

Rosa Fallahpourghadikolaei
fall6680@mylaurier.ca

Multiscale Mathematical Modelling of Nonlinear Nanowire Resonators for Biological Applications

© Rosa Fallahpourghadikolaei

Supervisor: Prof. Roderick Melnik

Department of Mathematics

Wilfrid Laurier University

A thesis submitted in fulfillment of the requirements for the degree of

Master of Science

April 2019

Abstract

Nanoscale systems fabricated with low-dimensional nanostructures such as carbon nanotubes, nanowires, quantum dots, and more recently graphene sheets, have fascinated researchers from different fields due to their extraordinary and unique physical properties. For example, the remarkable mechanical properties of nanoresonators empower them to have a very high resonant frequency up to the order of giga to terahertz. The ultra-high frequency of these systems attracted the attention of researchers in the area of bio-sensing with the idea to implement them for detection of tiny bio-objects. In this thesis, we originally propose and analyze a mathematical model for nonlinear vibrations of nanowire resonators with their applications to tiny mass sensing, taking into account thermal, piezoelectric, electromagnetic, surface, and external excitations. The mathematical models for such nanowires are formulated using the Euler-Bernoulli beam theory in conjunction with the nonlocal differential constitutive relations of Eringen type. In order to analyze the obtained nonlinear partial differential equation (PDE), we first use the Galerkin method in combination with a perturbation technique to obtain the primary resonance. After finding the primary resonance, a parametric sensitivity analysis is carried out to investigate the effects of key parameters on the sensitivity of the nanowire resonators in mass sensing. Our main hypothesis is that bio-particles attached to the surface of the nanowire resonator would result in a detectable shift in the value of the jump frequency. Therefore, a mathematical formula is developed based on the jump frequency to scrutinize the sensitivity of the considered nanowire resonators. Our mass sensitivity analysis aims at the improved capability of the nanowire resonators in detection

of tiny bio-particles such as DNA, RNA, proteins, viruses, and bacteria. Numerical solutions, obtained for the general nonlinear mathematical model of nanowire resonators, using the Finite Difference Method, are compared with the results obtained with a simplified approach described above. Finally, we investigate the sensitivity of the nanowire resonator for mass sensing using molecular dynamics simulations to provide a validation for our results from the obtained continuum models. It is expected that the results of this research may assist in our better understanding of key characteristics of nanowire resonators for their applications in detection of bio-particles, ultimately impacting the development of advanced approaches to disease diagnostics and treatments.

To my parents and husband ...

Acknowledgements

First and foremost, I would like to appreciate my research supervisor, Prof. Roderick Melnik, for his support, expertise and guidance. Working under his supervision was a great opportunity for me to learn the fundamental of research in the area of applied mathematics.

I also would like to acknowledge my committee members, Prof. Santoprete and Prof. Wei, for their time and valuable comments on my thesis.

I am deeply grateful to my respected parents for their endless sacrifices, love and support throughout my life. This achievement would not have been possible without them.

At the end, I would like to thank my husband, Hassan, for his boundless support, encouragement and belief in me.

Table of contents

List of figures

List of tables

Nomenclature

α_x	Coefficient of thermal expansion
δ	Classical macroscopic stress tensor
ε^s	Surface strain tensor
ε_t	Strain
ε_{LJ}	Energy well depth
ε_{xx}	Strain in x direction
Γ	Nonlocal coefficient
γ_s	Surface energy density
λ	Dielectric constant
μ	Damping coefficient
ν	Poisson ratio
Ω	Frequency of excitation
ω_n	Linear natural frequency
ϕ	Dihedral angle torsion

ψ	Electric potential
ρ	Nanowire density
ρ_0	Surface density
σ^s	Surface stress tensor
σ_θ	Axial thermal stress
σ_n	Nonlocal stress tensor
σ_{xx}	Stress in x direction
τ_0	Residual surface tension
τ_m	Material constant
θ	Bond angle
θ_0	Equilibrium bond angle
θ_t	Temperature
ζ_m	Magnetic permeability
A	Area
a	Acceleration
a_e	External characteristic length
a_i	Internal characteristic length
b	Width of nanowire
C	Fourth order elasticity tensor

C_i Coefficients of dihedral multi-harmonic

D Electric displacement

E Young modulus

e Piezoelectric constant

E^s Surface elastic modulus

e_0 Material constant

E_e Electric field

e_m Strength vectors of electric field

E_{ba} Bond angle energy

E_{bs} Bond stretch energy

E_{dh} Dihedral energy

E_{El} Electrostatic energy

E_{LJ} Lennard-Jones potential

F_i Force on atom i

f_L Lorenz force

f_u Axial load per length

f_{em} Electromagnetic force

G Shear modulus

H Function of residual surface tension and cross section shape

h	Height of nanowire
H_m	Magnetic field
h_m	Disturbing vectors of magnetic field
I_z	Second moment of area
J	Current density
K	Kernel function
k_1	Linear Winkler coefficient
k_3	Nonlinear Winkler coefficient
K_{ba}	Stiffness constant for bond angle
K_{bs}	Stiffness constant for bond stretch
L	Length of nanowire
M	Bending moment
m_i	Mass of atom i
m_p	Particle mass
N	Axial force
P	Potential energy of the system of atoms
q	Distributed transverse loading
Q_i	Charge in electron units
r	Bond stretch

r_0 Equilibrium bond stretch

r_c Cutoff distance

r_{ij} Distance between two atoms

R_{LJ} Distance at zero energy

U Vectors of displacement

u Axial deflection

V Transverse shear force

v Velocity

V_e Electric voltage

w Transverse deflection

x_p Position of applied force

Chapter 1

Introduction

1.1 Problem Statement

Detection of bio-objects such as DNA, RNA, proteins, viruses, and bacteria is very important for preventing, accurate diagnosing and effective curing different types of diseases. Accordingly, it is crucial to develop novel, practical, and effective techniques to detect tiny bio-objects. This important and interdisciplinary subject has prompted scientists, engineers, and applied mathematicians to propose and investigate innovative approaches for the detection of bio-objects. Recent years have witnessed rapid advances in the development of nanodevices for different applications such as self-powered sensing, energy harvesting and mass sensing with potential of bio-object detection. Several nanoresonators have been designed, modelled, optimized and fabricated for tiny mass sensing. These nanoresonators are made of carbon nanotubes, graphene sheets, and nanowires (NWs) [1–3]. Due to their ultra-high modulus of elasticity and resonant frequency, they received substantial attention of the researchers as they can be used as sensors for label-free detection of specific biological objects. Although a number of important studies have been undertaken in this field so far, in particular those aiming to implement nanoresonators for bio-object detection [4–9], there is still lack of robust and systematic modelling techniques for the nanoresonators. Specifically,

it concerns the application of nanowires in biological detection, taking into account some of the most important parameters. These include parameters connected with electromagnetic fields, thermal variations, external excitations, axial loads, nonlocal and surface effects, large oscillations, and nonlinear viscoelastic foundations. Having in mind applications in mass detection, it is highly important to develop a mathematical model, which can be used to investigate the effect of these parameters on frequency behavior of nanowires. In fact, the outstanding capability of nanomechanical resonators, specially nanowires for ultra-high resolution mass sensing applications, is significantly related to their dynamic characteristics [10]. Thus, dynamic characterization and parametric sensitivity analysis of nanomechanical resonators for sensing applications are crucial. It should be noted that when we refer to nanosensors, we deal with a resonator with dimensions in the order of nanometer, which has sensitivity in the nanoscale range, and its interaction distance with the object being detected in nanometer size. That is why a small perturbation with different sources of excitation such as temperature, electromagnetic field, nonlinearity due to large oscillations of the nanoresonators or their substrates should be taken into account for an adequate mathematical modelling of these devices.

In this thesis, we aim to study nanowire resonators for biological detection taking into account different parameters such as temperature variations, electromagnetic field, nonlinearity and surface effects. We will use both continuum modelling and molecular dynamics simulations to achieve a better understanding of nanowire resonators in terms of mass detection and to provide a multiscale modelling framework for the analysis of vibrations of nanowire resonators with application in tiny mass sensing and biological object detection.

1.2 Literature Review

Vibrations of nanoresonators including nanobeams, quantum dots, nanotubes, nanowires, graphene sheets, and nanoplates have been fascinating an interdisciplinary community

of researchers, working in the areas of applied mechanics and mathematics, structural analysis and vibrations. A number of works have been published so far to investigate the vibrations of the nanoresonators [11–14]. Reviewing the works done by the researchers in these areas shows that utilization of continuum theories is very popular for modelling the vibrations of nanoresonators [15, 16]. Generally, there exist two main categories of research in the modelling of nanoresonators. In the first category, the focus of researchers is on the use of different continuum theories such as Timoshenko, Euler-Bernoulli and Rayliegh to model vibrations of nanostructures such as nanowires [17, 18]. Based their investigations on the continuum theories, researchers have considered different effects such as thermal variations and piezoelectric potential to model vibrations of nanowires. In addition, a few researchers have combined classical and nonlocal beam theories to characterize the dynamics of nanowires. Using these combined models, they investigated the effect of different parameters such as size, surface and nonlocal parameters on the vibrations of nanowires [19, 20]. In section 1.2.1, we provide a review on different models and results presented by researchers for the modelling of nanowire resonators using classical and non-classical theories.

The second category is related to the models with focus on the applications of nanoresonators in mass sensing, biological detection and drug delivery [21, 22]. Similar to the first category of research in this area, researchers have used classical and non-classical theories to study the applications and potency of the nanowire resonators for the detection of tiny bio-objects and chemical atoms [23, 24]. In sections 1.2.2 and 1.2.3, we present a review of the current models, experimental and alanytical results proposed by researchers for the nanoresonators taking into account the above-mentioned applications.

An analysis of the state-of-the-art in this field shows that there is a lack of modelling results for nanowire resonators in mass detection application that take into account different critical parameters such as electromagnetic field, piezoelectric potential, nonlinearity, external

excitations and thermal variations. Furthermore, the literature survey shows that, ultimately, more refined models such as those based on molecular dynamics simulations are also needed for our better understanding of the vibration behavior of nanowires for mass and bio-object detection applications. These two shortcomings of current knowledge in this area have prompted us to work on the development, as well as on mathematical and numerical analysis, of a novel continuum model for nanowire resonators plus their molecular dynamics simulations.

1.2.1 Vibration Modelling of Nanowires

The use of continuum models for the vibrations analysis of nanowires started from the early 2000s (e.g. [25] and references therein). The main aim of the most published works on the vibrations of nanowires at that time was finding a closed-form for the natural frequency of the nanowires, and also providing a mathematical framework to predict the behavior of nanowires under different cases of oscillations. Thus far, researchers have included different effects in their modelling of vibrations of nanowires such as geometry, size, surface effects, current-carrying, boundary conditions, magnetic field, initial tensile force, and external sources of excitations. This section of the chapter reviews the evolution of modelling of nanowire resonators using both local and nonlocal continuum models.

One of the earliest efforts for modelling vibrations of nanowires was presented by Ustunel et al. [26] in which they proposed a one-dimensional model for NWs. In another pioneering work, Vincent et al. [27] studied self-sustained vibrations of nanowires under a constant electron beam . In an interesting work by Zhou et al., vibrations of zinc oxide nanowires were studied considering the electric field effects. Their developed partial differential equation was converted to a nonlinear ordinary differential equation with both quadratic and cubic nonlinearities [17]. One of the earliest attempts in which a continuum model was proposed for vibration analysis of nanowires was a paper by He and Liley where they developed a model

for the vibrations of NWs considering surface effects and different boundary conditions [20]. Effects of surface stress on both buckling and vibrations of piezoelectric nanowires were studied by Wang and Feng in 2010 [19]. They showed that the resonant frequency of piezoelectric nanowires can be adjusted using the applied electric potential. They also demonstrated that piezoelectricity and the surface stress have quite similar effects on the frequency response of the nanowire [19].

Kiani is one of the influential researchers in the area of vibration analysis of nanowires as he developed several models for NWs considering different effects [28]. In one of his early research papers in this area [28], a nonlocal continuum model was developed to study free longitudinal vibrations of tapered nanowires employing the perturbation techniques. In his study, he considered two different types of boundary conditions including fixed-fixed and fixed-free constraints. One of the main results of the research was related to the rate of change in NW radii. For higher values of the small scale effect parameter, the rate of change in radii is more pronounced on the variation of the natural frequencies and phase velocities [28]. Hasheminejad and Gheshlaghi [29] developed a dissipative surface stress model to investigate the influence of size-dependent surface dissipation on fundamental frequencies of nanowires. Euler–Bernoulli beam theory in conjunction with the classic Zener model was used to develop the fifth order differential equation which describes the flexural vibrations of NWs. Fu et al. [30] studied nonlinear free vibrations of NWs using nonlocal Timoshenko beam theory considering the surface effects. Askari and Esmailzadeh used nonlocal Timoshenko beam theory to study vibrations of nanowires considering geometrical nonlinearity and different surface areas using the variational iteration method [31, 32]. He and Lilley investigated the vibrations of nanowires considering the surface effects and using the Timoshenko beam theory. They obtained the quality factor of nanowire's vibrations, and showed that considering the surface stress decreases the stiffness of cantilever nanowire, and increases the stiffness of nanowires with simply supported boundary conditions [33]. Samaei

et al. [34] studied vibrations of piezoelectric nanowires considering surface effects. They developed a continuum model for the vibrations of nanowires, which takes into account the effects of surface elasticity, residual surface tension, and transverse shear deformation. The main conclusions of their work is that the surface effects increase the natural frequency for the lower modes.

Forced vibrations of a current-carrying nanowire in a longitudinal magnetic field was first studied by Kiani in 2014 [35]. He developed the governing equation of the considered system taking into account both surface energy and size effects. The research has shown the effects of different parameters on the the maximum transverse displacements of the nanowires. These effects include the magnetic field, electric current, pre-tension force, frequency of the applied load, surface and size effects. One of the main results of the work shows that the maximum transverse displacements of the current-carrying nanowire reduces as the small-scale parameter increases. In another work by Kiani, the vibrations of double nanowire systems as electric current carriers were studied [36]. Theoretical models for both in-plane and out of plane vibrations were developed in order to find the corresponding fundamental frequencies [36]. Kiani also studied the interactions of two parallel nanowires carrying electric currents under a longitudinal magnetic field employing Biot–Savart law and a surface elasticity model. Results of the work show that the fundamental frequency decreases as the strength of the magnetic field magnifies. In addition, it was concluded that the initial tensile force inside the nanowire plus the surface effects promote its stability [37]. Vibrations and instability of pretensioned current-carrying nanowires under suddenly exerted three-dimensional magnetic field were studied in [38]. Using Hamilton's principle, governing equations of the longitudinal and transverse vibrations of nanowire were developed. The simulation results show that the maximum longitudinal displacement of the nanowire nonlinearly increases for each of the components of the three-dimensional

magnetic field. In addition, stability of the nanostructure increases by the initial tensile force, and also the residual surface stress with positive sign [38].

Both free and forced vibrations of nanowire rested on an elastic substrate were studied by Su et al. They assumed Winkler-Pasternak foundations and generalized substrate models as the foundation model for the nanowire [18]. In their work, they obtained the characteristic equations, mode shapes and effective Young's moduli of the nanowires considering different forms of boundary conditions [18]. In another research [39], free and forced transverse vibrations of nanowires were studied taking into account the surface effects based on the Timoshenko beam theory. A comparison study was also performed by the authors to verify the obtained theoretical results for the fundamental frequencies with the FEM simulation [39]. Zhang et al. in [40] analyzed transverse vibrations of embedded nanowires under axial compression taking into account the higher order surface effects. Results of this research show that the axial load, surrounding elastic medium, and high-order surface stress are affecting the natural frequency of transverse vibrations of nanowires. Jin and Li studied nonlinear dynamics of silicon nanowire (SiNW) considering nonlocal effects. They performed a bifurcation analysis, which shows that the nonlocal effect causes the most significant impact when the excitation frequency equals to the natural frequency of the structure [41].

Sedighi and Bozorgmehri probed nonlinear vibrations along with adhesion instability of nonlocal nanowires with consideration of surface energy. They revealed that the critical Casimir value decreases by increasing the nonlocal parameter [42].

1.2.2 Nanoresonators in Mass Sensing

The extraordinary and unique mechanical properties of the nanostructures have made them an excellent candidate for mass sensing application. Different types of nanoresonators including nanowires, quantum dots, nanotubes and graphene sheets have been studied by researchers from different fields to be used for tiny object detection. In fact, the remarkable mechanical

properties of nanoresonators empower them to have a very high resonant frequency up to the order of giga to terahertz. The ultra-high frequency of these structures attracted attention of researchers in the area of bio-sensing to implement them for detection of tiny bio-objects. As a result, plenty of theoretical and practical approaches have been proposed for detection of tiny bio-particles. Using both theoretical and experimental approaches, researchers have shown the potential of nanoresonators in detection of tiny objects in the scale of zeptogram (zg) [43–45]. Nanoresonators, specifically semi-conducting nanowires, have shown a very unique reproducible and tunable conducting properties, which provide strong sensing approaches for medical applications [46]. This high resolution of sensing allows detection of tiny bio-objects such as DNA, RNA, proteins, viruses, bacteria and very small chemical atoms. As the literature shows, it is necessary to develop a full model for the vibrations of nanowire resonators considering different important parameters. Analysis of temperature variations is one of the well-addressed parameters, but for analyzing other significant parameters, the development of novel models is needed to provide a better understanding of nanoresonator's sensing resolution. This section of the chapter provides a review on the applications of nanoresonators such as nanoplates, nanotubes, and nanowires in detection of tiny bio-objects.

A pioneering research paper where a nanoresonator was proposed for mass detection has been the paper [21] by Fritz et al. The authors developed a mass sensor using a silicon nanometre-scale resonating cantilever with mass sensitivity of 10^{-19} gram. This high resolution is enough for detection of a single bio-molecule such as a medium size protein. One year later, Abadal et al. developed a simple linear electromechanical model for an electrostatically driven resonating cantilever with application in mass sensing. Their theoretical approach demonstrates sensitivity in the order of attogram [47].

Su et al. [48] developed a microcantilever based mechanical resonator for DNA detection utilizing gold nanoparticle-modified probes. Their proposed method is capable of detection of DNA at a concentration of 0.05 nM or lower. Volodin et al. proposed coiled carbon nanotubes

for mass and force sensing. The nanotube windings can be either electrically or acoustically excited, and its fundamental frequency is in the order of 400 GHz. The proposed sensor is suitable for measuring small forces and masses in the femtogram range [49].

In a very interesting article, Sone et al. [50] showed the potential of nanoresonators for allergy check. A femtogram mass sensitivity was demonstrated in water using a commercial piezoresistive cantilever. In addition, results of their papers show that the binding ratio between the antibody and antigen is about 1:2, and accordingly, the proposed sensor has the potential to monitor the reaction between an antibody and an antigen for allergy check. A zeptogram-scale mass sensing method was proposed by Yang et al. [43] in which they developed a very high frequency nanoelectromechanical systems with a mass resolution of approximately 7 zg which is equivalent to mass of 30 xenon atmos. Their proposed sensory device works based on the concept of frequency shift, which happens after adding a tiny mass to the nanoresonator. Pang et al. [22] proposed a nano-based piezoelectric resonator, which is sensitive to femtogram mass. They performed a preliminary vapor-detection measurement, which demonstrates the potential of the proposed device for a chemical and biological sensing platform. Barton et al. fabricated a nanomechanical mass sensor, which contains a nanofluidic channel, and is capable of detection of tiny bio-objects. Their fluid density measurements disclose a mass responsivity of 100 Hz/fg and a noise equivalent mass of 2 fg [51].

As one of the most implemented classes of nanostructures in mass sensing, one can refer to nanotubes because of their unique mechanical properties and ultra-high resonant frequencies. A number of researchers focused on carbon nanotube resonators for ultra-small mass sensing, and accordingly, developed new methods based on these types of materials [9, 52]. For example, Chiu et al. developed an atomic scale mass sensing scheme using doubly clamped carbon nanotube resonators. They showed that the carbon nanotube single-electron transistor properties allow self-detection of the nanotube vibration. They used the

resonant frequency shift to sense and determine the mass of atoms [53]. In another paper, the application of a carbon nanotube for zeptogram-level mass detection has been explored by Joshi et al. They used molecular structural mechanics approach for investigating the dynamic responses of chiral single walled carbon nanotube based nano bio-sensors. They showed that single-walled carbon nanotubes can reach the high sensitivity in the order of $0.12\ zg/GHz$ [44]. Cho et al. [1] developed a tunable, broadband nonlinear nanomechanical resonator for femtogram mass sensing at room temperature using carbon nanotubes. A mathematical model, considering the nonlinear vibrations of carbon nanotube resonators, was developed in their paper. They used the jump phenomenon to detect ultra-small objects. In a comprehensive analysis, Kiani et al. [24] developed a mathematical model using different beam theories including nonlocal Rayleigh, Timoshenko, and higher-order to investigate the potential of single-walled carbon nanotubes for arbitrarily attached nano-objects. Ali-Akbari et al. [8] studied the nonlinear performance of forced carbon nanotubes for bio-object sensing applications. They developed a nonlinear model for the vibrations of mechanically excited nanotubes using the Eringen's theory. Results of their research reveal that in the case of ultra-high Q-factor CNT-based resonators, a very small mechanical excitation results in the nonlinear oscillations of the nanotubes. Recently, Roudbari and Ansari developed a continuum model for single-walled boron nitride nanotube for mass sensing applications using nonlocal Rayleigh and Timoshenko beam theories [7].

Nanoplate is another type of nanostructures, which has been implemented for ultra-small mass sensing applications. For example, Adhikari and Chowdhury developed a mathematical framework for the use of graphene sheets in small mass sensing. They considered four different configurations for locating the small bio-objects, and developed both molecular dynamics and analytical simulations. The results of the paper indicates that the sensitivity of graphene sensors is in the order of gigahertz/zeptogram [45]. Kwon et al. [54] showed the potential of graphene-nanoribbon-based resonators for yoctogram mass sensing using

molecular dynamics simulations. In an interesting work, Duan et al.[55] revealed the potential of pillared graphene as an ultra-high mass sensing. Using molecular dynamics simulations, they showed that pillared graphene can reach at least 10^{-24} g resolution. Recently, they have also shown the ultra-high mass sensitivity and a very high quality factor of diamond nanothread based resonators based on molecular dynamics simulations [56]. Askari et al. [23] proposed a new approach for ultra-small mass sensing using a nanoplate, which operates based on the concept of jump phenomenon in nonlinear resonators. In addition, they implemented a system identification scheme to verify their obtained results by the new proposed technique. Results of their paper demonstrate the promising potential of the nanoplate for mass sensing in the order of femtogram. Nanoplate resonator can be also used as a self-powered mass sensing device. Asadi et al. [2] theoretically demonstrated that a nanoplate resonator not only can be used for detection of tiny bio-objects, but also has the potential to be used as a self-powered sensor.

Discovery of nanowires has opened new doors to novel methods for bio-sensing and bio-instrumentation. Generally, there are two main categories for nanowires based bio-sensors, which are electrical detection and optical detection. Following these techniques and probing new approaches, many papers have been published up to date about the use of nanowires in bio and nanoparticles (NPs) sensing. For example, Wasisto et al. [57] fabricated a SiNW-based resonators to sense aerosol nanoparticles by measuring resonant frequency shifts induced by the mass of NPs. Results of the research show that SiNW has the potential to detect NPs in the femtogram scale. Noteworthy also the paper by Li et al. [58], in which silicon nanowires were used to detect DNA through monitoring the electronic conductance of SiNWs. They showed that the sensitivity of the nanowire sensors strongly depends on the width of the wires. In addition, they observed a linear relationship between the response of the sensor and the surface to volume ratio of the nanowires. Gil-Santos et al. used two-dimensional vibrations of resonant nanowires for mass sensing and stiffness

spectroscopy. Using a superposition state of two orthogonal vibrations along with measuring different frequencies, they determined the mass and stiffness of the targeted system [59].

Despite of a number of published articles about the applications of nanoresonators in mass sensing, there are only a few published works in which authors addressed thermal effect on the resolution of nano-based mass sensing. As one pioneering example, Kim et al. have studied the resolution of mass detection by optical and capacitive methods in ambient atmosphere utilizing ultra-thin single-crystalline silicon microcantilevers. Results of their paper demonstrate that the detectable minimum mass by optical sensing increases slightly with decreasing cantilever size due to temperature fluctuation noise. In addition, they showed that the capacitive detection approach can detect a minimum mass below 1×10^{-14} gram [60]. Lassagne et al. proposed an ultra-sensitive mass sensing method using 1 *nm* carbon nanotubes. In their analysis, they considered the effect of thermal noise by cooling the nanotube down to 5 K. This low temperature resulted in improving the sensor resolution to 1.4 *zg* [61]. Biedermann et al. theoretically investigated thermal vibration response of the crystalline nanowire, and showed the effect of the thermal parameter on the eigen frequency of the targeted nanoresonators. In addition, they illustrated that the considered nanostructure has the potential to be used in ultra-small mass sensing, atomic force microscope force transducers, and highly sensitive acoustic sensors [62].

1.2.3 Nanoresonators in Other Bio Applications

Nanoresonators, such as those based on carbon nanotubes (CNTs), can be used for other medical applications such as drug delivery. Indeed, modified and functionalized CNTs have shown interesting and unique potential for drug delivery applications [63, 64]. They have excellent ability to cross cell membranes, very good biocompatibility, water solubility, a high drug loading efficiency and controlled drug release [65]. All of these unique features of CNTs have made them excellent drug delivery vehicles. CNTs have been used for delivering

bioactive peptides to the immune system. In addition, they also have been used for nucleic acid delivery. They have shown promising potential to target doxorubicin and even tumors [66].

Nanowires, which are in the main focus of this thesis, have also shown potential for drug delivery applications. The small diameter and magnetic properties of nanowires make them suitable for passing through the narrow capillaries using magnetic drug delivery [67]. This can be considered as a very effective technique for drug delivering at inaccessible parts inside the body [68].

1.3 Objectives

The principal aim of this thesis is to use mathematical modelling to better understand the frequency behavior of nanowire resonators for applications in biological detection. Using both continuum mechanics and molecular dynamics simulations, in this thesis, provides a multiscale modelling from the vibrations of nanowire resonators for mass sensing applications. In fact, developing such model is the fundamental goal of this study. The following objectives will be addressed in order to reach the principal aim of this thesis:

- We first provide a brief review on the current developed models for nanowire resonators using different continuum models to highlight the current advances in this field and to find the points that have not been addressed yet in the vibration modelling of nanowire resonators.

- We will discuss the potential of nanoresonators in mass sensing and biological object detection. A succinct review will be presented to show the potential of nanowires for this specific application.

- The principal objective is to develop a comprehensive continuum model for the vibrations of piezoelectric nanowires considering different parameters, critical for the

performance, such as electromagnetic fields, thermal variations, viscoelastic substrate, nonlocal and surface effects, added mass and nonlinearity due to large oscillations.

- Another important objective is to investigate the sensitivity of the frequency behavior of the nanowires to all of the above-mentioned parameters in both linear and nonlinear regions.

- We will also look at approximate solutions of the vibrations of nanowire resonators by using perturbation techniques.

- As another objective of this thesis, we will develop a numerical simulation technique for the presented continuum model of the vibrations of nanowire resonators.

- Finally, it is an important objective of this thesis to develop molecular dynamics simulations for the nanowire resonators with an added HIV virus at the middle of the nanoresonator. Therefore, we will look at the effects of added mass of HIV virus on the frequency shift of the nanowires using MD simulations, and provide a comparison with those results obtained from continuum mechanics models. In addition, we will use the MD simulations to investigate the effects of temperature and SiNW's size variation on the frequency behavior of nanowire resonators.

1.4 Thesis Structures

This Master's thesis contains six chapters, and its structure is as follows:

- Chapter 1 presents the problem statements, literature review with focus on modelling of nanowire resonators, applications of nanoresonators in mass sensing and bio-object detection, as well as drug delivery. The chapter ends with discussing the objectives of the thesis and its structure.

- Chapter 2 provides details on the modelling of the considered nanowire resonators and the related mathematical background. We first start with illustrating the Euler-Bernoulli beam theory, and then, its combination with the nonlocal Erigen theory. Mathematical equations related to the nonlocal form for the piezoelectric materials is also presented in this chapter. The formulations pertinent to the electromagnetic field effect, temperature variations, the mechanical stress induced by the piezoelectric potential, and also the surface effects are thoroughly discussed.

- Chapter 3 shows the use of perturbation analysis for the developed governing equation in order to study the effect of different parameters on the different resonance cases in the vibrations of nanowires. We provide details on the effect of the variation of different parameters on the frequency response of the nanowire resonators.

- In Chapter 4, we use the Finite Difference Method as a numerical approach to solve the governing equation of nanowire resonator for obtaining its frequency of oscillations.

- Chapter 5 presents the molecular dynamics simulations of the considered nanowire resonator.

- The last chapter discusses the conclusions and future works.

Chapter 2

Mathematical Model

2.1 Overview

The main challenges in the field of nanotechnology are connected with our ability to better understand materials properties of nanostructures, and also with our capability to correctly predict their behaviour under different conditions. It is an interdisciplinary field where scientists, engineers, and mathematicians are working together in determining materials properties of nanostructures, creating new nano-objects with enhanced capabilities, and developing necessary modelling tools, which give the power of a reliable predictive capacity.

In this chapter, we first provide geometrical representation and material parameters of our system of interest. Then, we discuss the dominant mechanical theories for the modelling of nanostructures. Section 2.3 describes the Euler-Bernoulli beam theory (EBT), the relevant stress-strain relations, and its connection with bending moment, shear and axial forces [69, 70]. Section 2.4 briefly describes the nonlocal theory and its application in nanoresonators and piezoelectric materials.

An introduction to the surface effects and its application in modelling of nanoresonators is presented in section 2.5. Section 2.6 provides the detailed procedure for finding the governing equation of considered nanoresonators using nonlocal EBT. Effect of different physical

parameters are considered in the modelling of nanowires including piezoelectricty, thermal effect, electromagnetic field, and surface tension. Given the focus of this thesis on tiny mass sensing, considering important effects of external disturbances, such as thermal, magnetic field, and electromechanical load, we note that a very small perturbation due to these effects can change the sensitivity of the nanowire resonator. It is assumed here that the nanowire resonator is rested on a nonlinear foundation with damping. Furthermore, an added mass is located at the middle of the nanowire resonator. The added mass is considered in our mathematical model, as this nanowire is intended to detect mass of tiny bio-objects. An external periodic load is also exerted to the considered nanowire resonator. The considered boundary and initial conditions are presented in sections 2.7 and 2.8, respectively.

2.2 Geometry and Material Parameters

In this chapter we aim to model the vibrations of piezoelectric nanowires, taking into account electromagnetic, thermal, nonlocal and surface effects with an external load rested on a Winkler foundation [71]. Figure 2.1(a) shows the geometry of the considered nanowire resonator in this thesis. There exist different types of nanowire resonators with distinct forms of cross sections such as circular and rectangular. In our model, it is supposed that the nanowire has a rectangular cross section as it can provide a flat surface on its top for locating the added mass, comparing to the circular cross section. The nanowire resonator has the length of L, height of $2h$, and width of b, as indicated in Figure 2.1(b). Figure 2.2 represents a 3D view of the nanowire resonator. In the first approximation, we will represent our nanowire as a beam.

Based on ref. [72] we consider the following sizes for the nanowire: $h = 1\ nm$, $b = 3\ nm$ and $L = 15\ nm$. Regarding the material of our nanoresonator, we use the properties of silicon nanowire, presented in Appendix B. Silicon nanowire has shown a promising potential for

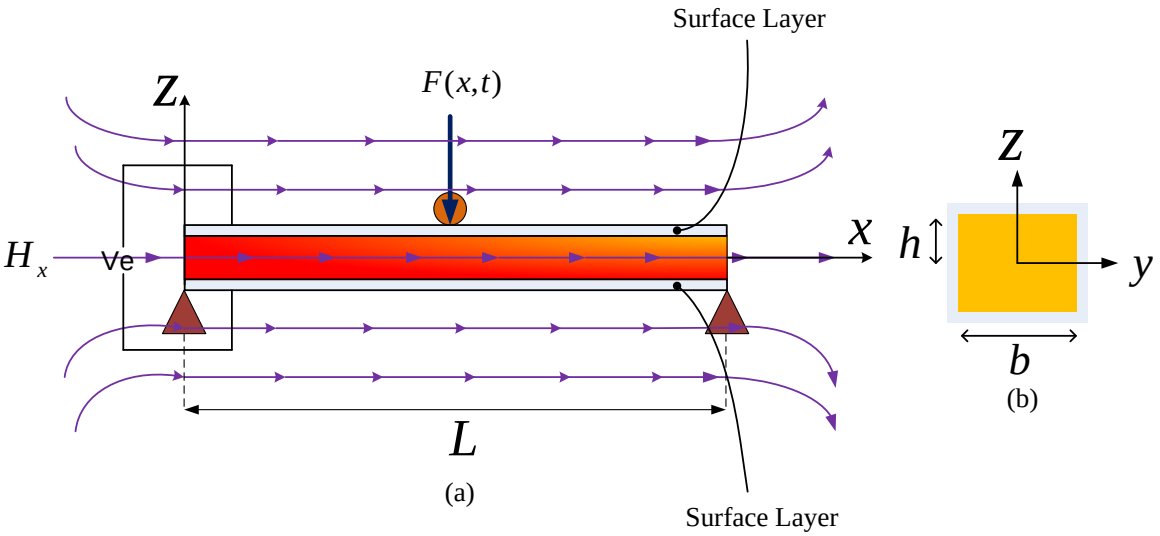

Fig. 2.1 Schematic of the nanoresonator, (a) a piezoelectric nanowire under harmonic load, thermal and electromagnetic field effects, (b) cross section of the nanowire

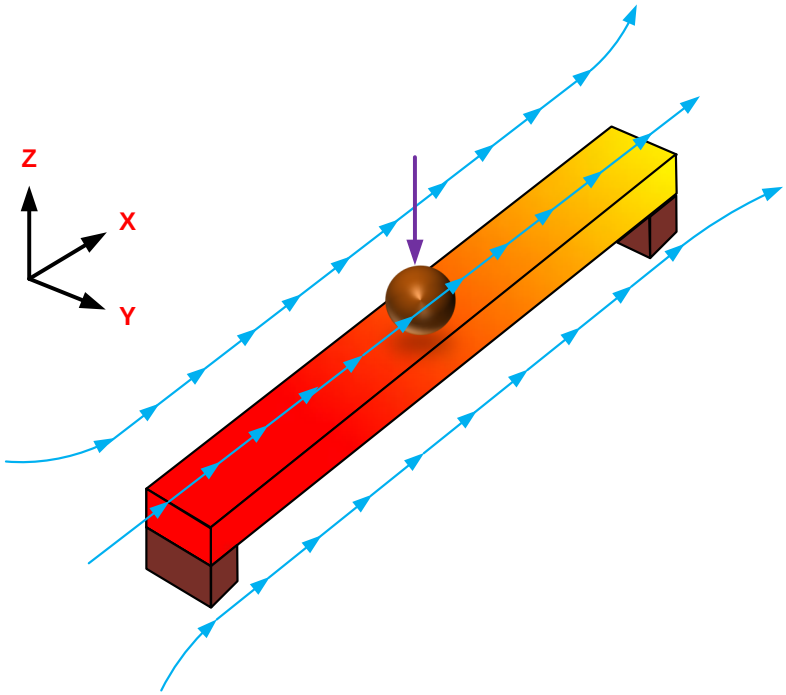

Fig. 2.2 3D view of the nanowire resonator

ultra-high resolution sensing because of its high modulus of elasticity, and accordingly, its high resonant frequency [3].

In the next section, we start with presenting the Euler-Bernoulli theory for the vibrations of a beam, and then it is extended to the nonlocal formulation, taking into account other important features such as piezoelectricty and surface effects.

2.3 The Euler-Bernoulli Beam Theory

The Euler-Bernoulli Theory (EBT) is used in order to obtain the governing equation of elastic nanowires. This theory can be applied to thin beams in which the length and deflections are much larger and much smaller than the depth, respectively. The main assumptions of EBT are as follows:

First, it is supposed that the cross-section is infinitely rigid in its own plane. Second, it is assumed that the cross-section of a beam remains in the plane after deformation. Furthermore, the cross-section remains normal to the deformed axis of the beam [73].

Based on EBT, the displacement field can be found by the following equations [69, 70]:

$$u_a = u(x,t) - z\frac{\partial w(x,t)}{\partial x}, \qquad u_b = 0, \qquad u_c = w(x,t), \tag{2.1}$$

in which u and w represent the axial and transverse deflection, respectively. According to the nonlinear von Karman theory [74], the only nonzero strain of the Euler-Bernoulli beam theory is as following:

$$\varepsilon_{xx} = \frac{\partial u(x,t)}{\partial x} + \frac{1}{2}\left(\frac{\partial w(x,t)}{\partial x}\right)^2 - z\frac{\partial^2 w(x,t)}{\partial x^2}, \tag{2.2}$$

where ε_{xx} is the strain in x direction.

In accordance with the EBT, we have the following relations between transverse shear forces V, bending moment M and the axial forces N:

$$\frac{\partial V(x,t)}{\partial x} = \frac{\partial^2 M(x,t)}{\partial x^2} + N(x,t)\frac{\partial^2 w(x,t)}{\partial x^2}, \tag{2.3}$$

and

$$\frac{\partial N(x,t)}{\partial x} + f_u = 0, \tag{2.4}$$

where f_u is the distributed axial load (measured per unit undeformed length) [69, 70, 73].

Axial forces and bending moment can be represented as the following relationships:

$$N = \int \sigma_{xx} dA = \int E\varepsilon_{xx} dA = EA\left[\frac{\partial u(x,t)}{\partial x} + \frac{1}{2}\left(\frac{\partial w(x,t)}{\partial x}\right)^2\right], \tag{2.5}$$

and

$$M = \int z \cdot \sigma_{xx} dA = \int z \cdot E\varepsilon_{xx} dA = -EI\frac{\partial^2 w(x,t)}{\partial x^2}, \tag{2.6}$$

in which, σ_{xx} represents the axial stress. Using the Euler-Bernoulli beam theory, this set of equations (Eq.(2.3)-Eq.(2.6)), will be utilized as the basis of our modelling to find the governing equation of the considered nanowire resonator. It should be noted that in our modelling we extend the Euler-Bernoulli beam theory to piezoelectric nanowires considering the piezoelectric effect. The details of this is provided in the next section, which we start from the description of the basis of the nonlocal theory.

2.4 Nonlocal Theories

The classical continuum models are not capable of modelling the length scales of the nanoresonators. In fact, continuum models cannot consider the material microstructure (such as lattice spacing between individual atoms), which are highly important in the modelling

of nanostructures [75, 76]. Although the implementation of atomic and molecular models results in an accurate analysis of nanoresonators, they are difficult to use, and highly time consuming in terms of computation. Nonlocal models empower the classical continuum approaches to account for the length scale in nanoresonators. Indeed, the use of nonlocal theory results in adding the internal length scale into the constitutive equations simply as a material parameter. The basis of nonlocal continuum theory was first proposed by Eringen [77, 78].

In accordance with the Eringen form of the nonlocal elasticity [77, 78], the stress field at a point is a function of strains at all other points in an elastic continuum. This would lead to an integral form of constitutive relations. Therefore, the nonlocal stress tensor σ_n at point x is represented as [74] :

$$\sigma_n = \int_V K(|x' - x|, \tau_m) S(x') dx', \tag{2.7}$$

where $S(x)$ is classical macroscopic stress tensor at point x and $K(|x' - x|, \tau_m)$ is the kernel function which implies the nonlocal modulus. $|x' - x|$ and τ_m are the distance in the Euclidean norm and material constant, respectively. According to the Hooke's law, there is a relationship between $S(x)$ at a point x in a Hookean solid and strain , ε_t , at the point, which can be written as follows:

$$S(x) = C(x) : \varepsilon_t(x), \tag{2.8}$$

in which C shows the fourth-order elasticity tensor and symbol : represents the double-dot product (see ref. [79]). Equations (2.7) and (2.8) are the constitutive equations, which can describe the nonlocal constitutive behavior of a Hookean solid. Since, it is difficult to use the integral constitutive relation shown in Eq. (2.7), it has been redefined in an equivalent differential form as:

$$(1 - \tau_m^2 a_e^2 \nabla^2)\sigma_n = S(x), \qquad \tau_m = \frac{e_0 a_i}{a_e}, \tag{2.9}$$

where e_0, a_i and a_e are material constant, internal and external characteristic lengths, respectively. We can represent the stress resultants in terms of the strains in different beam theories by the following equation [74]:

$$\Xi = 1 - \Gamma\nabla^2, \qquad \Gamma = e_0^2 a_i^2. \tag{2.10}$$

In the next section, we present the nonlocal stress theory for beams.

2.4.1 Nonlocal Stress Relations for Beams

The nonlocal theory yields a differential relation between stress resultants and the strains. Considering an immaterial nonlocal behaviour in the thickness ($2h$ in Fig. 2.1) direction of beam, Eq. (2.10) takes the following form [74]:

$$\Xi(\sigma_{xx}) = E\varepsilon_{xx}, \qquad \Xi(\sigma_{xz}) = 2G\varepsilon_{xz}, \qquad \Xi = 1 - \Gamma\frac{\partial^2}{\partial x^2}, \tag{2.11}$$

in which E is the Young modulus and G represents shear modulus. Γ implies the nonlocal parameter, which is equal to zero in the local theory.

Following [70, 80], we have the axial force-strain relation, which is identical in all beam theories:

$$\Xi(N) = N - \Gamma\frac{\partial^2 N}{\partial x^2} = EA\Big[\frac{\partial u}{\partial x} + \frac{1}{2}\Big(\frac{\partial w}{\partial x}\Big)^2\Big], \tag{2.12}$$

and

$$A = \int_A dA, \qquad \int_A z dA = 0,$$

where the x axis passes through the geometric centroid of the beam.

Accordingly, the constitutive relationship between bending moment and strain is constructed as below [80]:

$$M - \Gamma \frac{\partial^2 M}{\partial x^2} = -EI \frac{\partial^2 w}{\partial x^2}. \tag{2.13}$$

In the next part, we will introduce the nonlocal theory for piezoelectric materials.

2.4.2 Extension of Nonlocal Theories in Piezoelectric Nanowires

According to the nonlocal piezoelectricity theory, the stress and the electric displacement at a point do not only depend on the strain and electric-field at the point, but on all other points of the body. The nonlocal constitutive relationships for the piezoelectric nanowire are given by the following equations [81, 82]:

$$\sigma_n = \int_V K(|x' - x|, \tau_m)[C\varepsilon_t(x') - eE_e(x')]dx, \tag{2.14}$$

$$D = \int_V K(|x' - x|, \tau_m)[e\varepsilon_t(x') - \in E_e(x')]dx. \tag{2.15}$$

The differential constitutive equations corresponding to the integral form of equations (2.14) and (2.15), can be reconstructed as below:

$$\sigma_n - \Gamma \nabla^2 \sigma_n = C\varepsilon_t - eE_e, \tag{2.16}$$

$$D - \Gamma \nabla^2 D = e\varepsilon_t + \lambda E_e, \tag{2.17}$$

in which D, E_e, C, e and λ are electric displacement, electric field, fourth-order elasticity tensor, piezoelectric constants and dielectric constants, respectively. The description of surface effects is provided next.

2.5 Surface Effects

There are two important effects due to the nanoscale free surfaces. The first effect is surface stress and the second one is the surface elasticity. Both effects occur due to the fact that surface atoms in nanomaterials have a distinct bonding configuration as compared to atoms lying within the bulk material. Surface energy can be utilized in order to investigate the surface effects. There is a relationship between surface stress tensor σ^s, surface energy density γ_s and surface strain tensor ε^s as below [83, 84]:

$$\sigma^s = \gamma_s \delta + \frac{\partial \gamma_s}{\partial \varepsilon^s}. \tag{2.18}$$

Considering the one-dimensional and linear form of the surface stress tensor, we can write the Eq. (2.18) as the following equation for the surface stress of the nanowire:

$$\sigma^s_{xx} = \tau_0 + E^s \varepsilon^s_{xx}, \tag{2.19}$$

in which τ_0 and E^s represent the residual surface tension and surface elastic modulus, respectively. In the classical EBT, flexural rigidity EI_z, is considered as a significant quantity, due to the fact that it can be used to analyze the beam deformation. The flexural rigidity consists of E and I_z which are Young's modulus and the second moment of area, respectively. For a nanowire with rectangular cross section, we have the following equation for I_z:

$$I_z = b\frac{(2h)^3}{12}, \tag{2.20}$$

where b is the width and $2h$ is the height of a rectangular cross section of the nanowire (see Fig. 2.1).

By modeling a very thin isotropic elastic layer below the surface, the surface elasticity impact can be investigated. E_1 is defined as the Young's modulus of the surface layer, and a

is considered as the thickness of considered layer. We assume that a is approaching to zero, keeping $E_1 a$ as the constant of surface stiffness E^s, in order to recreate the idealized surface with zero thickness considered in the surface elasticity theory. Therefore, surface elasticity effects on the bending of a beam can be considered by replacing EI_z with the following effective flexural rigidity [84]:

$$(EI)^* = \frac{1}{12}Ebh^3 + \frac{1}{2}E^s bh^2 + \frac{1}{6}E^s h^3. \tag{2.21}$$

In accordance with the Laplace-Young equation [85], the jump of the normal stress $(\sigma^u_{mj} - \sigma^l_{mj})v_m v_j$ across a surface is given by the following equation:

$$(\sigma^u_{mj} - \sigma^l_{mj})v_m v_j = \tau_0 c, \tag{2.22}$$

in which c and v_m are the curvature of the surface and the unit vector normal to the surface, respectively. Considering $w(x)$ as the deflection at the position x, the second derivative of $w(x)$ with respect to x, $w''(x)$, is an approximation of the curvature of a bending beam. In a deformed beam, the residual surface tension will produce a distributed transverse loading, $q(x)$, along the longitudinal direction, which is opposed to the undeformed beam, in which $w''(x) = 0$. We have the Laplace-Young equation as below:

$$q(x) = Hw''(x), \tag{2.23}$$

where H is a function of residual surface tension and the cross-sectional shape. For the rectangular cross section nanowire we have H as follows [84]:

$$H = 2\tau_0 b. \tag{2.24}$$

The above equation is considered as the applied surface tension to the nanowire and will be used in our system of mathematical modelling in section 2.6.

2.6 Governing Equation of Nonlinear Nanowire Resonator

As we plan to mathematically model a piezoelectric nanowire resonator, the core of our model is based on the theories described in sections 2.3-2.5. Specifically, in our modelling, we use the nonlocal Euler-Bernoulli beam theory presented in section 2.4.1, accounting for piezoelectric and surface effects, discussed in sections 2.4.2 and 2.5, respectively.

In order to develop the mathematical model of the considered nanoresonator, we need to find the corresponding axial load N, shear force V, and bending moment M. This will lead us to having all required mechanical terms in Eq. (2.3) based on the Euler-Bernoulli beam theory.

We first start with modelling the surface effects in our nanowire resonator. As we deal with a nanoresonator, due to the small ratio of the volume to area, it is important to account for the surface effects in the modelling in order to be able to carry out a more practical and accurate analysis of the mass sensitivity of the nanowire resonator. The surface stresses of the nanowire can be described by Eq. (2.19) and the following equation:

$$\sigma_{xz} = \tau_0 \frac{\partial w}{\partial x}. \tag{2.25}$$

As it is required to fully satisfy the equilibrium conditions between nanowire's main core and it's corresponding surface layers, the following equations for both the upper and lower surfaces must be satisfied [86]:

$$\sigma^{up}_{mj,m} - \sigma^{up}_{jz} = \rho_0 \frac{\partial^2 u^{up}_j}{\partial t^2}, \qquad \sigma^{l}_{mj,m} + \sigma^{l}_{jz} = \rho_0 \frac{\partial^2 u^{l}_j}{\partial t^2}, \tag{2.26}$$

where the up and l signs represent the upper and lower surfaces, respectively, ρ_0 is the surface density of surface layers. We have $m = x, y$ and $j = x, y, z$. Considering Eq. (2.1) and Eq. (2.25), Eq. (2.26) can be reconstructed for the transverse vibrations of the nanowire as follows (see ref. [86], pages $2-3$):

$$\sigma_{zz}^{up} = \tau_0 \frac{\partial^2 w}{\partial x^2} - \rho_0 \frac{\partial^2 w}{\partial t^2}, \qquad \sigma_{zz}^{l} = -\tau_0 \frac{\partial^2 w}{\partial x^2} + \rho_0 \frac{\partial^2 w}{\partial t^2}. \tag{2.27}$$

The following equation displays the linear variation of σ_{zz} through the nanowire thickness:

$$\sigma_{zz} = \frac{1}{2}(\sigma_{zz}^{up} + \sigma_{zz}^{l}) + \frac{z}{2h}(\sigma_{zz}^{up} - \sigma_{zz}^{l}). \tag{2.28}$$

Substituting Eq. (2.27) into Eq. (2.28), results in the following equation for σ_{zz} :

$$\sigma_{zz} = \frac{z}{h}\left(\tau_0 \frac{\partial^2 w}{\partial x^2} - \rho_0 \frac{\partial^2 w}{\partial t^2}\right). \tag{2.29}$$

Based on the Laplace-Young equation, illustrated in section 2.5, we assume two distributed loads are exerted along the x coordinate due to the effect of residual surface stress. Accordingly, the following forms are considered for the distributed loads pertinent to the surface stress effects:

$$g_1(x) = b\tau_0^{up} \frac{\partial^2 w}{\partial x^2}, \qquad g_2(x) = b\tau_0^{l} \frac{\partial^2 w}{\partial x^2}. \tag{2.30}$$

It is supposed that, both upper and lower surfaces have analogous properties, therefore, the resultants of the above-mentioned distributed loads are presented as below [86]:

$$G_s(x) = g_1(x) + g_2(x) = 2b\tau_0 \frac{\partial^2 w}{\partial x^2}. \tag{2.31}$$

Temperature variations can change the sensitivity of the nanowire resonator for mass sensing. For understanding the effect of thermal variations on the response of the nanowire resonator,

we should consider the exerted stress due to the thermal load in our modelling. In order to account for the thermal effect in our model, we need to add the thermal stress-strain term to Eq. (2.2). The thermal stress term can be written as follows:

$$\sigma_\theta = -\frac{E}{1-2\nu}\alpha_x\theta_t, \tag{2.32}$$

where σ_θ, ν, α_x, and θ_t represent the axial thermal stress, Poisson ratio, the coefficient of thermal expansion in the direction of x axis, and temperature, respectively. Accounting for large amplitudes of oscillations of the nanowire and the axial load due to the thermal stress, we have the following relation for the longitudinal displacement u as a function of transverse deformation w [87]:

$$u = -\frac{1}{2}\int_0^L \left(\frac{\partial w}{\partial x}\right)^2 dx + \frac{x}{2L}\int_0^L \left(\frac{\partial w}{\partial x}\right)^2 dx - \frac{1}{2}\int_0^L \left(\frac{1}{1-2\nu}\right)\alpha_x\theta_t dx. \tag{2.33}$$

Substituting Eq. (2.33) and Eq. (2.2) into Eq. (2.4) results in:

$$T = \frac{EA}{2L}\left(\int_0^L \left(\frac{\partial w}{\partial x}\right)^2 dx - \frac{1}{1-2\nu}\alpha_x\theta_t\right), \tag{2.34}$$

where T represents two terms of the axial load owing to thermal stress and the large oscillations of the nanowire.

Another important term that should be taken into account is the electromagnetic field effect. Several researchers have shown that the magnetic field is affecting the vibrations of nanowire [35]. In accordance with this observation, it is critical to take into account the effect of electromagnetic field in our modelling of nanowire resonators with application in mass sensing. To include the electromagnetic field effect into the governing equations of nanowire resonators, based on the Maxwell equations [88, 89], we have the following set of equations

in the Cartesian coordinates, (x,y,z), as presented in Fig. 2.1:

$$J = \nabla \times h_m, \tag{2.35}$$

$$\nabla \times e_m = \zeta_m \frac{\partial h_m}{\partial t}, \tag{2.36}$$

$$\nabla . h_m = 0, \tag{2.37}$$

$$e_m = -\zeta_m \frac{\partial U}{\partial t} \times H_m, \tag{2.38}$$

$$h_m = \nabla \times (U \times H_m), \tag{2.39}$$

where J, e_m, h_m, U and ζ_m represent current density, strength vectors of electric field, disturbing vectors of magnetic field, the vectors of displacement, and the magnetic permeability, respectively. In order to obtain the magnetic field, which applies the transverse force to the nanowire, we first consider the general case of $U = (u,v,w)$ as the displacement vector. Accordingly, we assume a longitudinal magnetic field vector as $H_m = (H_x,0,0)$. Therefore, we obtain:

$$h_m = \nabla \times (U \times H_m) = -H_x \left(\frac{\partial v}{\partial y} + \frac{\partial w}{\partial x} \right) \hat{i} + H_x \frac{\partial v}{\partial x} \hat{j} + H_x \frac{\partial w}{\partial x} \hat{k} \tag{2.40}$$

and

$$J = \nabla \times h_m = H_x \left(\frac{\partial^2 v}{\partial x \partial z} + \frac{\partial^2 v}{\partial x \partial y} \right) \hat{i} - H_x \left(\frac{\partial^2 v}{\partial y \partial z} + \frac{\partial^2 v}{\partial x^2} + \frac{\partial^2 w}{\partial z^2} \right) \hat{j} + H_x \left(\frac{\partial^2 v}{\partial x^2} + \frac{\partial^2 v}{\partial y^2} + \frac{\partial^2 w}{\partial y \partial z} \right) \hat{k}. \tag{2.41}$$

The Lorentz force f_L exerted by the longitudinal magnetic field is obtained using the following equation[88, 89]:

$$f_L = \zeta_m(J \times H_m) = \zeta_m \left[0\hat{i} + H_x^2 \left(\frac{\partial^2 v}{\partial x^2} + \frac{\partial^2 v}{\partial y^2} + \frac{\partial^2 w}{\partial y \partial z} \right) \hat{j} + H_x^2 \left(\frac{\partial^2 w}{\partial x^2} + \frac{\partial^2 w}{\partial y^2} + \frac{\partial^2 v}{\partial y \partial z} \right) \hat{k} \right]. \tag{2.42}$$

Therefore, the components of Lorentz force in x,y, and z directions are defined as follows:

$$f_x = 0, \tag{2.43}$$

$$f_y = \zeta_m H_x^2 \left(\frac{\partial^2 v}{\partial x^2} + \frac{\partial^2 v}{\partial y^2} + \frac{\partial^2 w}{\partial y \partial z} \right), \tag{2.44}$$

$$f_z = \zeta_m H_x^2 \left(\frac{\partial^2 w}{\partial x^2} + \frac{\partial^2 w}{\partial y^2} + \frac{\partial^2 v}{\partial y \partial z} \right). \tag{2.45}$$

As we only investigate the transverse vibrations of the nanowire, the Lorentz force in z-direction is implemented as:

$$f_{em} = f_z = \zeta_m H_x^2 \frac{\partial^2 w}{\partial x^2}. \tag{2.46}$$

The above equation is used in our governing equation of the transverse vibration, Eq. (2.58), as the term of electromagnetic force.

For the piezoelectric effect, we should find its corresponding axial load. Accordingly, the electric displacement can be given by the following equations [90, 91]:

$$E_x = -\frac{\partial \psi}{\partial x}, \qquad E_z = -\frac{\partial \psi}{\partial z}, \tag{2.47}$$

and we have:

$$D_x = \lambda_{11} E_x, \qquad D_z = e_{31} \varepsilon_{xx} + \lambda_{33} E_z, \tag{2.48}$$

$$\frac{\partial D_x}{\partial x} + \frac{\partial D_z}{\partial z} = 0, \tag{2.49}$$

where λ_{11} and λ_{33} are dielectric constants, D_x, D_z, e_{31}, and ψ show the electric displacements, piezoelectric coefficient, and the electric potential, respectively. E_x and E_z represent the components of the electric field. For the considered nanowire resonator, we suppose that the electrical potential ψ varies between $-h$ to h across the height of the nanowire. Accordingly, we can consider a uniform piezoelectric distribution along the NW. It implies that $\psi_x \ll \psi_z$, therefore, we can neglect the electric displacement D_x in comparison with D_z. Based on this assumption, Eq. (2.49) will be written in the following form:

$$\frac{\partial D_z}{\partial z} = 0. \tag{2.50}$$

We consider the following boundary conditions for the electrical potential distribution to solve the above differential equation and combine the term related to the piezoelectric effect with the boundary conditions for the vibrations of the nanowire:

$$\psi(x,-h) = 0, \qquad \psi(x,h) = 2V_e. \tag{2.51}$$

Using Eqs. (2.17), (2.47), (2.48) and Eq. (2.50) and assuming the above boundary conditions results in the following form of electrical potential (derivation is provided in Appendix C) :

$$\psi(x,z) = -\frac{e_{31}}{\lambda_{33}}\left(\frac{z^2-h^2}{2}\right)\frac{\partial^2 w}{\partial x^2} + \left(1+\frac{z}{h}\right)V_e, \tag{2.52}$$

where V_e is the electric voltage [86]. The exerted axial load by piezoelectric potential is obtained using the following equation:

$$p_e = b\int_{-h}^{h} \sigma_{xx} dz. \tag{2.53}$$

Substituting Eq. (2.47) and Eq. (2.52) into Eq. (2.17), and then into Eq. (2.53) results in the following form of the axial load:

$$p_e = 2V_e b e_{31}. \tag{2.54}$$

Combining Eq. (2.53), Eq. (2.31) and Eq. (2.34), the following equation is obtained for the axial load, N, indicated in Eq. (2.55):

$$N = P_e + \frac{EA_{eff}}{2L}\int_0^L \left(\frac{\partial w}{\partial x}\right)^2 dx - \frac{1}{1-2v}\alpha_x\theta_t + 2b\tau_0. \tag{2.55}$$

Turning to Figure 2.1(a) and using the Newton's law, we can write the following formulation for the shear force applied to the nanowire:

$$\begin{aligned}\frac{\partial V}{\partial x} = (\rho A)_{eff}\frac{\partial^2 w(x,t)}{\partial t^2} + m_p\delta(x-x_p)\frac{\partial^2 w(x,t)}{\partial t^2} + \\ \mu\frac{\partial w(x,t)}{\partial t} + k_1 w(x,t) + k_3 w^3(x,t) - F(x,t) - f_{em},\end{aligned} \tag{2.56}$$

where ρ, V, μ, m_p, x_p, k_1 and k_3 are density, shear force, damping coefficient, particle mass, position of applied force, linear and nonlinear Winkler coefficient, respectively. The terms $k_1 w(x,t)$ and $k_3 w^3(x,t)$ are the forces exerted to the nanowire resonator by the assumed linear and nonlinear foundations, respectively.

Substituting Eqs. (2.55) and (2.56) into Eq. (2.3), and then using Eq. (2.13), results in the following governing equation for the vibrations of piezoelectric nanowire considering an added mass:

$$(EI)_{eff}\frac{\partial^4 w}{\partial x^4} + \left(1 - \Gamma\frac{\partial^2}{\partial x^2}\right)\Psi = 0, \tag{2.57}$$

where

$$\Psi = (\rho A)_{eff}\frac{\partial^2 w(x,t)}{\partial t^2} + m_p\delta(x-x_p)\frac{\partial^2 w(x,t)}{\partial t^2} + \mu\frac{\partial w(x,t)}{\partial t} + k_1 w(x,t) - 2b\tau_0\frac{\partial^2 w}{\partial x^2} + k_3 w^3(x,t) - F(x,t) - \zeta_m A H_x^2\frac{\partial^2 w}{\partial x^2} + 2V_e b e_{31}\frac{\partial^2 w}{\partial x^2} - \left(\frac{(EA)_{eff}}{2L}\int_0^L\left(\frac{\partial w}{\partial x}\right)^2 dx - N_\theta\right)\frac{\partial^2 w}{\partial x^2}, \tag{2.58}$$

where [90]

$$(\rho A)_{eff} = \rho A + 2b\rho_0, \tag{2.59}$$

$$(EI)_{eff} = EI + 2E^s + 4E^s\frac{h^3}{3} - vI\frac{\tau_0}{h} + \frac{2be_{31}^2 h^3}{3\lambda_{33}}, \tag{2.60}$$

$$(EA)_{eff} = Ebh + 2E^s(b+h), \tag{2.61}$$

$$F(x,t) = \bar{F}\delta(x-x_p)cos(\Omega t), \tag{2.62}$$

$$N_\theta = \frac{1}{1-2v}\alpha_x\theta_t. \tag{2.63}$$

We need to develop the dimensionless form of the above equation by defining the following variables: $\xi = \frac{x}{L}$, $\bar{W} = \frac{w}{L}$, $\tau = \omega_n t$. Considering these new variables, Eqs. (2.57) and (2.58) are rewritten as follows:

$$\frac{\partial^4\bar{W}}{\partial\xi^4} + \Pi\frac{\partial^2\bar{W}}{\partial\tau^2} - \Upsilon\Pi\frac{\partial^4\bar{W}}{\partial\tau^2\partial\xi^2} + \kappa\frac{\partial^2\bar{W}}{\partial\tau^2} - \Upsilon\kappa\frac{\partial^4\bar{W}}{\partial\tau^2\partial\xi^2} + \Delta\frac{\partial\bar{W}}{\partial\tau} - \Delta\Upsilon\frac{\partial^3\bar{W}}{\partial\tau\partial\xi^2} + \psi\bar{W} - \psi\Upsilon\frac{\partial^2\bar{W}}{\partial\xi^2} - 2\frac{\tau_0}{L}\frac{\partial^2\bar{W}}{\partial\xi^2} + 2\Upsilon\frac{\tau_0}{L^2}\frac{\partial^4\bar{W}}{\partial\xi^4} - F\left(\frac{\xi}{L},\frac{\tau}{\omega_n}\right) + \Upsilon\frac{\partial^2}{\partial\xi^2}F\left(\frac{\xi}{L},\frac{\tau}{\omega_n}\right) - \Lambda\frac{\partial^2\bar{W}}{\partial\xi^2} + \Upsilon\Lambda\frac{\partial^4\bar{W}}{\partial\xi^4} - \gamma_1\frac{\partial^2\bar{W}}{\partial\xi^2} + \Upsilon\gamma_1\frac{\partial^4\bar{W}}{\partial\xi^4} + \psi_1\bar{W}^3 + \Upsilon\frac{\partial^2}{\partial\xi^2}\psi_1\bar{W}^3 - \psi_2\left(\int_0^1\left(\frac{\partial\bar{W}}{\partial\xi}\right)^2 d\xi + N_\theta\right)\frac{\partial^2\bar{W}}{\partial\xi^2} + \psi_2\Upsilon\frac{\partial^2}{\partial\xi^2}\left(\int_0^1\left(\frac{\partial\bar{W}}{\partial\xi}\right)^2 d\xi + N_\theta\right)\frac{\partial^2\bar{W}}{\partial\xi^2} = 0, \tag{2.64}$$

where

$$\Upsilon = \left(\frac{e_0 a}{L}\right)^2, \qquad \Pi = \frac{L(\rho A)_{eff}\omega_n^2}{\Lambda_1}, \qquad \Lambda_1 = \frac{(EI)_{eff}}{L^3}, \qquad \Delta = \frac{\mu L \omega_n}{\Lambda_1},$$

$$\kappa = \frac{m_p \delta(1-\frac{x_p}{L})\omega_n^2 L}{\Lambda_1}, \qquad \psi = \frac{K_1 L}{\Lambda_1}, \qquad \psi_2 = \frac{(EA)_{eff}}{\Lambda_1 L^3}, \qquad \Lambda = \frac{\xi A H_x^2}{L\Lambda_1}, \qquad \gamma_1 = \frac{2Vbe_{31}}{L\Lambda_1}.$$

The obtained governing equation of the nanowire resonator will be analyzed in Chapter 3 by using perturbation techniques and Chapter 4 by utilizing the numerical approaches. The equation contains different effects which will be both qualitatively and quantitatively analyzed in the next chapters of this thesis.

2.7 Boundary Conditions

As we are studying a piezoelectric nanowire, the boundary conditions (BCs) of this nanowire corresponding to different types of end supports should also be examined. In this thesis, we investigate two different cases for our BCs which are simply supported ends and clamped-clamped (CC) ends. In a simply supported nanowire, one end is considered as pinned support and the other one as roller support. In this case, the deflection and bending moment are zero. In a clamped nanowire, the end is assumed to be fixed and there is no deflection and slope being considered.

In order to develop the dimensionless form of the governing equation of nanowire resonators, presented by Eq. (2.57), we defined the following variables: $\xi = \frac{x}{L}$, $\bar{W} = \frac{w}{L}$. Based on this definition and the initial length of the nanowire, L (see Figure 2.1), we conclude that $\xi = [0 \;\; 1]$. The following table represents the BCs for the nanowire, taking into account for the dimensionless form of the governing equation (see Eq. (2.64)):

Table 2.1 Boundary Conditions of Nanowire

Boundary Condition	At left end ($\xi = 0$)	At right end ($\xi = 1$)
Simply Supported Ends	$\bar{W}(0,\tau) = 0, \frac{\partial^2 \bar{W}}{\partial \zeta^2}(0,\tau) = 0$	$\bar{W}(1,\tau) = 0, \frac{\partial^2 \bar{W}}{\partial \zeta^2}(1,\tau) = 0$
Clamped-Clamped End	$\bar{W}(0,\tau) = 0, \frac{\partial \bar{W}}{\partial \zeta}(0,\tau) = 0$	$\bar{W}(1,\tau) = 0, \frac{\partial \bar{W}}{\partial \zeta}(1,\tau) = 0$

2.8 Initial Conditions

The following general form of the initial conditions is assumed for the nanowire resonator:

$$\bar{W}(\xi, \tau = 0) = \bar{W}_0 \tag{2.65}$$

and

$$\frac{\partial \bar{W}}{\partial \tau}(\xi, \tau = 0) = \dot{\bar{W}}_0. \tag{2.66}$$

In the next chapter, we use the perturbation technique to quantify the effect of different parameters introduced in the developed governing equation of the nanowire resonator.

Chapter 3

Perturbation Analysis

3.1 Overview

In Chapter 2, we developed a mathematical model for the vibrations of nanowire resonators accounting for different parameters. The developed model will be analyzed in this chapter using the method of multiple scales (MMS). In fact, the main focus of the present chapter is on the implementation of MMS to provide a qualitative analysis for the vibrations of nanowire resonators with an added mass, modelled in Chapter 2. In section 3.2, we use the Galerkin method to extract the time dependent part of the model proposed in Chapter 2. This will lead us to a nonlinear differential equation, which will be solved in section 3.4 by using MMS. Applying MMS to the obtained nonlinear differential equation gives the primary resonance formulation. The developed form of the primary resonance is used then for our parametric sensitivity analysis presented in section 3.4.2 considering simply supported boundary conditions for the nanowire resonators. We investigate the effect of different parameters including the added mass, electromagnetic fields, temperature variations, piezoelectric voltage and nonlocal parameters on both linear frequency and nonlinear primary resonance of nanowire resonators. Section 3.4.3 provides details of a sensitivity analysis based on the primary resonance for nonlinear vibrations of nanowire resonators. The effect

of boundary conditions is discussed in section 3.4.4. A super-harmonic resonance analysis is presented in section 3.4.5 based on the perturbation technique. Chapter ends with a sensitivity analysis in accordance with the obtained super-harmonic resonance case.

3.2 Galerkin Method

In this chapter, we aim at finding the primary resonance and frequency behavior of the oscillations of nanowires based on the developed model in Chapter 2. In order to analyze the oscillations of nanowire resonators and obtain the primary resonance using MMS, the first step is to apply the Galerkin method [92], which discretizes the time dependent part of Eq. (2.64). Accordingly, we consider the following form for $\bar{W}(\xi,\tau)$ in order to discretize Eq. (2.64) taking into account the primary mode of nanowire oscillations [92]:

$$\bar{W}(\xi,\tau) = \phi(\xi)\bar{u}(\tau), \tag{3.1}$$

where $\phi(\xi)$ defines the dimensionless deflection shape of the beam and it can be found from Table 2.1 based on the assumed boundary conditions. In Eq. (3.1), $\bar{u}(\tau)$ represents the dimensionless time dependent part of the oscillations of nanowires. Since our focus is on the vibration and frequency analysis of nanowire resonators, we use the separation of variables to find the time dependent part of the developed model in Chapter 2 [92]. Using the Galerkin method, we substitute Eq. (3.1) into Eq. (2.64) and then taking the integral from both sides of the equation, the following nonlinear ordinary differential equation is obtained:

$$\ddot{\bar{u}} + \frac{\alpha_1}{\alpha_0}\dot{\bar{u}} + \frac{\alpha_2}{\alpha_0}\bar{u} + \frac{\alpha_3}{\alpha_0}\bar{u}^3 = \frac{\alpha_F}{\alpha_0} cos\left(\frac{\Omega}{\omega_n}\tau\right), \tag{3.2}$$

in which

$$\alpha_0 = \Pi(\int_0^1 \phi^2(\xi)d\xi - \Upsilon\int_0^1 \phi''(\xi)\phi(\xi)d\xi) + \kappa(\int_0^1 \phi^2(\xi)d\xi - \Upsilon\int_0^1 \phi''(\xi)\phi(\xi)d\xi), \tag{3.3}$$

$$\alpha_1 = \Delta(\int_0^1 \phi^2(\xi)d\xi - \Upsilon\int_0^1 \phi^{"}(\xi)\phi(\xi)d\xi), \tag{3.4}$$

$$\begin{aligned}\alpha_2 = \Pi(&\int_0^1 \phi^2(\xi)d\xi - \Upsilon\int_0^1 \phi''(\xi)\phi(\xi)d\xi) - \\ &\psi(\int_0^1 \phi^2(\xi)d\xi - \Upsilon\int_0^1 \phi''(\xi)\phi(\xi)d\xi) + \\ &\frac{2\tau_0}{L}(\int_0^1 \phi^2(\xi)d\xi - \Upsilon\frac{2\tau_0}{L^2}\int_0^1 \phi''(\xi)\phi(\xi)d\xi) - \\ &\gamma_1(\int_0^1 \phi''(\xi)\phi(\xi)d\xi - \Upsilon\int_0^1 \phi''''(\xi)\phi(\xi)d\xi) \\ &\Lambda(\int_0^1 \phi''(\xi)\phi(\xi)d\xi - \Upsilon\int_0^1 \phi''''(\xi)\phi(\xi)d\xi) \\ -\psi_2\frac{1}{1-2\nu}\alpha_x\theta_t(&\int_0^1 \phi''(\xi)\phi(\xi)d\xi) - \Upsilon\int_0^1 \phi''''(\xi)\phi(\xi)d\xi),\end{aligned} \tag{3.5}$$

$$\alpha_3 = -\psi_2\int_0^1 \phi'(\xi)^2\phi''(\xi)\phi(\xi)d\xi + \Upsilon\frac{\partial^2}{\partial^2\xi}(\psi_2\int_0^1 \phi'(\xi)^2\phi'(\xi)\phi(\xi)d\xi), \tag{3.6}$$

and

$$\alpha_F = \bar{F}\left[\int_0^1 \delta\left(1-\frac{x_p}{L}\right)\phi(\xi)d\xi - \Upsilon\frac{\partial^2}{\partial\xi^2}\int_0^1 \delta\left(1-\frac{x_p}{L}\right)\phi(\xi)d\xi\right], \tag{3.7}$$

where δ is the Dirac function. In order to analyze the Eq. (3.2), the Method of Multiple Scales [93] will be employed in the next section. The main aim of using MMS is to find the

primary and other types of resonances of nanowire vibrations, and then to investigate the effect of different parameters on such vibrations. The next section will illustrate the MMS.

3.3 Method of Multiple Scales

The Method of Multiple Scales assumes that the expansion of the solution to a specific problem is a function of multiple independent variables, or scales, instead of a single variable t. The independent variables are considered as [94, 95]:

$$T_n = \varepsilon^n t, \tag{3.8}$$

where ε is a small dimensionless parameter. It is supposed that the solution of interest can be described by an equation in the following form [93]:

$$q(t,\varepsilon) = q_0(T_0,T_1,T_2,...) + \varepsilon q_1(T_0,T_1,T_2,...) + \varepsilon^2 q_2(T_0,T_1,T_2,...) + ..., \tag{3.9}$$

in which the number of independent time scales relies on the order of the MMS that is utilized. Generally, with employing Eq. (3.9) into a nonlinear differential equation and collecting coefficients of equal powers of ε results in a system of $n+1$ differential equations. In order to find the solution of the original nonlinear differential equation, the system of ODEs requires to be solved sequentially for $k = 1,2,...,n-1$, along with neglecting the secular terms, those terms that will become large when t increases, in the process at each order ε^k for $k = 1,2,...,n$. This will provide the following form of the solution for the original problem [94]:

$$q(t,\varepsilon) = \sum_{k=0}^{n-1} q_k(T_0,T_1,T_2,...,T_n) + O(\varepsilon^n). \tag{3.10}$$

Indeed, instead of finding q as a function of t, we determine q as a function of $T_0,T_1,T_2,....$ Therefore, the independent variable in the original nonlinear equation is altered from t to

a set of variables $T_0, T_1, T_2, \ldots$. Using the chain rule, the following forms of derivatives are obtained based on the set $T_0, T_1, T_2, \ldots$:

$$\frac{d}{dt} = \frac{\partial}{\partial T_0} + \varepsilon \frac{\partial}{\partial T_1} + \varepsilon^2 \frac{\partial^2}{\partial T_2} + \ldots = D_0 + \varepsilon D_1 + \varepsilon^2 D_2 + \ldots, \tag{3.11}$$

$$\begin{aligned} \frac{d^2}{dt^2} = \frac{\partial^2}{\partial {T_0}^2} + 2\varepsilon \frac{\partial^2}{\partial T_0 \partial T_1} + \varepsilon^2 \left(2\frac{\partial^2}{\partial T_0 \partial T_2} + \frac{\partial^2}{\partial {T_1}^2} \right) + \ldots = D_0^2 \\ + 2D_0 D_1 \varepsilon + (D_1^2 + 2D_0 D_2)\varepsilon^2 + \ldots . \end{aligned} \tag{3.12}$$

In the next section, we will apply MMS to analyze Eq. (3.2) and investigate the vibration behavior of nanowire resonators.

3.4 Implementation of MMS for Nanowire Resonators

In order to solve Eq. (3.2), we first rewrite it with implementation of small parameter ε. Accordingly, we have the following nonlinear differential equation [95]:

$$\ddot{\bar{u}} + 2\varepsilon \bar{\mu} \dot{\bar{u}} + \omega_l^2 \bar{u} + \varepsilon \bar{\beta} \bar{u}^3 = \varepsilon f cos(\Omega_1 \tau), \tag{3.13}$$

where $2\bar{\mu} = \frac{\alpha_1}{\alpha_0}$, $\omega_l^2 = \frac{\alpha_2}{\alpha_0}$, $\bar{\beta} = \frac{\alpha_3}{\alpha_0}$, $f = \frac{\alpha_F}{\alpha_0}$, and $\Omega_1 = \frac{\Omega}{\omega_n}$. For the primary resonance case analysis of the nanowire resonator, modelled in Chapter 2, the frequency of external excitation Ω_1 should be approximately equal to that of natural frequency ω_l of the nanowire. Hence, to delineate the nearness of Ω_1 to ω_l , one may use a detuning parameter σ, and by using the dimensionless small parameter (ε) it can be written as:

$$\Omega_1 = \omega_l + \varepsilon \sigma. \tag{3.14}$$

Now, we can expand $\bar{u}$ as the following equation:

$$\bar{u}(\tau,\varepsilon) = \bar{u}_0(T_0,T_1) + \varepsilon\bar{u}_1(T_0,T_1). \tag{3.15}$$

Accordingly, by using Eqs. (3.11), (3.12) and substituting Eq. (3.15) into Eq. (3.13), and then by separating the similar power of ε, will result in the following set of differential equations:

$$D_0^2\bar{u}_0 + \omega_l\bar{u}_0 = 0, \tag{3.16}$$

$$D_0^2\bar{u}_1 + \omega_l\bar{u}_1 = -2D_0D_1\bar{u}_0 - 2\bar{\mu}\bar{u}_0 - \bar{\beta}\bar{u}_0^3 + f\cos(\omega_l T_0 + \sigma T_1). \tag{3.17}$$

The solution of Eq. (3.16) can be considered as:

$$u_0 = A(T_1,T_2)\exp(i\omega_l T_0) + \bar{A}(T_1,T_2)\exp(-i\omega_l T_0). \tag{3.18}$$

By substituting Eq. (3.18) into Eq. (3.17), we obtain the following form of equation:

$$\begin{aligned} D_0^2\bar{u}_1 + \omega_l\bar{u}_1 = &-[2i\omega_l(A' + \bar{\mu}A) + 3\bar{\beta}A^2\bar{A}]\exp(i\omega_l T_0) \\ &-\bar{\beta}A^3\exp(3i\omega_l T_0) + \frac{1}{2}f\exp[i(\omega_l T_0 + \sigma T_1] + c.c.\ , \end{aligned} \tag{3.19}$$

where $c.c.$ stands for the complex conjugate terms. The term which contains $\exp(i\omega_l T_0)$ is the secular term. In order to have a bounded solution, the secular terms should be neglected as presented below [94]:

$$2i\omega_l(A' + \bar{\mu}A) + 3\bar{\beta}A^2\bar{A} - \frac{1}{2}f\exp(i\sigma T_1) = 0. \tag{3.20}$$

Exerting $A = \frac{a}{2}\exp(iB)$ into Eq. (3.20) and separating the real and imaginary parts, we obtain the following set of ordinary differential equations:

$$a' = -\bar{\mu}a + \frac{1}{2}\frac{f}{\omega_l}\sin(\sigma T_1 - B), \tag{3.21}$$

$$aB' = \frac{3}{8}\frac{\bar{\beta}}{\omega_l}a^3 - \frac{1}{2}\frac{f}{\omega_l}\cos(\sigma T_1 - B). \tag{3.22}$$

By defining $\bar{\lambda} = \sigma T_1 - B$, Eqs. (3.21) and (3.22) are rewritten as below:

$$a' = -\bar{\mu}a + \frac{1}{2}\frac{f}{\omega_l}\sin(\bar{\lambda}), \tag{3.23}$$

$$a\bar{\lambda}' = a\sigma + \frac{3}{8}\frac{\bar{\beta}}{\omega_l}a^3 - \frac{1}{2}\frac{f}{\omega_l}\cos(\bar{\lambda}). \tag{3.24}$$

We can find a steady state solution of the system of equations (3.23)-(3.24) by equating a' and $\bar{\lambda}'$ to zero. We know that the amplitude and phase of the system do not depend on the time and hence the time derivative terms of both terms are equal to zero. Therefore, we can have the following equations:

$$\bar{\mu}a = \frac{1}{2}\frac{f}{\omega_l}\sin(\bar{\lambda}), \tag{3.25}$$

and

$$a\sigma - \frac{3}{8}\frac{\bar{\beta}}{\omega_l}a^3 = \frac{1}{2}\frac{f}{\omega_l}\cos(\bar{\lambda}). \tag{3.26}$$

Squaring and adding the above equations, the following closed-form relationship is obtained [95]:

$$\left[\bar{\mu}^2 + \left(\sigma - \frac{3}{8}\frac{\bar{\beta}}{\omega_l}a^2\right)^2\right]a^2 = \frac{f^2}{4\omega_l^2}. \tag{3.27}$$

The above equation is 6th order polynomial in terms of a. It is also a quadratic equation in terms of σ. Solving the above equation for σ, we obtain the following form as the frequency

response curve for the Eq. (3.13):

$$\sigma = \frac{3}{8}\frac{\bar{\beta}}{\omega_l}a^2 \pm \left[\frac{f^2}{4\omega_l^2} - \bar{\mu}^2\right]^{\frac{1}{2}}. \tag{3.28}$$

The obtained relationship will be used in section 3.4.3 to quantify the effect of different parameters on the primary resonance of the nanowire resonator.

3.4.1 Simply Supported Boundary Conditions

Based on section 2.7, we consider simply supported boundary conditions for the nanowire resonator. In particular, we have:

$$\phi(\xi) = \sin(\pi\xi). \tag{3.29}$$

Implementing Eq. (3.29) into Eq.(3.3) to Eq. (3.7) will result in the following coefficients:

$$\begin{aligned}\alpha_1 = 0.5\pi^4 + 0.5\psi + 0.5\psi\Upsilon\pi^2 + \frac{\tau_0}{L}\pi^2 + \Upsilon\frac{\tau_0}{L^2}\pi^4 + \\ \frac{\Lambda}{2}\pi^2 + \frac{\Upsilon\Lambda}{2}\pi^4 + \gamma_1\frac{\pi^2}{2} + \frac{\Upsilon\lambda_1}{2}\pi^4 - \\ \psi_2\frac{2}{\pi}\left(\frac{1}{1-2\nu}\right)\alpha_x\theta_t - \psi_2\frac{\pi^4}{4}\left(\frac{1}{1-2\nu}\right)\alpha_x\theta_t,\end{aligned} \tag{3.30}$$

and

$$\alpha_2 = 0.5\Delta + \Delta\Upsilon\frac{\pi^2}{2}, \tag{3.31}$$

and

$$\alpha_3 = \psi_2\frac{\pi^4}{4} + \Upsilon\psi_2\frac{\pi^6}{4} + \frac{3}{8}\psi_1, \tag{3.32}$$

and

$$\alpha_0 = 0.5\Pi + 0.5\Pi\Upsilon, \tag{3.33}$$

where all main constants in the right-hand sides of (3.30)-(3.33) have been defined in section 2.6. In the next section, we provide a sensitivity analysis considering different parameters such as thermal, electromagnetic, piezoelectric, nonlocal and added mass.

3.4.2 Sensitivity Analysis: Linear Vibrations

This section provides a sensitivity analysis on the effect of different parameters on the vibration frequency of the nanowire resonator with simply supported boundary conditions. In our analysis, we have considered the material characteristics of silicon nanowire defined in Table B.1 (see Appendix). Figures of this section have been plotted based on the dimensionless linear frequency of the nanowire resonator with respect to dimensionless added mass. The dimensionless linear frequency is defined by the following equation:

$$\bar{\omega} = \frac{\omega_l}{\omega_0}, \tag{3.34}$$

where ω_0 is the linear frequency of the nanowire resonator without added mass and it can be obtained by using Eq. (3.3) and Eq. (3.5) (see Appendix, Eq. (E.1)). The dimensionless mass $\bar{m}$ is defined as below:

$$\bar{m} = \frac{m_p}{m_{nw}}, \tag{3.35}$$

where m_p and m_{nw} represent the masses of the added particle and the nanowire, respectively. Figure 3.1 shows the effect of dimensionless nonlocal parameter ($\frac{e_0 a}{L}$) and added mass ($\bar{m}$) on the dimensionless linear frequency. As the figure demonstrates, increasing the added mass results in decreasing the frequency. In addition, the value of frequency decreases by increasing the nonlocal parameter for a given added mass.

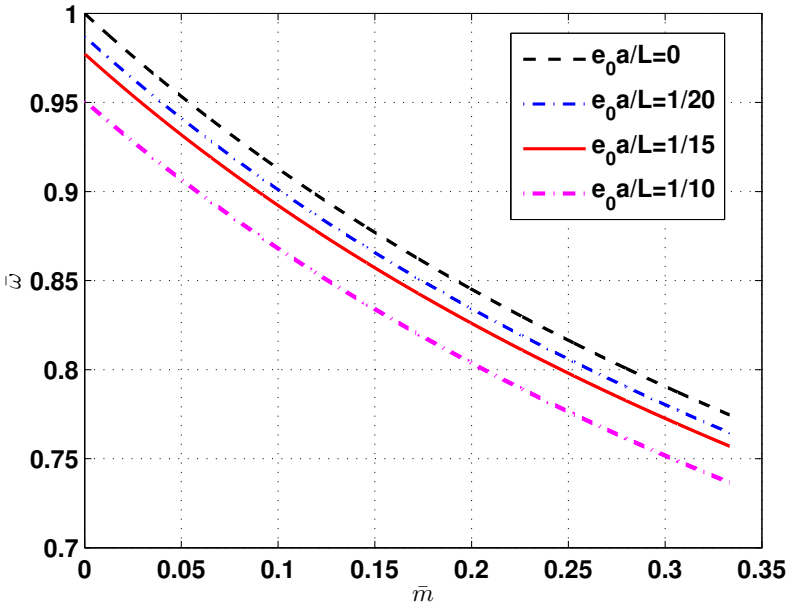

Fig. 3.1 Effect of the nonlocal parameter and added mass on the linear frequency of the SiNW

Figure 3.2 represents the effect of temperature on the linear frequency of the nanowire. Based on this figure, increasing temperature results in decreasing the linear natural frequency for a given added mass. Although temperature variations result in a small shift in the frequency of the nanowire for a specific added mass, it may affect the sensitivity of the nanowire resonator for small mass sensing such as bio-objects, significantly.

The effect of piezoelectric voltage is presented in Figure 3.3. As displayed by this figure, increasing the piezoelectric voltage decreases the frequency of oscillations of nanowire the resonator. In addition, it shows that the piezoelectric voltage has a more pronounced effect on the vibration behavior of the nanowire resonator in comparison with thermal variations. This figure shows that the piezoelectric voltage significantly changes the sensitivity of the nanowire resonator. Accordingly, the frequency of the nanowire resonator can be adjusted by using a specific piezoelectric voltage. The effect of magnetic field is presented in Figure 3.4. This figure shows that the magnetic field can be used for increasing the natural frequency of the nanowire. Therefore, it can be utilized as a design parameter to adjust the frequency of the

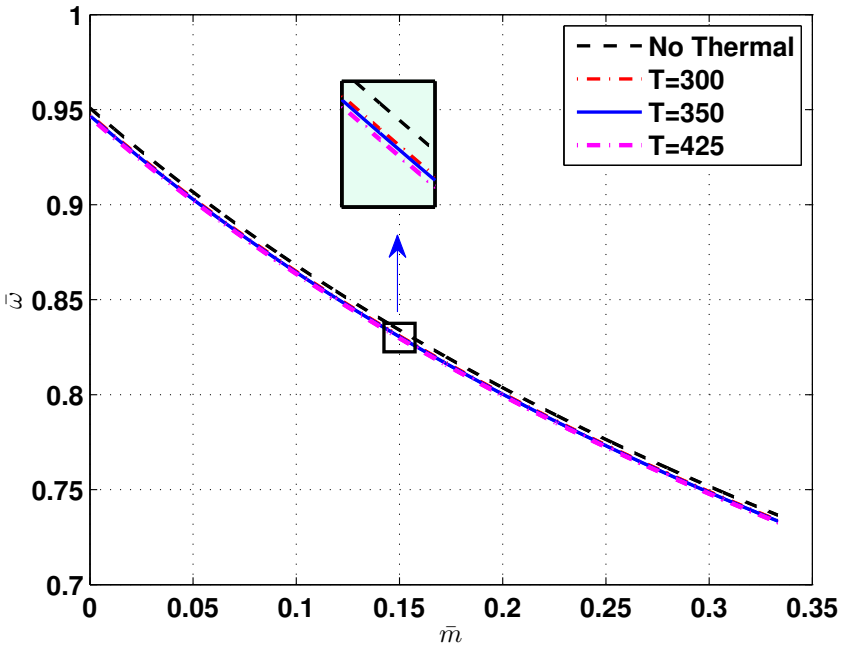

Fig. 3.2 Effect of the temperature $[^oK]$ variations and added mass on the linear frequency of SiNW

nanowire to a specific value required for a mass sensing application. It must be noted that the effect of electromagnetic fields on the vibrations of resonators, described by the model developed in Chapter 2, is not very big but it is considerable for sensing applications with high precision. All of these figures show that adding a tiny mass to a nanowire would result in a detectable frequency shift. This frequency shift can be measured and used for detection of the added mass in the case of experimental analysis. Therefore, our developed mathematical model from Chapter 2 that accounts for magnetic, thermal and piezoelectric effects, along with the provided solution procedure in Chapter 3, are useful for analytical calculations of the added mass to the nanowire.

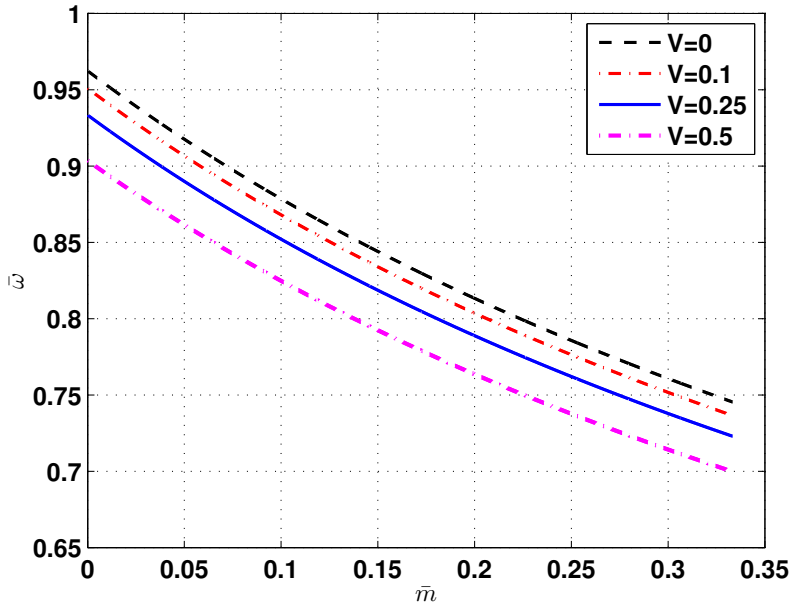

Fig. 3.3 Effect of the piezoelectric voltage [V] and added mass on the linear frequency of SiNW

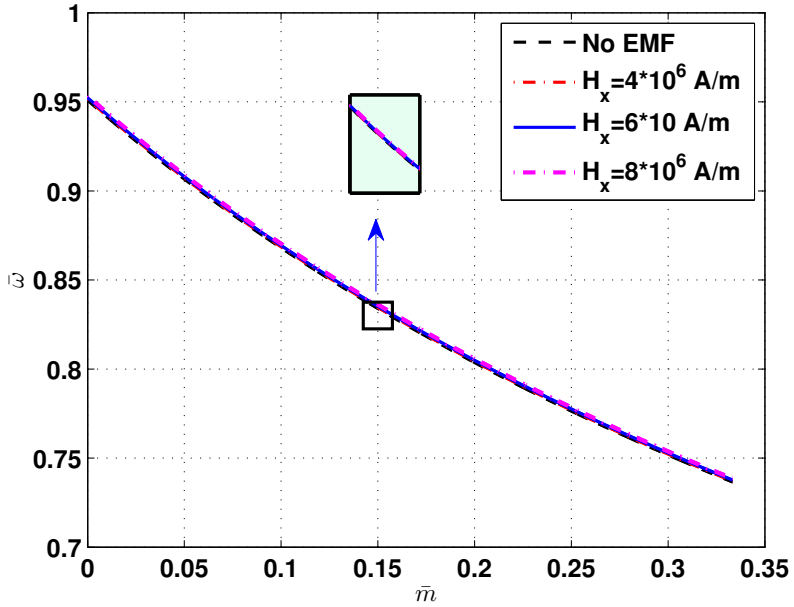

Fig. 3.4 Effect of the magnetic field and added mass on the linear frequency of SiNW

3.4.3 Sensitivity Analysis: Nonlinear Vibrations

In this part, we study nonlinear vibrations of the nanowire using the obtained primary resonance in section 3.4, accounting simply supported boundary conditions. Similar to section 3.4.2, we have considered the material characteristics of silicon nanowire defined in Table B.1 (see Appendix). Based on Eq. (3.28) developed in section 3.4, we investigate the effect of added mass on the primary resonance of nanowire resonators. Figure 3.5 represents the effect of the added mass on the primary resonance of nanowire resonators. As the figure shows, adding a small mass (e.g., $m_p = 10^{-18}g$) to the nanowire results in a detectable shift in the jump frequency. This jump can be observed in the experimental analysis [1]. This observation can be analyzed using the provided model in Chapter 2. In addition, this figure shows a high sensitivity of the nanowire resonator to a very small mass. It affects both the jump frequency and also amplitude of oscillations. Accordingly, it can be concluded that nanowire resonators have a high potential for detection of tiny particles such as bio-objects. Figure 3.6 shows the effect of thermal variations on the primary resonance of the nanowire resonator. As the figure presents, increasing temperature results in increasing the amplitude of oscillations. In fact, increasing temperature reduces the stiffness of the resonator, and therefore, both amplitude of oscillations and the value of jump frequency increase. Analogous results can be obtained when the piezoelectric voltage increases (see Fig. 3.7). Increasing the piezoelectric voltage results in increasing the amplitude of oscillations and also the value of the jump frequency. Accordingly, these two parameters can be used for adjusting the amplitude and the jump frequency of the nanowire resonator. In many practical situations of sensing, it is important to consider the effect of these two parameters in measurements as they affect both vibration amplitude and also frequency. The effect of electromagnetic fields is presented in Figure 3.8 based on the obtained primary resonance in section 3.4. As the figure demonstrates, increasing the value of the magnetic field reduces the value of jump frequency of the nanowire resonator. In addition, the value of amplitude of

oscillations of the nanowire resonator decreases with increasing the value of the magnetic field.

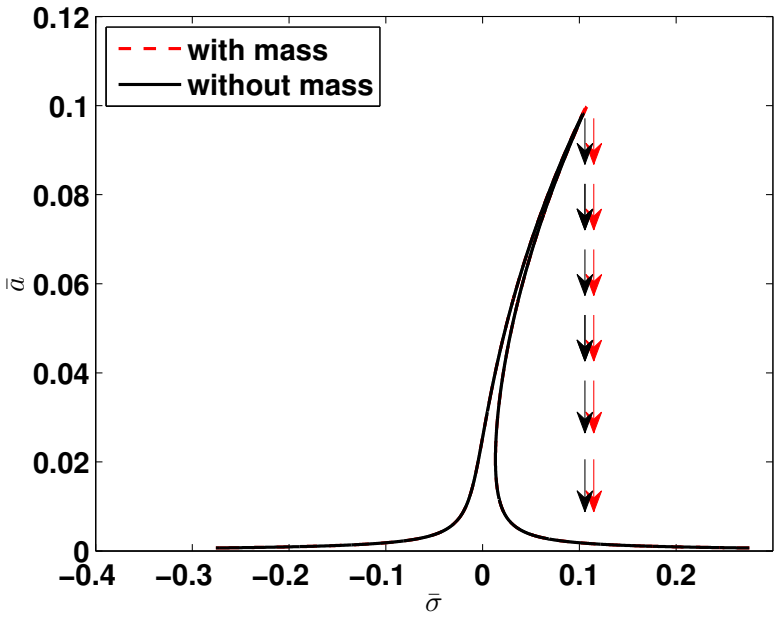

Fig. 3.5 Effect of the added mass on the primary resonance of SiNW

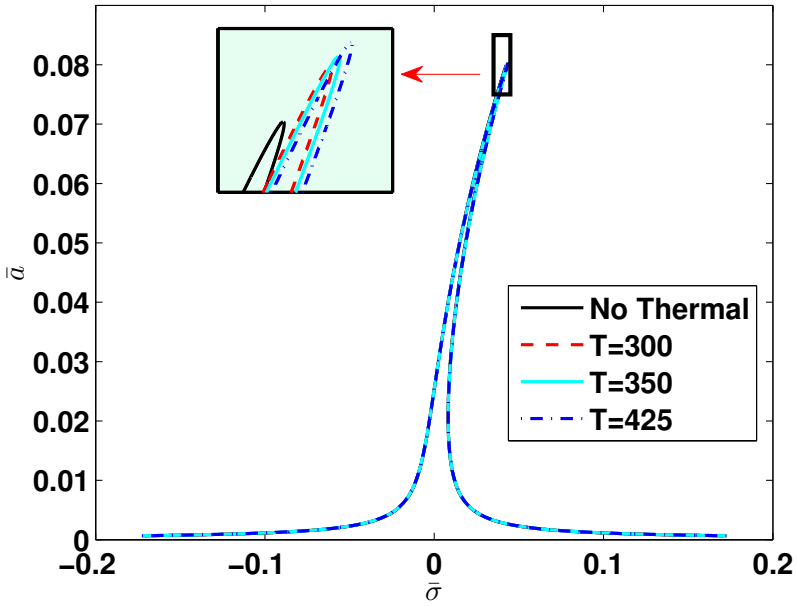

Fig. 3.6 Effect of the temperature $[^{o}K]$ variations on the primary resonance of the SiNW

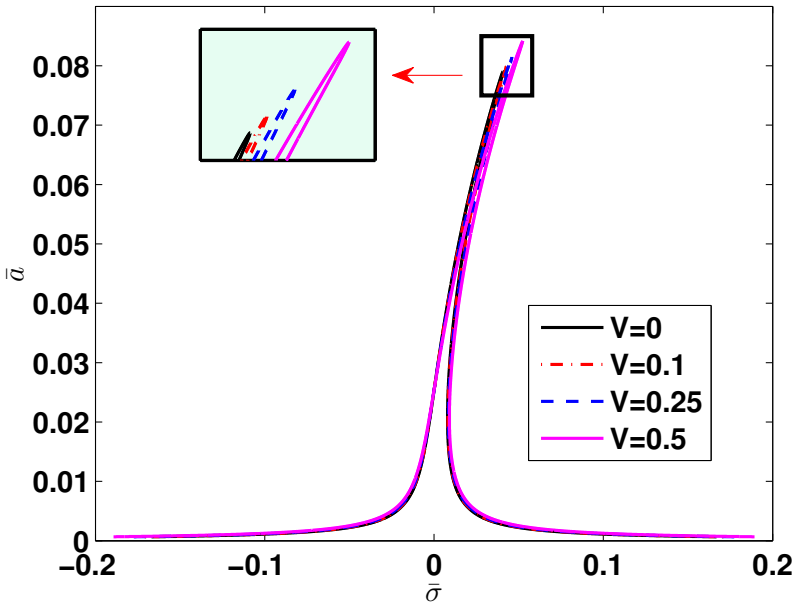

Fig. 3.7 Effect of the piezoelectric voltage $[V]$ on the primary resonance of SiNW

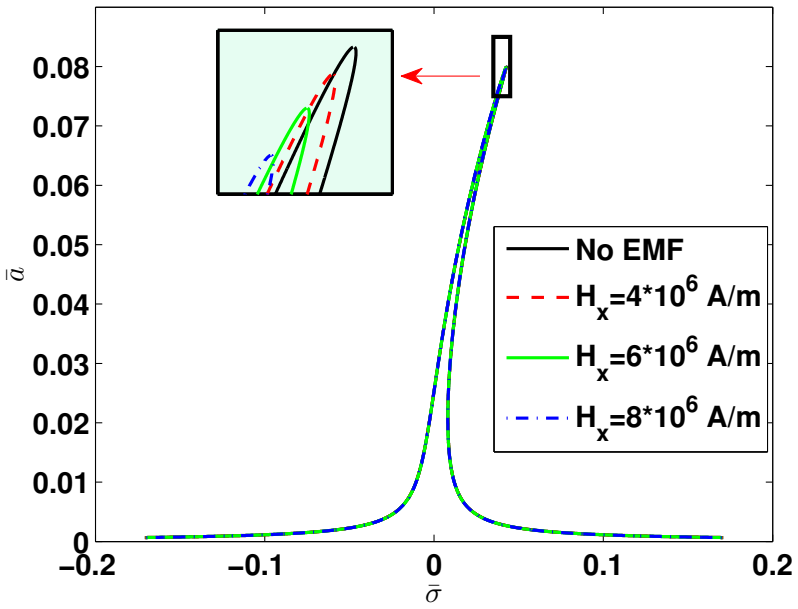

Fig. 3.8 Effect of the magnetic field on the primary resonance of SiNW

3.4.4 Clamped-Clamped Boundary Conditions

In this section, we study the effect of boundary conditions on the vibration behavior of the nanowire resonator with the model developed in Chapter 2, considering the material properties presented in Table B.1 (see Appendix). Figure 3.9 shows the effect of boundary conditions and added mass on the linear frequency of the nanowire resonator, illustrated in section 3.4.2. Based on this figure, the nanowire resonator with clamped-clamped boundary conditions has a higher frequency of vibrations in comparison with simply supported boundary conditions for a given added mass. It shows that not only variations in physical parameters can change the frequency of vibrations in nanowire resonators, but also, boundary conditions can significantly affect the frequency variation of nanowire resonators. Therefore, boundary conditions can be considered as another important factor in order to study nanowire resonators for mass detection applications.

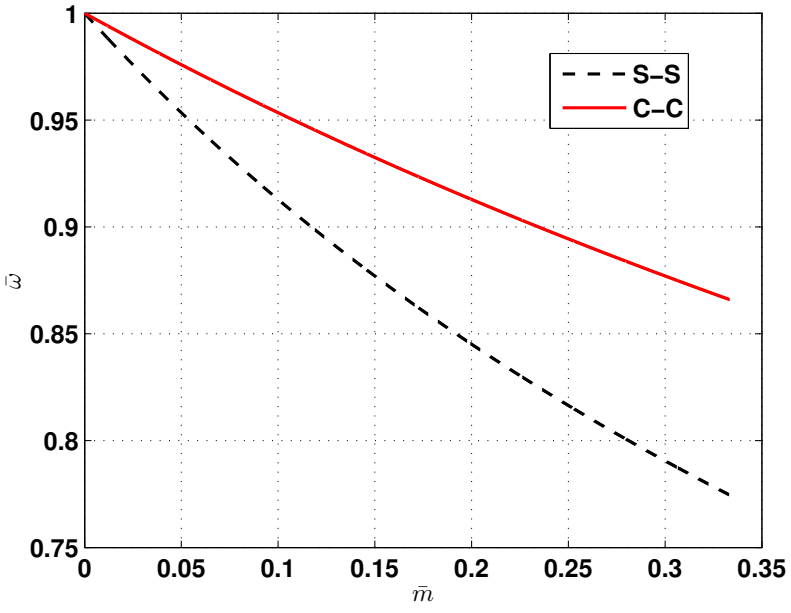

Fig. 3.9 Effect of the added mass and different boundary conditions on the linear frequency of SiNW

3.4.5 Super-Harmonic Resonance

The other resonance case that we can use for the sensitivity analysis of the considered nanowire resonators is the super-harmonic resonance case. The super-harmonic case occurs when $\Omega_1 \simeq \frac{1}{3}\omega_l$ [93]. This resonance case can also be considered for finding the effect of the added mass on the frequency behavior of nanowire resonators. In order to assess this case, following [93], we define the super-harmonic resonance case as:

$$3\Omega_1 = \omega_l + \varepsilon\sigma. \tag{3.36}$$

We assume the solution of Eq. (3.2) in the following form [93]:

$$\bar{u}_0 = A(T_1)\exp(i\omega_l T_0) + \bar{\Gamma}\exp(i\Omega_1 T_0) + c.c. \tag{3.37}$$

Substituting Eq. (3.37) into Eq. (3.2) results in:

$$\begin{aligned} D_0^2\bar{u}_1 + \omega_l\bar{u}_1 = -[2i\omega_l(A' + \bar{\mu}A) + 3\bar{\beta}A^2\bar{A} + 6\bar{\beta}A\bar{\Gamma}^2]\exp(i\omega_l T_0) \\ -\bar{\beta}[A^3\exp(3i\omega_l T_0) + \bar{\Gamma}^3\exp(3i\Omega_1 T_0) + 3A^2\bar{\Gamma}\exp[i(2\omega_l + \Omega_1)T_0 \\ 3\bar{A}^2\bar{\Gamma}\exp[i(\Omega_1 - 2\omega_l)T_0] + 3A\bar{\Gamma}^2\exp[i(\omega_l + 2\Omega_1)T_0] + \\ 3\bar{A}\bar{\Gamma}^2\exp[i(\omega_l - 2\Omega_1)T_0]] - \bar{\Gamma}[2i\bar{\mu}\Omega_1 + 3\bar{\beta}\bar{\Gamma}^2 + 6\alpha A\bar{A}]\exp(i\Omega_1 T_0) + c.c., \end{aligned} \tag{3.38}$$

where,

$$\bar{\Gamma} = \frac{f}{2\times(\omega_l^2 - \Omega_1^2)}. \tag{3.39}$$

For this resonance case, we must follow the resonance condition as below [93]:

$$3\Omega_1 T_0 = (\omega_l + \varepsilon\sigma)T_0 = \omega_l T_0 + \varepsilon\sigma T_0. \tag{3.40}$$

Now, we can eliminate the secular and near secular terms in Eq. (3.38) which leads to following equation:

$$2i\omega_l(A' + \bar{\mu}A) + 6\bar{\beta}\bar{\Gamma}^2 A + 3\bar{\beta}A^2\bar{A} + \bar{\beta}\bar{\Gamma}^3\exp(i\sigma T_1) = 0. \tag{3.41}$$

Using $A = \frac{a}{2}\exp(iB)$ and separating the real and imaginary parts, we obtain:

$$a' = -\bar{\mu}a - \frac{\alpha\bar{\Gamma}^3}{\omega_l}\sin(\sigma T_1 - B), \tag{3.42}$$

$$aB' = \frac{3\bar{\beta}}{\omega_l}\left(\bar{\Gamma}^2 + \frac{1}{8}a^2\right)a - \frac{\bar{\beta}\bar{\Gamma}^3}{\omega_l}\cos(\sigma T_1 - B). \tag{3.43}$$

Using the defined $\bar{\lambda}$ in section 3.4, we obtain the following equations:

$$a' = -\bar{\mu}a - \frac{\alpha\bar{\Gamma}^3}{\omega_l}sin(\bar{\lambda}), \tag{3.44}$$

$$a\bar{\lambda}' = \left(\sigma - \frac{3\bar{\beta}\bar{\Gamma}^2}{\omega_l}\right)a - \frac{3\bar{\beta}}{8\omega_l}a^3 - \frac{\bar{\beta}\bar{\Gamma}^3}{\omega_l}\cos(\bar{\lambda}). \tag{3.45}$$

We can find a steady state solution of Eqs. (3.44)-(3.45) by equating a' and $\bar{\lambda}'$ to zero. Accordingly, the following set of equations is obtained:

$$\bar{\mu}a = -\frac{\alpha\bar{\Gamma}^3}{\omega_l}\sin(\bar{\lambda}), \tag{3.46}$$

$$\left(\sigma - \frac{3\bar{\beta}\bar{\Gamma}^2}{\omega_l}\right)a = \frac{3\bar{\beta}}{8\omega_l}a^3 + \frac{\bar{\beta}\bar{\Gamma}^3}{\omega_l}\cos(\bar{\lambda}). \tag{3.47}$$

Eliminating $\bar{\lambda}$ in the above equations, the following closed form relation can be obtained:

$$\left[\bar{\mu}^2 + \left(\sigma - 3\frac{\bar{\beta}\bar{\Gamma}^2}{\omega_l} - \frac{3\bar{\beta}}{8\omega_l}a^2\right)^2\right]a^2 = \frac{\bar{\beta}^2\bar{\Gamma}^6}{\omega_l^2}. \tag{3.48}$$

Solving the above equation based on the detuning parameter (σ) and amplitude of oscillations (a), we obtain the following closed form relationship for the super-harmonic resonance case:

$$\sigma = 3\frac{\bar{\beta}\bar{\Gamma}^2}{\omega_l} + \frac{3\bar{\beta}}{8\omega_l}a^2 \pm \sqrt{\frac{\bar{\beta}^2\bar{\Gamma}^6}{\omega_l^2 a^2} - \bar{\mu}^2}. \tag{3.49}$$

Following [93], the maximum amplitude for the case of super-harmonic resonance can be found using the following formula:

$$a_p = \frac{\bar{\beta}\bar{\Gamma}^3}{\bar{\mu}\omega_l}. \tag{3.50}$$

Therefore, the super-harmonic resonance in the case of maximum amplitude of oscillation is given as follows [93]:

$$\sigma_p = \frac{3\bar{\beta}\bar{\Gamma}^2}{\omega_l}\left[1 + \frac{\bar{\beta}\bar{\Gamma}^4}{8\bar{\mu}^2\omega_l^2}\right]. \tag{3.51}$$

In the next section, we will use the obtained super-harmonic resonance for the parametric sensitivity analysis of the nanowire resonator described by the model developed in Chapter 2.

3.4.6 Parametric Sensitivity Analysis

In this section, we focus on the super-harmonic resonance case of our silicon nanowire resonator and the effect of different parameters on the peak amplitude defined by Eq. (3.50) and its corresponding σ_p obatined in Eq. (3.51). All figures of this section are obtained based on Eq. (3.50) and Eq. (3.51) using parameters defined in Table B.1 (see Appendix) with simply supported boundary conditions (section 3.4.1). In these figures, the blue and green lines are related to the amplitude of oscillations and super-harmonic resonance, respectively. Furthermore, the natural frequency (ω_l) is approximately equal to 66.6 GHz. Figure 3.10 shows the effect of temperature variations on both dimensionless peak amplitude (a_p) and its corresponding detuning parameter (σ_p). The corresponding values are obtained for four different temperatures: $T = 273,\ 300,\ 350$, and $450\ ^\circ K$ [96]. Based on this figure, the detuning parameter of the super-harmonic resonance, σ_p, is 5.38 GHz at the tempera-

ture of 425 $^{\circ}K$. The corresponding amplitude of oscillations, a_p, is 0.25 nm. As the figure demonstrates, increasing environmental temperature increases both a_p and σ_p. Therefore, not only we can look at the primary resonance to understand the behavior of the nanowire under thermal variations, but also, we can investigate the super-harmonic resonance as an alternative approach for understanding the response of the nanowire resonator under different thermal conditions. As it was expected both primary and super-harmonic resonance cases show similar behaviors under thermal loads.

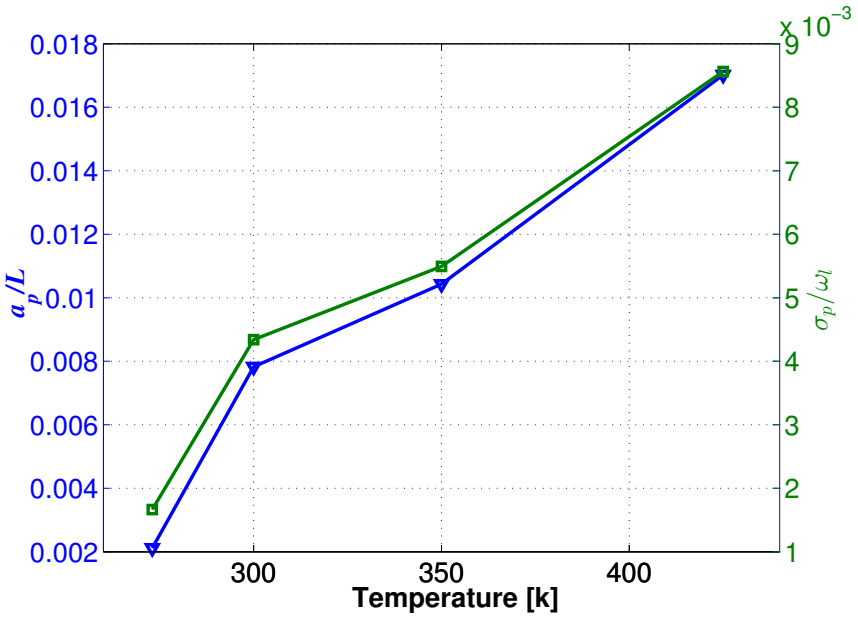

Fig. 3.10 Effect of temperature on the peak amplitude and the detuning parameter of the super-harmonic resonance of SiNW

Figure 3.11 reveals the effect of magnetic field on the super-harmonic resonance of nanowire resonators. The figure shows the relation of both a_p and σ_p to the variation of magnetic flux density for the super-harmonic resonance case. Similar to the primary resonance, increasing the magnetic flux density decreases both a_p and σ_p . It should be noted that $\bar{H}_x$ represents the dimensionless form of the magnetic flux density.

Figure 3.12 shows the effect of piezoelectric voltage on both a_p and σ_p. As the figure depicts, increasing the piezoeletric voltage enhances both a_p and σ_p of the nanowire resonator.

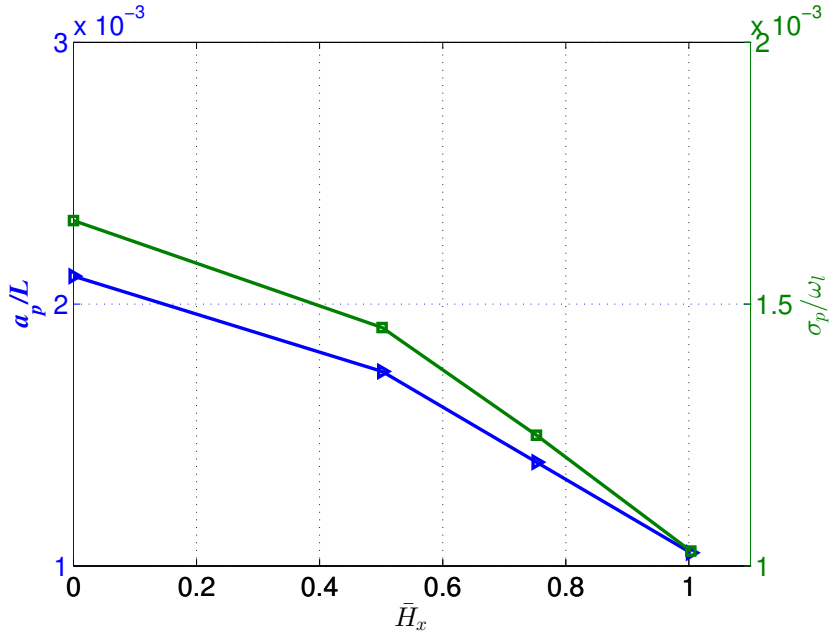

Fig. 3.11 Effect of magnetic field on the peak amplitude and the detuning parameter of the super-harmonic resonance of SiNW

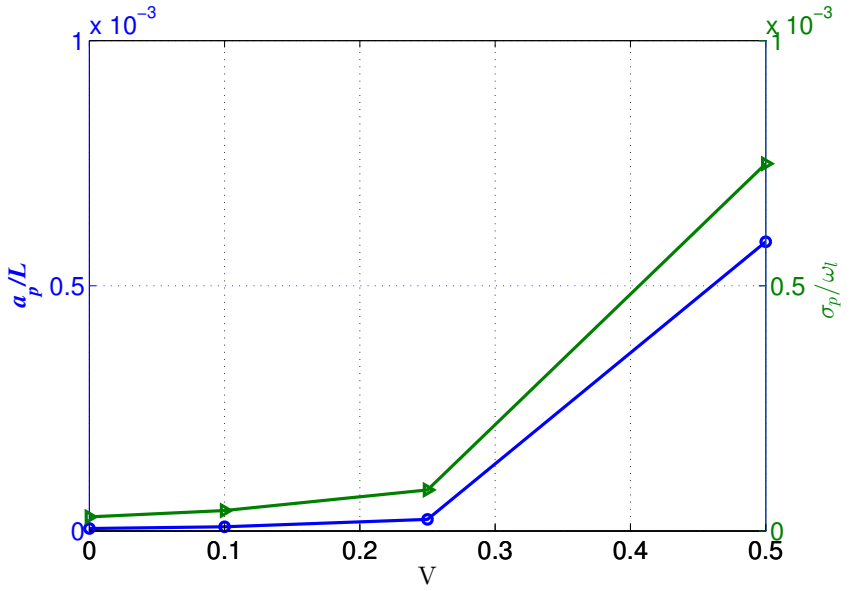

Fig. 3.12 Effect of piezoelectric voltage on the peak amplitude and the super-harmonic resonance of SiNW

To plot this graph (Fig. 3.12), we have chosen the value of 0, 0.1, 0.25, and 0.5 $[V]$ for the piezoelectric voltage in Eqs. (3.50) and (3.51). In accordance with this figure, the

detuning parameter of the super-harmonic resonance, σ_p, is 0.47 GHz at the piezoelectric voltage of 0.5 $[V]$. The corresponding amplitude of oscillations, a_p, is 7.5 pm. As shown by this figure, the super-harmonic resonance follows a similar behavior as the primary resonance with respect to the variation of piezoelectric voltage.

This chapter has provided a qualitative framework for the vibration analysis of the silicon nanowire resonator with added mass considering several parameters developed in Chapter 2. The provided analysis can give a better insight into the behavior of nanowire resonators under different external conditions such as variations in temperature, electromagnetic fields, added mass, and piezoelectric voltage. In the next chapter, we numerically investigate the mathematical model developed for the consiered nanowire resonator.

Chapter 4

Numerical Analysis

4.1 Overview

There are two categories of computational methods, based on numerical and analytical procedures respectively, that can be utilized for structural analysis. In the previous chapter, we used the perturbation analysis as an analytical method to investigate the vibrational behaviour of our considered nanowire described by the model developed in Chapter 2. Although the techniques based on analytical methods require less computational efforts and virtual storage, numerical methods provide an easier implementation and a wider practical applicability. In addition, they can provide a more accurate solution in comparison with perturbation methods. In order to use perturbation methods for the nonlinear vibration analysis of nanowire resonators, it is necessary to add small parameter ε to Eq. (3.2), which reduces the accuracy of this technique in comparison with more general numerical approaches. Hence, in this chapter, we study the vibration of our developed system using numerical techniques. By using a numerical approach, we can reach a more reliable analysis for the developed model of nanowire resonators. In order to apply a numerical analysis to our nanowire, we use the Finite Difference Method (FDM) as an established tool for structural analysis applications [97, 98]. Using this technique, we analyze the frequency response of the model developed in

Chapter 2 for nonlinear vibrations of nanowire resonators. In the next section of this chapter, we first briefly illustrate the FDM approach for solving partial differential equations. We note that this numerical method has been used by other researchers for vibration analysis of nanoresonators, and it has shown its high efficiency for the frequency analysis of nanostructures [97, 98]. Then in section 4.3, we apply the FDM to the governing equation of nanowire resonators developed in section 2.6. Finally, by using the obtained solution from the FDM, in section 4.4, we present a sensitivity analysis to investigate the effect of different parameters on the vibrations of nanowire resonators.

4.2 Finite Difference Method

Finite-difference methods are a generic class of numerical methods [99], which are being used for solving differential equations by approximating them with difference equations, where finite differences approximate the derivatives. FDMs require a discretization of the computational domain. The domain is partitioned in both space and time, and the approximations of the solution are computed at points of the grid, resulted from the domain discretization. We use Figure 4.1 to illustrate the FDM. As depicted in this figure, the computational domain is covered by a time grid (t), and a space grid (x).

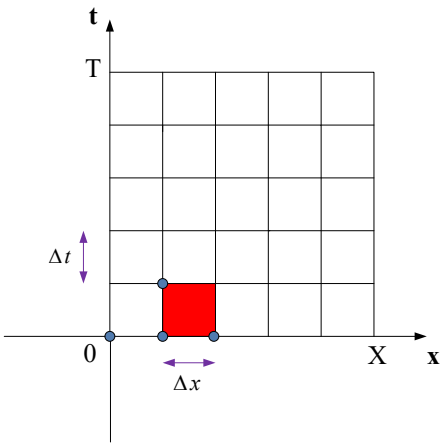

Fig. 4.1 Discretization of grid

Based on the FDM method, the discretized equations based on the first, second, third and fourth derivatives with respect to x are as follows [97, 100, 101]:

$$\frac{\partial w}{\partial x} \approx \frac{w_{i+1} - w_{i-1}}{2\Delta x}, \tag{4.1}$$

$$\frac{\partial^2 w}{\partial x^2} \approx \frac{w_{i+1} - 2w_i + w_{i-1}}{(\Delta x)^2}, \tag{4.2}$$

$$\frac{\partial^3 w}{\partial x^3} \approx \frac{w_{i+3} - 3w_{i+2} + 3w_{i+1} - w_i}{(\Delta x)^3} \tag{4.3}$$

$$\frac{\partial^4 w}{\partial x^4} \approx \frac{w_{i-2} - 4w_{i-1} + 6w_i - 4w_{i+1} + w_{i+2}}{(\Delta x)^4}, \tag{4.4}$$

where

$$\Delta x = \frac{Length\ of\ X}{Number\ of\ Steps\ in\ X}. \tag{4.5}$$

The accuracy of approximations (4.1), (4.2) and (4.4) at the grid point x_i, is of the second order, and approximation (4.3) is of the first order, with respect to (Δx). In the next section, we apply FDM to our developed governing equation, Eq. (2.57), to provide a numerical analysis for the frequency of nanowire resonators. It should be mentioned that Eq. (2.57) includes the second and fourth order derivatives with respect to x, so we just apply (4.2) and (4.4) approximations to study the FDM approach.

4.3 Implementation of FDM for Nanowire Resonators

In this section, we apply FDM to the governing equation (Eq. (2.57)) of nanowire resonators. In order to use FDM to analyze the developed model, we assume that the displace-

ment of the nanowire resonator can be given in the following form [97]:

$$w(x,t) = w(x)e^{i\omega t}, \tag{4.6}$$

where ω is the frequency of the nanowire resonator. We first consider the linear part of Eq. (2.57) developed in Chapter 2. Substituting Eq. (4.6) into the linear part of Eq. (2.57) results in:

$$(P)\frac{\partial^4 w(x)}{\partial x^4} + (Q)\frac{\partial^2 w(x)}{\partial x^2} + k_1 w(x) = \bar{M}\omega^2 w(x). \tag{4.7}$$

By substituting the approximate derivatives, Eq. (4.2) and Eq. (4.4), into Eq. (4.7), the following form is obtained:

$$\begin{aligned} G_1(w_{i-2} - 4w_{i-1} + 6w_i - 4w_{i+1} + w_{i+2}) + G_2(w_{i+1} - 2w_i + w_{i-1}) + k_1 w_i = \\ \omega^2\big[-G_3 w_i - G_4(w_{i+1} - 2w_i + w_{i-1})\big], \end{aligned} \tag{4.8}$$

where

$$G_1 = \frac{(EI)_{eff} + 2\Gamma b\tau_0 + \Gamma\zeta AH_x^2 + 2\Gamma vbe_3 1 + \Gamma\frac{(EA)_{eff}}{2L}N_\theta}{(\Delta x)^4}, \tag{4.9}$$

$$G_2 = \frac{-2b\tau_0 - \zeta_m AH_x^2 - 2vbe_3 1 - \frac{(EA)_{eff}}{2L}N_\theta - \Gamma k_1}{(\Delta x)^2}, \tag{4.10}$$

$$G_3 = \rho A + m_p, \tag{4.11}$$

$$G_4 = \Gamma\frac{m_p + \rho A}{\Delta x^2}, \tag{4.12}$$

and

$$\bar{M} = \big[-G_3 w_i - G_4(w_{i+1} - 2w_i + w_{i-1})\big]. \tag{4.13}$$

Using Eq. (4.5) for $i = 1, ..., N$, we can represent Δx as below:

$$\Delta x = \frac{L}{N-1}. \tag{4.14}$$

By considering clamped-clamped boundary conditions for the nanoresonator (defined in Table 2.1), we will have the following equations for both ends of the nanowire:

$$\text{at } x = 0: \; w_1 = 0, \quad \& \quad \frac{w_2 - w_0}{2\Delta x} = 0, \tag{4.15}$$

and

$$\text{at } x = N: \; w_N = 0, \quad \& \quad \frac{w_{N+1} - w_{N-1}}{2\Delta x} = 0. \tag{4.16}$$

Based on Eq. (4.15) and Eq. (4.16), we obtain the following relations:

$$w_0 = w_2, \qquad\qquad w_{N+1} = w_{N-1}. \tag{4.17}$$

It should be mentioned that w_0 and w_{N+1} are fictitious values which can be eliminated in our governing equation by using Eq. (4.17). Now, in order to solve Eq. (4.7) using FDM, we substitute $i = 2, ..., N-1$ into Eq. (4.8), which results in a system of equations as follows:

$$\begin{bmatrix} A_1 & B_1 & C_1 & 0 & \dots & 0 & 0 & 0 & 0 \\ A_2 & B_2 & C_2 & D_2 & \dots & 0 & 0 & 0 & 0 \\ . & . & . & . & \dots & . & . & . & . \\ . & . & . & . & \dots & . & . & . & . \\ . & . & . & . & \dots & . & . & . & . \\ 0 & 0 & 0 & 0 & \dots & A_{N-3} & B_{N-3} & C_{N-3} & D_{N-3} \\ 0 & 0 & 0 & 0 & \dots & 0 & A_{N-2} & B_{N-2} & C_{N-2} \end{bmatrix} \begin{bmatrix} w_2 \\ w_3 \\ . \\ . \\ . \\ w_{N-2} \\ w_{N-1} \end{bmatrix} = \omega^2 \tag{4.18}$$

$$\begin{bmatrix} G_3 - 2G_4 & G_4 & \dots & 0 & 0 \\ G_4 & G_3 - 2G_4 & \dots & 0 & 0 \\ . & . & \dots & . & . \\ . & . & \dots & . & . \\ . & . & \dots & . & . \\ 0 & 0 & \dots & G_3 - 2G_4 & G_4 \\ 0 & 0 & \dots & G_4 & G_3 - 2G_4 \end{bmatrix} \begin{bmatrix} w_2 \\ w_3 \\ . \\ . \\ . \\ w_{N-2} \\ w_{N-1} \end{bmatrix},$$

where

$$A_1 = 7G_1 - 2G_2 + k_1, \qquad B_1 = -4G_1 + G_2, \qquad C_1 = G_1, \tag{4.19}$$

$$A_2 = -4G_1 + G_2, \qquad B_2 = 4G_1 - 2G_2 + k_1, \qquad C_2 = -4G_1 + G_2, \qquad D_2 = G_1, \tag{4.20}$$

$$A_{N-3} = G_1, \qquad B_{N-3} = -4G_1 + G_2, \qquad C_{N-3} = 6G_1 - 2G_2 + k_1, \tag{4.21}$$

$$D_{N-3} = -4G_1 + G_2,$$

and

$$A_{N-2} = G_1, \qquad B_{N-2} = -4G_1 + G_2, \qquad C_{N-2} = 7G_1 - 2G_2 + k_1. \tag{4.22}$$

Hence, Eq. (4.18) can be rewritten in the following form:

$$\big(-[\bar{M}]\omega^2 + [K]\big)\{w\} = 0, \tag{4.23}$$

where $w = \{w_2, w_3, ...w_{N-2}, w_{N-1}\}^T$, $\bar{M}$ and K are the mass and stiffness matrices, respectively. $\bar{M}$ is defined by the following matrix:

$$\bar{M} = \begin{bmatrix} G_3 - 2G_4 & G_4 & ... & 0 & 0 \\ G_4 & G_3 - 2G_4 & ... & 0 & 0 \\ . & . & ... & . & . \\ . & . & ... & . & . \\ . & . & ... & . & . \\ 0 & 0 & ... & G_3 - 2G_4 & G_4 \\ 0 & 0 & ... & G_4 & G_3 - 2G_4 \end{bmatrix}. \tag{4.24}$$

K represents the stiffness matrix, and it can be found as follows:

$$K = \begin{bmatrix} A_1 & B_1 & C_1 & 0 & ... & 0 & 0 & 0 & 0 \\ A_2 & B_2 & C_2 & D_2 & ... & 0 & 0 & 0 & 0 \\ . & . & . & . & ... & . & . & . & . \\ . & . & . & . & ... & . & . & . & . \\ . & . & . & . & ... & . & . & . & . \\ 0 & 0 & 0 & 0 & ... & A_{N-3} & B_{N-3} & C_{N-3} & D_{N-3} \\ 0 & 0 & 0 & 0 & ... & 0 & A_{N-2} & B_{N-2} & C_{N-2} \end{bmatrix}. \tag{4.25}$$

In order to obtain the linear frequency of the vibrations of the nanowire resonator, we need to find the solution of Eq. (4.23). A non-trivial solution of Eq. (4.23) can be obtained when the determinant of coefficient matrix equals to zero as below:

$$\Big|\big[-[\bar{M}]\omega^2+[K]\big]\Big|=0. \tag{4.26}$$

Solving the above equation would lead to finding the frequency of the nanowire resonator described with the model developed in Chapter 2. For the nonlinear part of the governing equation, Eq. (2.57), we have:

$$\begin{aligned} NL := -\frac{EA_{eff}}{2L}\left[\int_0^L\left(\frac{\partial w(x,t)}{\partial x}\right)^2 dx\right]\frac{\partial^2 w(x,t)}{\partial x^2}+k_3 w^3(x,t)-\Gamma k_3\frac{\partial^2}{\partial x^2}[w^3(x,t)] \\ +\Gamma\frac{EA_{eff}}{2L}\left[\int_0^L\left(\frac{\partial w(x,t)}{\partial x}\right)^2 dx\right]\frac{\partial^2 w(x,t)}{\partial x^2}. \end{aligned} \tag{4.27}$$

The integral term in our governing equation can be approximated by the following relationship:

$$\int_0^L\left(\frac{\partial w(x,t)}{\partial x}\right)^2 dx\approx\frac{L}{2}\left[\left(\frac{\partial w(x,t)}{\partial x}\right)^2\Big|_{i=1}+\left(\frac{\partial w(x,t)}{\partial x}\right)^2\Big|_{i=N}\right]. \tag{4.28}$$

Based on the defined boundary condition in Eqs. (4.15)-(4.16) and the nonlinear terms presented by Eq. (4.27), we have the following relation to obtain the nonlinear frequency of the considered nanowire resonator developed in Chapter 2:

$$\big(-[\bar{M}]\omega^2+[K]+[K_{NL}]\big)\{w\}=0. \tag{4.29}$$

To obtain the nonlinear natural frequency, we first need to solve the linear equation to obtain the eigen values and vectors. Then, we utilize the obtained solution as an initial approximation for the nonlinear equation defined in Eq. (4.29). By substituting the derived

eigen values and vectors into Eq. (4.29), and also coupling the linear and nonlinear stiffness matrices with the mass matrix, the nonlinear frequency and mode shape can be calculated [69]. Then, implementing the iteration method, the nonlinear frequency is recalculated in order to find an approximate frequency, when the iterations converge with pre-defined accuracy. In the next section, we discuss the results obtained based on FDM.

4.4 Parametric Sensitivity Analysis

In this section, a parametric sensitivity analysis is carried out by using the obtained numerical solution in section 4.3, for the vibration of the nanowire resonator described by the model developed in Chapter 2. All figures of this section are obtained based on Eq. (4.26) using parameters defined in Table B.1 (see Appendix) with clamped-clamped boundary conditions defined by Eqs. (4.15) and (4.16). We have investigated the sensitivity of dimensionless frequency, $\bar{f}_n$, obtained by numerical simulation presented in section 4.3 with respect to variations in temperature, piezoelectric voltage, nonlocal parameter, and the added mass. The dimensionless frequency, $\bar{f}_n$, is obtained using the following equation:

$$\bar{f}_n = \frac{\omega}{\omega_0}, \tag{4.30}$$

where both ω and ω_0 can be obtained by using Eq. (4.26). The constant ω_0 is the frequency of the nanoresonator without considering the effect of added mass. Figure 4.2 shows the effect of temperature on the frequency behavior of silicon nanowire resonator using Eq. (4.30). As the figure shows, increasing the temperature reduces the frequency value of nanowire resonator. This figure represents a similar trend of what we observed in Figure 3.2 based on the perturbation analysis presented in section 3.4.2. Using Eq. (4.30) based on the FDM solution presented in section 4.3, we have performed a sensitivity analysis with respect to the piezoelectric voltage. Increasing the piezoelectric voltage reduces the frequency of

silicon nanowire resonator modelled in Chapter 2. Again, this FDM-based result regarding the piezoelectric voltage and its effect on the frequency of the nanowire resonator verifies our qualitative analysis based on the perturbation method presented in Figure 3.3 (see section 3.4.2).

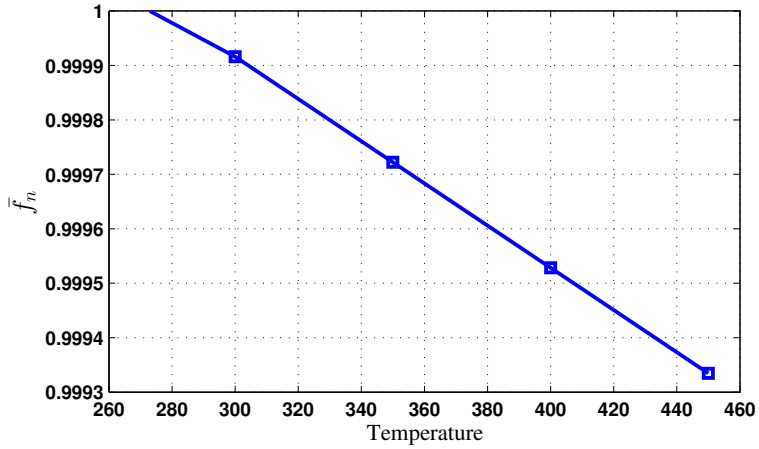

Fig. 4.2 Effect of temperature [$^{\circ}K$] on the frequency behavior of SiNW using FDM

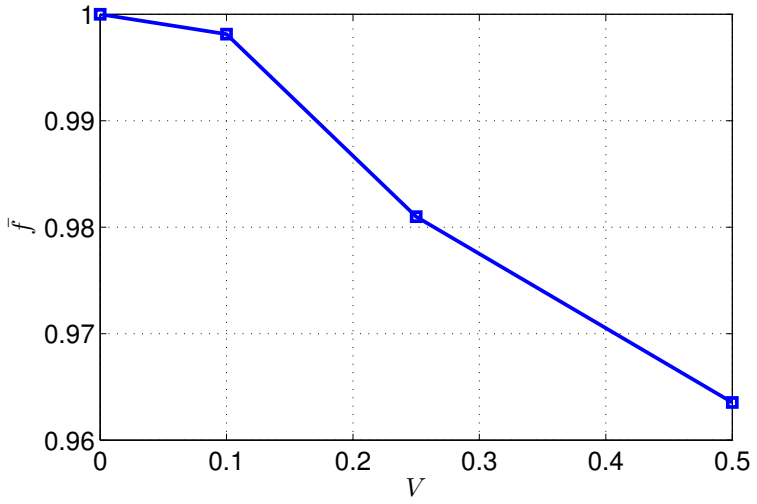

Fig. 4.3 Effect of piezoelectric voltage on the frequency behavior of SiNW using FDM

Figure 4.4 depcits the effect of dimensionless nonlocal parameter ($\frac{e_0 a}{L}$) on the frequency behavior of the silicon nanowire resonator modelled in Chapter 2. This figure has been plotted by using Eq. (4.30) based on the FDM solution provided in section 4.3. As the figure

reveals, increasing the nonlocal parameter reduces the frequency of nanowire resonator. This result confirms our analysis based on the perturbation method presented in Figure 3.1 of Chapter 3.

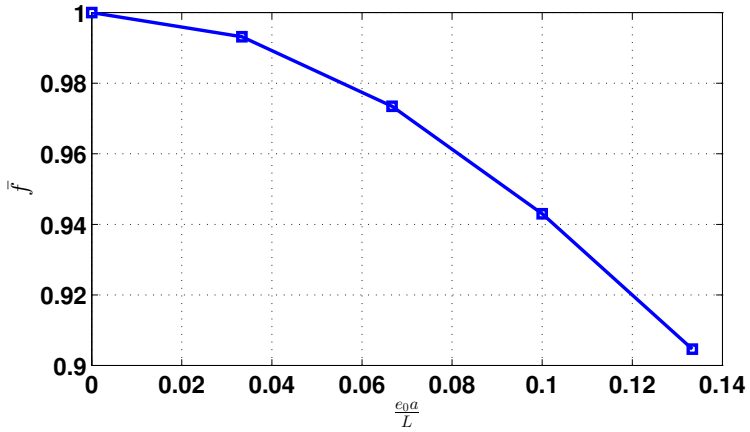

Fig. 4.4 Effect of dimensionless nonlocal parameter on the frequency behavior of SiNW using FDM

Figure 4.5 shows the effect of added mass on the frequency behavior of SiNW using Eq. (3.35) and Eq. (4.30). As the figure shows, increasing the mass of added particle reduces the frequency of SiNW resonator. This result supports the prediction of analytical investigation presented in section 3.4.2 of Chapter 3.

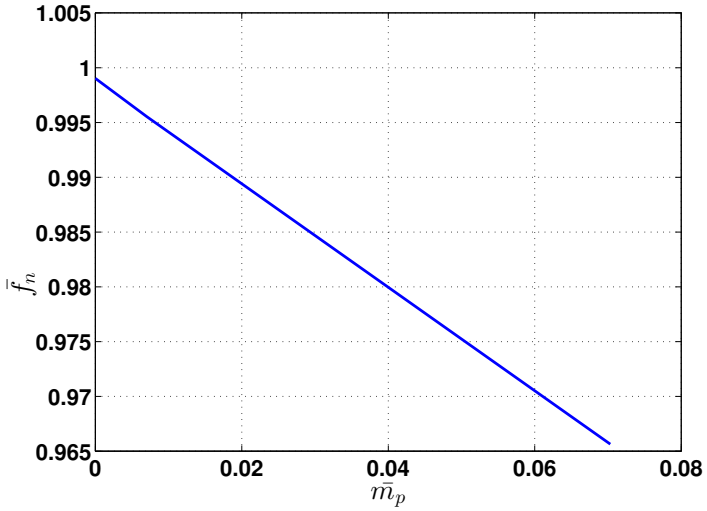

Fig. 4.5 Effect of added mass on the frequency behavior of SiNW using FDM

In order to investigate the convergence of our solution presented in section 4.3 for the developed model of silicon nanowire resonator using the iterative technique in conjunction with the FDM discussed in the context of Eq. (4.29), we have plotted the obtained nonlinear frequency of each iteration with respect to its corresponding number of iteration, M. Fig. 4.6 shows that by using the iterative technique for the nonlinear part, we can reach to the convergent frequency after a few iterations with the accuracy of 10^{-4}.

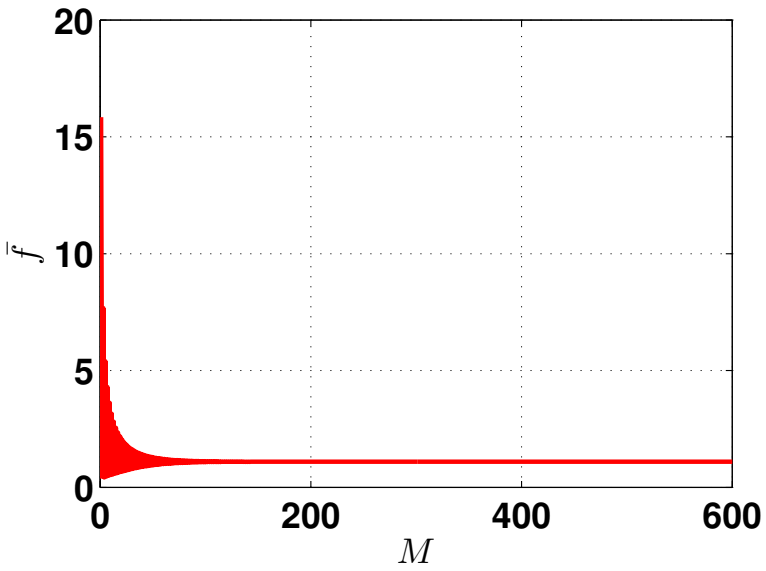

Fig. 4.6 Convergence analysis of the frequency response of FDM

The comparison of the FDM and the perturbation method shows when we use the perturbation method, it is necessary to simplify the developed PDE, presented in Eq. (2.57). For instance, in order to apply the perturbation analysis in Chapter 3, we should define the small parameter, ε, which reduces the accuracy of the method in comparison with numerical approaches such as the FDM [95]. However, the qualitative results obtained from the perturbation analysis, shown in section 3.4.3 to section 3.4.6, verify the numerical results based on the FDM. In fact, both the FDM and perturbation method predict similar behavior for the vibrations of nanowire resonators taking into account different parameters.

4.5 Other Numerical Techniques in Structural Analysis of Nanoresonators

We note that several other numerical approaches such as the Finite Element Method (FEM) [102], Generalized Differential Quadrature (GDQ) method [103], and Variational Differential Quadrature (VDQ) method [104] have been used in the literature to analyze the structural behavior of nanoresonators. For example, recently, the FEM was used by Aria and Friswell to study buckling and vibrations of functionally graded nanobeam [105]. El-Taher et al. [15] utilized the FEM to investigate vibrations of nanobeam, developed based on the nonlocal Euler-Bernoulli beam theory. Phadikar and Pradhan [106] used the FEM to find non-dimensional critical buckling load and non-dimensional frequency of both nanoplate and nanobeam. In their analysis, they considered the effect of geometry and boundary conditions. Ansari et al. [107] employed the GDQ to develop a numerical solution for the forced vibration of nanobeam considering the surface effect based on the Timoshenko beam theory. In fact, preliminary numerical results in analyzing nanoresonators in this thesis have been obtained based on the GDQ technique. Shahabodini et al. [108] used the VDQ to analyze the vibration of carbon nanotube resonators. They showed that the VDQ has a fast rate of convergence for analyzing vibration models of the CNT resonator. All of the above-mentioned techniques can be considered as possible alternative numerical approaches for analyzing the presented model of this thesis. However, for the considered geometry of our structure analyzed in this thesis, we have used the FDM, as it provides both relative simplicity and flexibility of implementation.

Chapter 5

Molecular Dynamics Simulations

5.1 Overview

In Chapters 3 and 4, we both analytically and numerically investigated the vibration behavior of the nanowire resonator described by the model developed in Chapter 2. In our study, we examined the effect of different multi-physics parameters on the frequency of the silicon nanowire and also considered an added particle on the scale of bio-objects located at the middle of the nanoresonator (see Fig. 2.1). In this chapter, the aim is to develop molecular dynamics (MD) simulations for the silicon nanowire resonator with an added mass. Specifically, our main results in this chapter are exemplified by an HIV molecule. MD simulations enable studying nanomaterials properties with comparable results to those obtained with experimental techniques [109]. In fact, MD simulations are considered as an essential technique for the investigation of nanomaterials dynamics. Based on MD simulations, we can obtain important information about interatomic interactions of nanomaterials and molecular complexes plus the trajectories prediction of millions of atoms in the targeted nanosystem [110]. Although MD simulations can provide a formidable analysis of nanoresonators, it is time consuming in comparison with continuum models, such as those developed in the previous chapters of this thesis. Accordingly, here by having both types of analyses (MD

simulations and continuum models), we can verify the potential of continuum models for qualitatively studying vibrations of silicon nanowire resonators by comparing the results obtained with such models to the results of MD simulations. In addition, the MD simulations of the silicon nanowire resonator can provide a deeper understanding of the dynamics of targeted nanoresonators. We briefly illustrate the molecular dynamics simulations method and fundamentals of it in sections 5.2 and 5.3, respectively. We also discuss the force fields used in our modelling in section 5.4 and provide a description of our simulations methodology in section 5.5.

Furthermore, we study the effect of temperature variations on the frequency response of the SiNW. Then, in our MD simulations, we locate a molecule of HIV as an added particle in the middle of silicon nanowire to probe its effect on the vibration properties of silicon nanowire resonator (see section 5.6). We conclude this chapter with a discussion on the advantages and challenges of MD simulations in comparison with continuum models.

5.2 Molecular Dynamics Simulations Method

In Chapter 2, we provided a theoretical modelling of our nanostructure using continuum mechanics methodologies. Generally, continuum models require less computational effort and provide a relatively straightforward formulation, which can give a qualitative insight into the dynamic behavior of nanoresonators. On the other hand, continuum models neglect the structural discontinuities at the atomic scale, which is the intrinsic limitation of such models. This crucial limitation averts continuum models from providing more accurate results, and accentuate the need for MD simulations in analyzing the vibration properties of nanostructures. MD simulations can provide a reliable and precise insight into vibrations of nanoresonators. Indeed, among different techniques for simulation of the atomic level, MD has shown a great potential for vibration analysis of nanoresonators, and it is a potent tool for understanding mechanical behaviors of nanoscale systems [109, 111, 112]. MD simulations

were proposed by Alder and Wainwright in the late 50s to study the phase transition of hard spheres [113], and it is now an advanced simulation tool, which is commonly used for simulations of thousands of atoms with having appropriate computer facilities [114]. It is being considered as a reliable simulation technique for the systems even with biological interactions and tiny nanoresonators [114, 115]. During the last decade, several types of simulation techniques have been developed based on molecular dynamics for particular systems such as solvated proteins, protein-DNA complexes as well as lipid systems, graphene sheets, nanotubes, and nanowires [109, 116, 111].

In this chapter, we use MD simulations to study the vibration behavior of nanowire resonators. In our continuum model, developed in Chapter 2, we have considered the added tiny particle, and investigated its effect on the frequency response of the nanowire resonator using perturbation method (see Chapter 3) and numerical simulation (see Chapter 4). We first model a silicon nanowire to study its frequency of vibrations using MD simulations, and then we add a molecule of HIV virus as a special case to investigate the potential of SiNW resonator for the detection of tiny bio-objects.

5.3 Fundamental of Molecular Dynamics Simulations

The fundamental concept behind the MD simulations is the numerical, step-by-step, solution of the classical equations of motion of an atomic system with the assumption of point-like masses atoms, which interact with each other based on a given potential energy [117, 118]. Following points are the main assumptions behind MD simulations [117, 118]:

- The main postulation is that molecules or atoms are considered as a system of interacting material points. Vector of instantaneous positions and velocities is used to dynamically describe the motion of molecules or atoms.

- It is supposed that there is no mass change in the system. Accordingly, the number of atoms remains the same.

As the system of interacting atoms follows Hamiltonian dynamics, the force interaction of atoms can be modelled by using the Newton's law as follows [117, 118]:

$$F_i = m_i \frac{d^2 r_i}{dt^2} = -\nabla P(r_1, r_2, ..., r_N), \tag{5.1}$$

where m_i is the mass of atom i, F_i represents the force on that atom, P is the potential energy of the system of atoms, N is total number of simulated atoms, and r_i represents a complete set of 3D atomic coordinates. One of the efficient techniques for solving Eq. (5.1) is the velocity-Verlet algorithm proposed by Allen and Tildesley [118], which is used as the solution method for classical MD simulations in LAMMPS (Large-scale Atomic/Molecular Massively Parallel Simulator) [109, 119, 120]. This algorithm is the direct solution of second order differential equation Eq. (5.1), which is based on positions $r(t)$, velocity $v(t)$, and acceleration $a(t)$. Further information about this algorithm can be found, e.g., in ref. [118]. For simulating a system using Eq. (5.1) with the velocity-Verlet algorithm, we need to isolate the whole system from any variation in number of atoms (N), total volume (V) and the total energy (E), which is known as an NVE ensemble. The other popular ensemble is called NVT in which it is supposed that the number of atoms (N), the volume (V) and the present temperature (T) of the systems are constant. These two ensembles are mostly utilized in the modeling of nanosystems [120, 121].

5.4 Force Fields

The empirical potentials, called force fields, are used in classical MD to demonstrate interactions between atoms. These potentials consist of bonded and non-bonded forces. Bonded interactions [122] depend on the particular connections (bonds) of the structure and non-

bonded interactions depend only on the distance between the atoms. Bonded forces including chemical bonds, bond angles, and bond dihedrals, and non-bonded forces, i.e., van der Waals (vdW) forces, and electrostatic (El) charges, contain parameters such as equilibrium bond length, angle, dihedral atomic charge and vdW parameters which are obtained through a fitting process using quantum mechanical simulations or experiments. A general form for the total energy can be shown as the following relationship: [109, 123]:

$$E_T = E_{bd} + E_{nonbd}, \tag{5.2}$$

where

$$E_{bd} = E_{bs} + E_{ba} + E_{dihedral}, \tag{5.3}$$
$$E_{nonbd} = E_{El} + E_{vdW}.$$

In (5.2)-(5.3) E_T, E_{bd}, E_{nonbd}, E_{bs}, E_{ba}, $E_{dihedral}$, E_{El} and E_{vdW} represent total, bonded, non-bonded, bond stretch (length), bond angle, dihedral, electrostatic and van der Waals energies, respectively. In this study, we utilize the DREIDING generic force field to apply the bonded and non-bonded interactions between HIV virus atoms, and also the Tersoff empirical potential for silicon nanowires in order to perform our MD simulations. We discuss these potentials in the next two sections.

5.4.1 The DREIDING Force Field

In this thesis, we use the DREIDING force field for our MD simulations of tiny biological objects exemplified here by HIV viruses. Researchers have shown that this generic force field is suitable for predicting structures and dynamics of biological molecules [122]. Also, for complex and variable organic materials, which contains C, H, N, and O, implementation of the DREIDING force fields reduces computational burden and expedites the simulation

of larger systems in comparison with other force fields [124]. The DREIDING force field consists of four different terms, which play important roles for this potential: bond stretch, bond angle bend, dihedral angle torsion, and van der Waals non-bonded interactions [125]. The relationship used in this study to define the bond stretch is a harmonic function, which is given as [122, 126, 127]:

$$E_{bs}(r) = \frac{1}{2}K_{bs}(r - r_0)^2, \tag{5.4}$$

where K_{bs} and r_0 are stiffness constant for the bond stretch and equilibrium bond stretch, respectively. Harmonic function is utilized as the default function for DREIDING, since it results in drastically large restoring forces as r increases [122]. The functional form of three-body bond angle (two bonds which share the common atom) applied in this simulations, is also a harmonic function. It is given by the following relationship [122, 126, 127]:

$$E_{ba}(\theta) = \frac{1}{2}K_{ba}(\theta - \theta_0)^2, \tag{5.5}$$

where K_{ba} represents the stiffness constant for the bond angle potential and θ_0 is the equilibrium bond angle. Another functional form of bonded energy is related to the dihedral angle which is obtained as [122]:

$$E_{dh}(\phi) = \sum_{i=0}^{n} C_i(\cos\phi)^i, \tag{5.6}$$

where variables C_i correspond to the coefficients of dihedral multi-harmonics. In order to include the van der Waals non-bonded interactions in our simulations, we utilized the Lennard-Jones potential as follows [122, 126, 127]:

$$E_{LJ}(r_{ij}) = 4\varepsilon_{LJ}\left[\left(\frac{R_{LJ}}{r_{ij}}\right)^{12} - \left(\frac{R_{LJ}}{r_{ij}}\right)^{6}\right], \qquad r \leq r_c \tag{5.7}$$

where r_{ij}, R_{LJ}, ε_{LJ} and r_c indicate the distance between two atoms, distance at zero energy, energy well depth and cutoff distance, respectively. The values of all the parameters related to the DREIDING force field (Eqs. (5.4)-(5.7)), used in this study, are provided in Tables D.1-D.3 (see Appendix). The electrostatic non-bonded energy is also calculated using Coulomb's law as [109, 123]:

$$E_{El} = 332.0637 \frac{Q_i Q_j}{\lambda r_{ij}}, \tag{5.8}$$

where Q_i and Q_j represent charges in electron units.

5.4.2 The Tersoff Potential

In this study, we utilized the Tersoff empirical potential to demonstrate the structural and thermal behaviour of silicon nanowire by molecular dynamics simulations. We employed this many-body empirical potential, for silicon-silicon interactions, since it has been shown that using the Tersoff functions [128] can properly explain the structural properties of variety of materials, such as carbon and silicon [111, 129]. The Tersoff potential is suitable to be used for the lattice constant and binding energy of a number of silicon lattices [130]. Since the silicon crystal structure is diamond-like, the Tersoff potential fits its elastic constants and vacancy formation energies [110, 131]. In addition, because of the high ratio of surface area to volume of the nanowire resonator, the Tersoff potential seems to be more reasonable to describe the silicon NW, as it shows adequate surface reconstruction [131]. The values of the Tersoff potential parameters of Si-Si, used in this study, can be found in ref. [129].

5.5 Simulation Procedures

In our MD simulations, we employed LAMMPS which uses the velocity-Verlet algorithm [118] in order to simulate the silicon nanowire resonator and an HIV virus as a biological

added mass, adopting the DREIDING and Tersoff force fields for the interaction potentials. In the present work, timestep of 0.55 fs is employed to provide a proper conservation of temperatures (e.g. 50, 300, 425 and 600 $^{\circ}K$ [96]) using a NVT thermostat. After relaxing the system for 55 ps, we utilized the NVE thermostat to simulate the structure for 275 ps. The simulation time is chosen based on the high frequency of silicon nanowire resonator [109, 132]. 1112 atoms of silicon at both ends of the nanowire are fixed to simulate the clamped-clamped boundary conditions. The middle part of the silicon nanowire (which contains different numbers of silicon atoms depending on the size of SiNW) is allowed to vibrate under an applied force at the middle of SiNW at y direction (see Fig. 5.1). In order to investigate the frequency change of the nanoresonator after adding biological mass, we located the HIV virus in the middle of the nanowire (Fig. 5.17). The trajectories of an atom at the center of the silicon nanowire are recorded, and then the Fast Fourier Transform (FFT) method is employed to obtain the vibration frequencies of the nanoresonator. In the next section, the results gained by our MD simulations are provided.

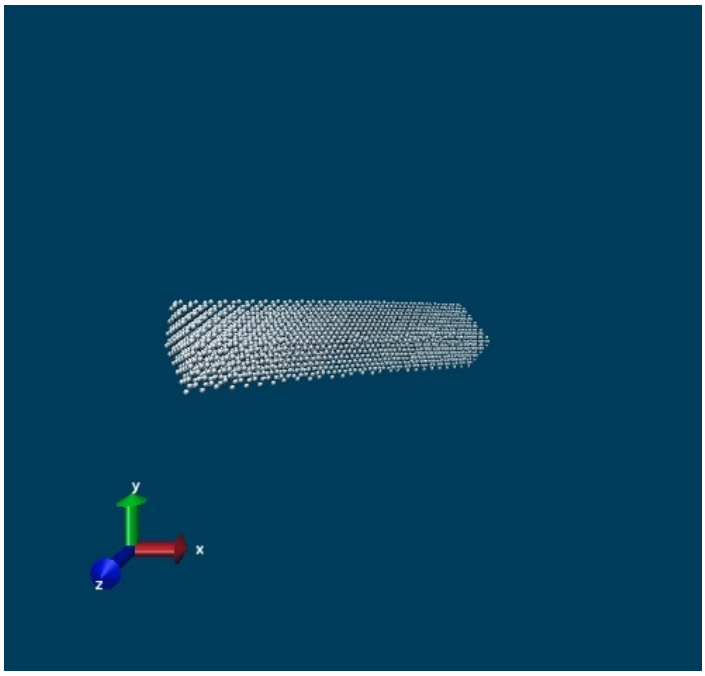

Fig. 5.1 SiNW with fixed boundary atoms (clamped-clamped) at $T = 300\ ^{\circ}K$

5.6 Results

In Chapters 3 and 4, we have investigated the effect of temperature variations on the vibration behavior of SiNW based on the continuum model developed in Chapter 2. In order to have a deeper insight into the impact of temperature change, and also to examine the limitations of our results based on the continuum model, (see Eq. (2.57)), we use MD simulations to probe the vibration behavior of SiNW resonator with respect to temperature alterations. Figures 5.2-5.5 show the effect of variations in temperature on the SiNW resonator's central atom displacement and its corresponding frequency [96]. In our MD simulations for temperature variations, we considered four different temperatures which includes a very low ($T = 50\ ^{\circ}K$) and a very high ($T = 600\ ^{\circ}K$) temperature [133, 134], to provide a wide range of temperature variations for examining the molecular dynamics behaviour of nanowire resonators. It should be noted that, in some biological object detection, the frequency shift measurement is restricted to a few conditions such as ultra-high vacuum and low temperature [135, 4]. Analyzing these figures illustrate that increasing temperature enhances the amplitude of oscillations of the central atom displacement of the SiNW resonator. Figure 5.6 provides a comparison between the central atom displacement of SiNW resonator for different temperatures. This figure confirms our qualitative analysis presented in section 3.4.3 in which we have shown that increasing temperature enhances the amplitude of oscillations of SiNW resonator. However, the observation of frequency change based on our perturbation (Figure 3.2) and numerical (Figure 4.2) analysis cannot be confirmed based on MD simulations. Our MD simulations show that the change in temperature practically does not affect the frequency response of SiNW resonator. The values of frequency for each of temperature cases are displayed in Figures 5.2 (b)-5.5 (b).

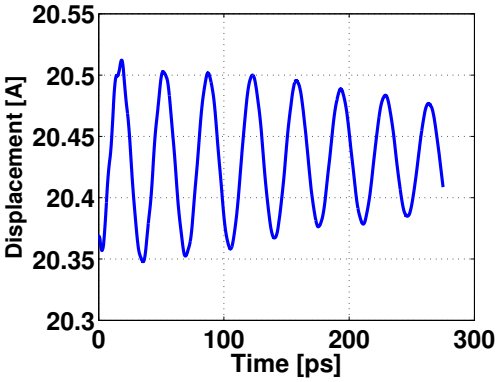

(a) Central atom displacement

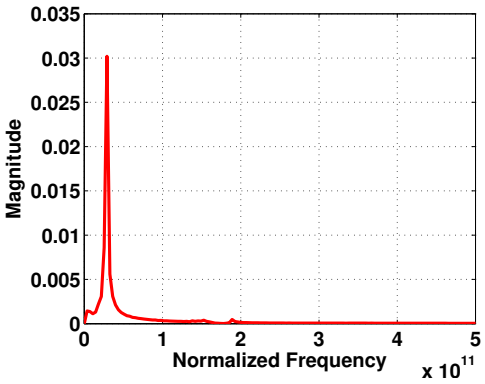

(b) FFT

Fig. 5.2 CC SiNW at $T = 50\ ^{\circ}K$

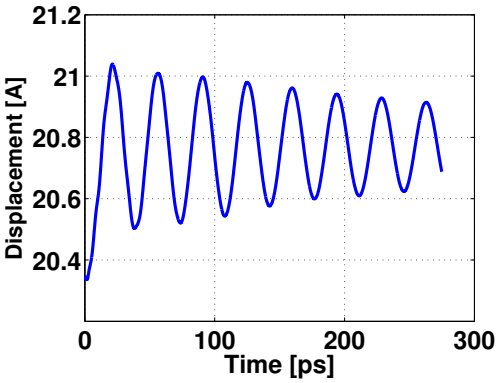

(a) Central atom displacement

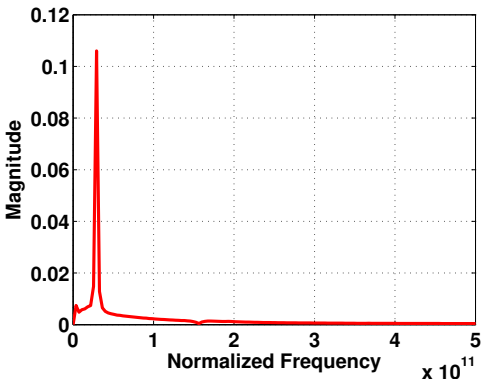

(b) FFT

Fig. 5.3 CC SiNW at $T = 300\ ^{\circ}K$

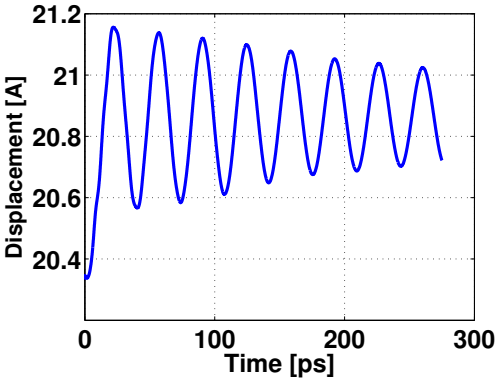

(a) Central atom displacement

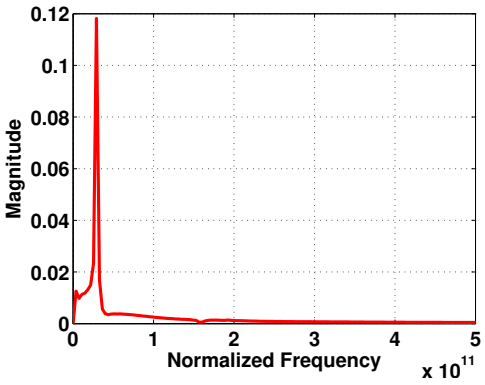

(b) FFT

Fig. 5.4 CC SiNW at $T = 425\ ^{\circ}K$

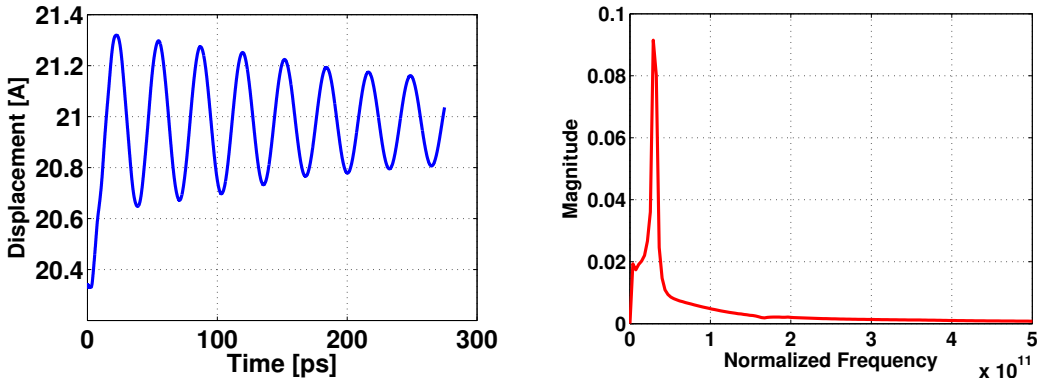

(a) Central atom displacement (b) FFT

Fig. 5.5 CC SiNW at $T = 600\ ^{\circ}K$

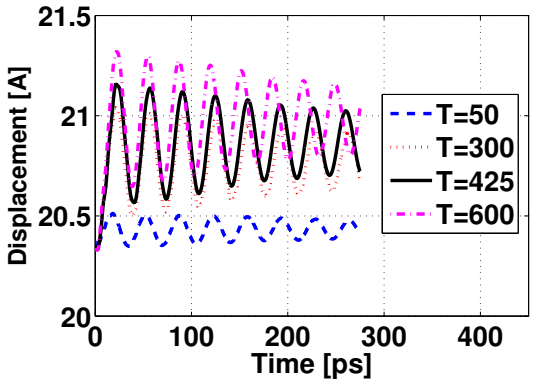

Fig. 5.6 Central atom displacements at four different temperatures

We have also studied the effect of different sizes of the rectangular cross sectional area for the SiNW [72] on its vibration behavior. This analysis gives a better insight into frequency response of SiNW resonators considering the size variations for the rectangular cross section. Figures 5.7-5.11 show the effect of variations in cross sectional area on the central atom displacement and the frequency behavior of SiNW with the length of 15 *nm*, at the temperature of 300 $^{\circ}K$. These figures show that increasing the area of cross section enhances the frequency of oscillations in the SiNW resonator. Fig. 5.11 highlights the effect of cross section on the frequency behavior of SiNW. This figure shows that changing the area of cross section of SiNW from 4 nm^2 to 16 nm^2 drastically increases its frequency.

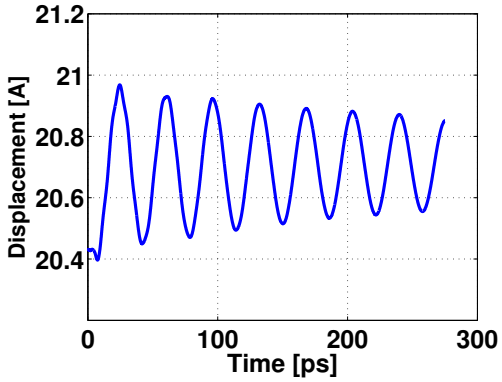

(a) Central atom displacement

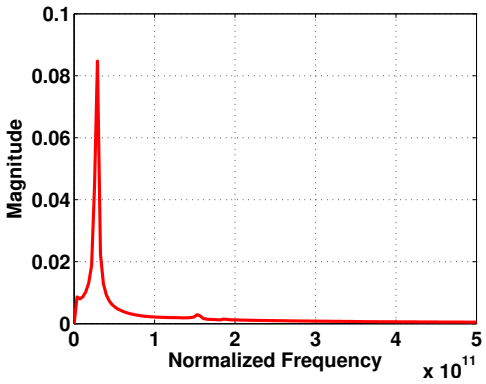

(b) FFT

Fig. 5.7 CC SiNW with length of 15 nm and cross sectional area of 4 nm^2 at $T = 300\ ^\circ K$

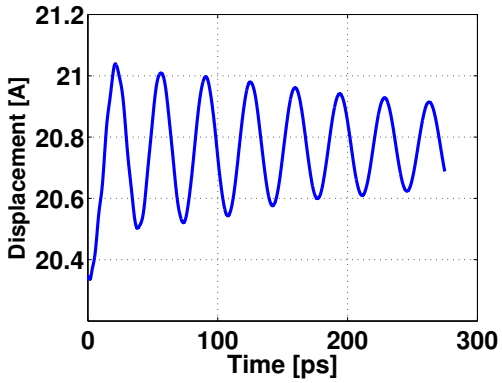

(a) Central atom displacement

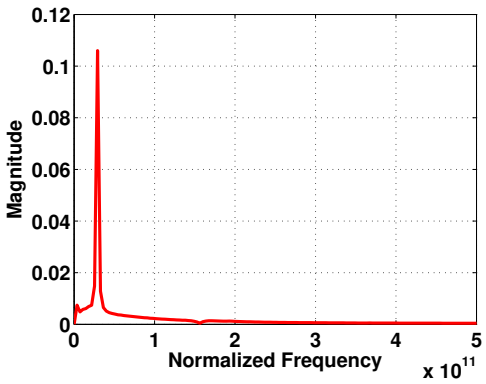

(b) FFT

Fig. 5.8 CC SiNW with length of 15 nm and cross sectional area of 6 nm^2 at $T = 300\ ^\circ K$

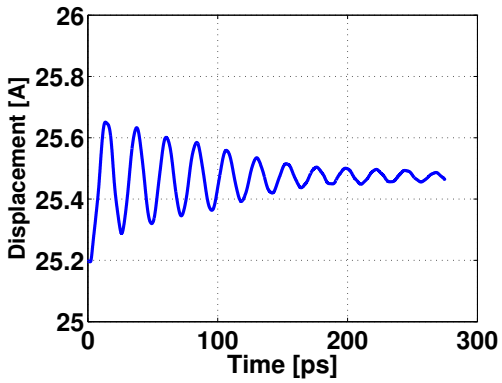

(a) Central atom displacement

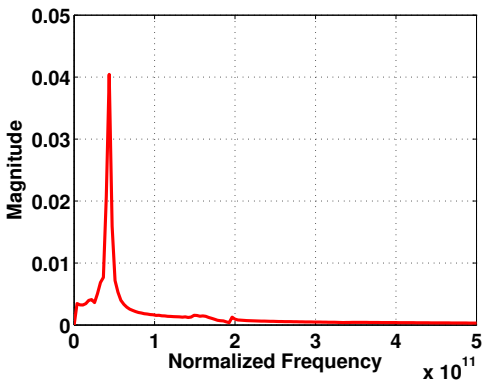

(b) FFT

Fig. 5.9 CC SiNW with length of 15 nm and cross sectional area of 12 nm^2 at $T = 300\ ^\circ K$

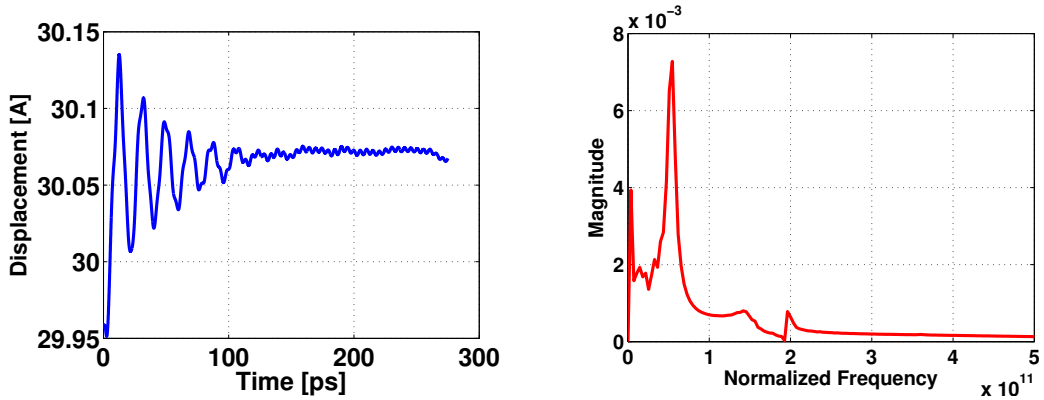

(a) Central atom displacement (b) FFT

Fig. 5.10 CC SiNW with length of 15 nm and cross sectional area of 16 nm^2 at $T = 300\ ^\circ K$

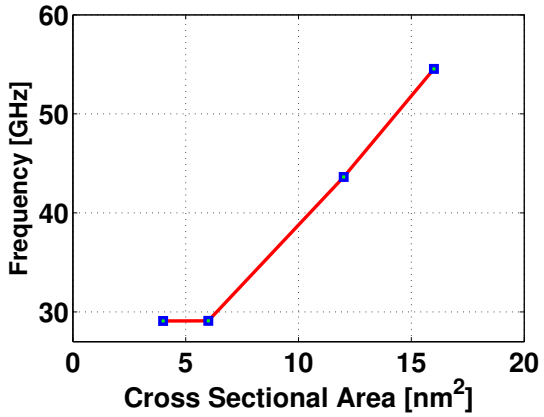

Fig. 5.11 Frequency of CC SiNW with different sizes of cross sectional area at $T = 300\ ^\circ K$

In order to study the effect of variations in length of the SiNW, we simulate the SiNW for four different lengths [72] considering the same cross section of $6nm^2$ and the temperature of $300^\circ K$. Figures 5.12-5.15 depict the effect of SiNW's length on its central atom displacement and frequency of vibrations. As Figures 5.12 (b)-5.15 (b) demonstrates, increasing the length of SiNW decreases its frequency of oscillations. Figure 5.16 is plotted to provide a better insight into the change of SiNW resonator frequency with respect to its length variations. As the figure illustrates, increasing the length of SiNW from 8 nm to 15 nm decreases its frequency from 94 GHz to 29 GHz.

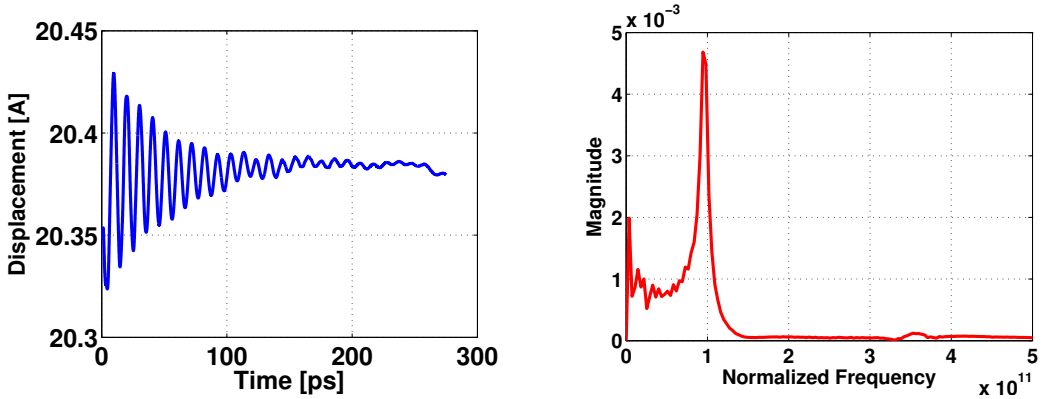

(a) Central atom displacement (b) FFT

Fig. 5.12 CC SiNW with length of 8 nm and cross sectional area of 6 nm^2 at $T = 300\ ^\circ K$

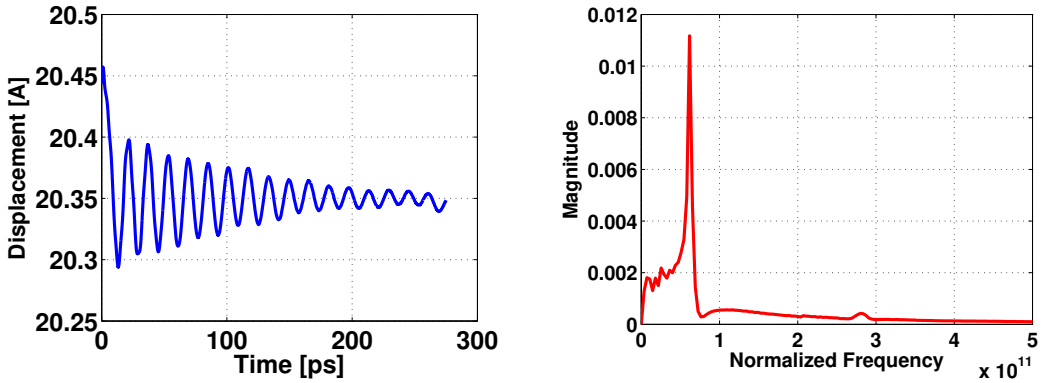

(a) Central atom displacement (b) FFT

Fig. 5.13 CC SiNW with length of 10 nm and cross sectional area of 6 nm^2 at $T = 300\ ^\circ K$

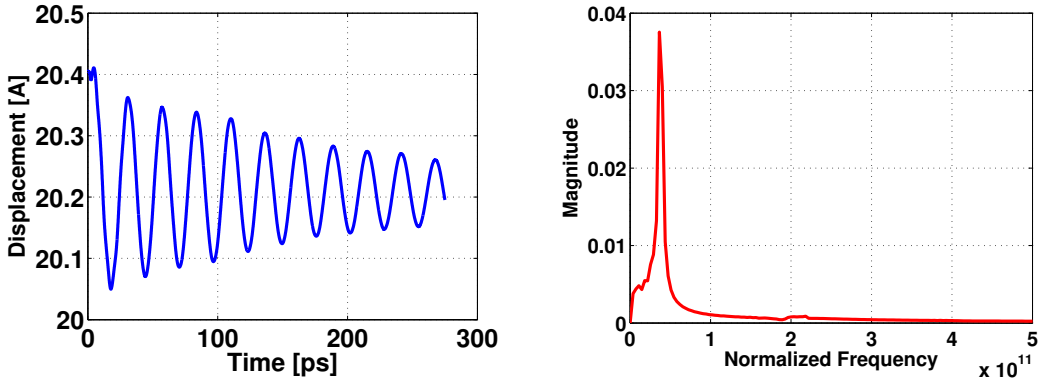

(a) Central atom displacement (b) FFT

Fig. 5.14 CC SiNW with length of 13 nm and cross sectional area of 6 nm^2 at $T = 300\ ^\circ K$

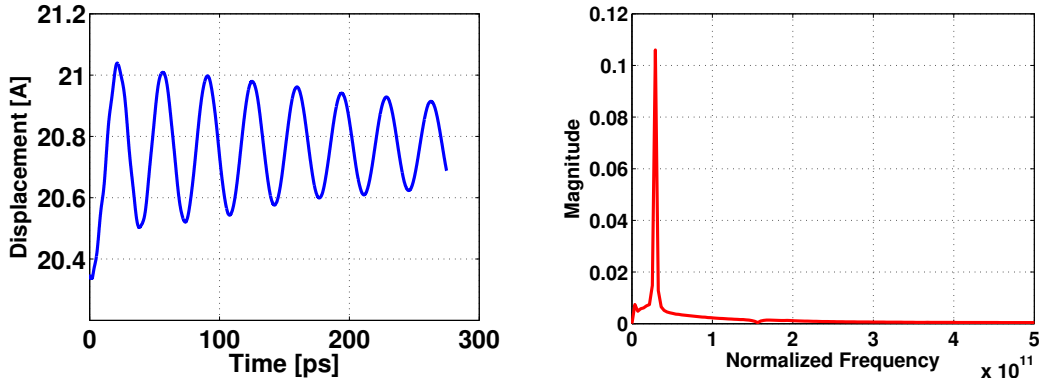

(a) Central atom displacement (b) FFT

Fig. 5.15 CC SiNW with length of 15 nm and cross sectional area of 6 nm^2 at $T = 300\ ^\circ K$

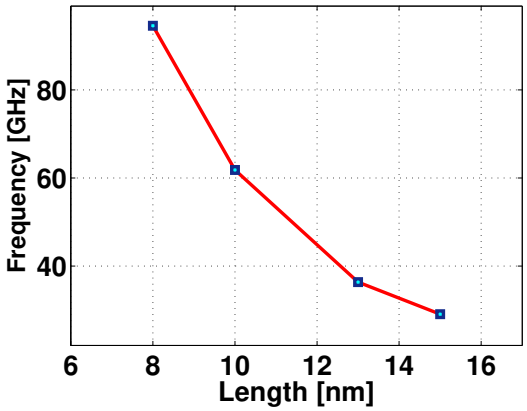

Fig. 5.16 Frequency of CC SiNW with different lengths at $T = 300\ ^\circ K$

In order to investigate the potential of SiNW for detection of biological objects, we use MD simulations to analyze the frequency response of nanowire resonator after adding an HIV virus. This methodology is much more computationally time consuming, compared the methodologies based on continuum models, we developed in the previous chapters. We locate an HIV virus in the middle of a SiNW resonator as shown in Figure 5.17. The mass of our considered HIV virus approximately equals to $4.42 \times 10^{-21} g$. The selected nanoresonator for this simulation has the cross sectional area of $12 nm^2$ and length of $15 nm$. We first examine the silicon nanowire resonator without an added HIV molecule and obtain its frequency, as presented in Figure 5.9. For this case, the value of the obtained frequency using

MD simulations is 43.63 GHz. After adding the molecule of HIV virus, using the higher amplitude peak as a reference [136], it is concluded that the frequency of SiNW resonator decreases to 21.81GHz, as presented in Figure 5.18.

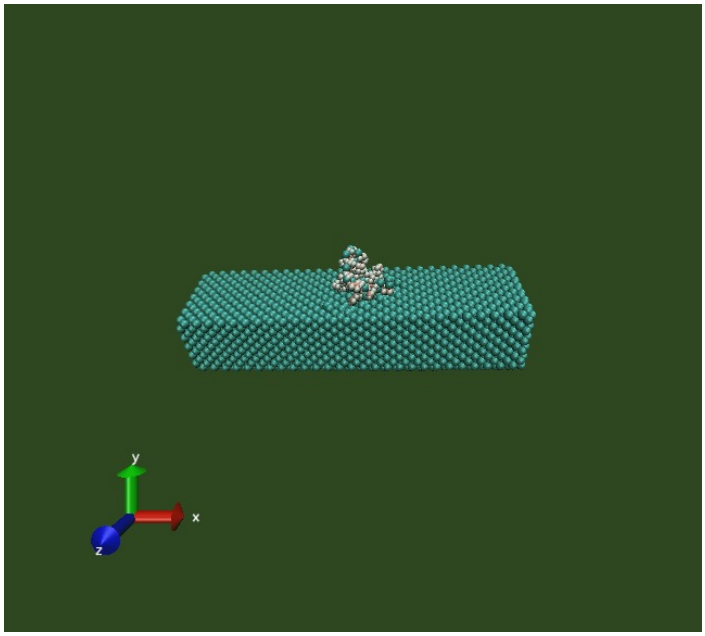

Fig. 5.17 CC SiNW with cross sectional area of 12 nm^2 and attached mass (HIV virus) at $T = 300\ ^\circ K$

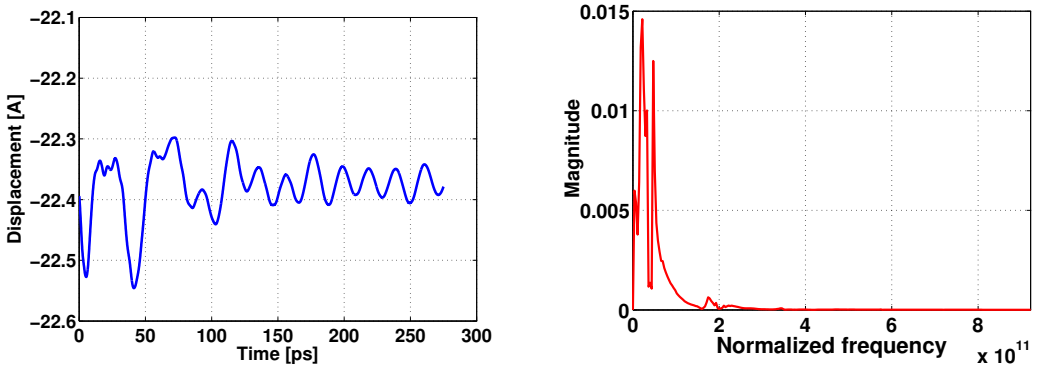

(a) Central atom displacement (b) FFT

Fig. 5.18 CC SiNW with cross sectional area of 12 nm^2 and attached mass (HIV virus) at $T = 300\ ^\circ K$

This in line with our postulation regarding the shift of frequency after adding a tiny mass to our nanoresonator, similar to what we discussed in sections 3.4.2 and 4.4. However, our continuum model predicts less variation in frequency of nanowire resonator after adding the small particle in comparison with MD simulations. Based on the observed frequency shift from MD simulations, we conclude that the silicon nanowire resonator is capable of detecting tiny bio-objects in the scale of zeptogram.

Chapter 6

Conclusions and Future Work

In this thesis, the potential of the nanowire resonator for detection of tiny masses with focus on biological objects was investigated. We first presented a mathematical model for the vibrations of nanowire resonators taking into account critical parameters. With the implementation of the Euler-Bernoulli beam theory in conjunction with the Eringen nonlocal theory, a nonlinear model was developed to study the vibrations of nanowire resonators, considering surface and thermal effects, as well as the effects of electromagnetic field, piezoelectric potential, external load, nonlinear foundation, added mass and large oscillations. The obtained governing equation for the vibrations of nanowire resonators was solved by both analytical and numerical techniques. In order to obtain an analytical solution for the vibrations of nanowires, the method of multiple scales was used to find primary and super-harmonic resonances of the device. Based on the obtained information, we then investigated the frequency shift due to the tiny added mass to a SiNW resonator. In addition, using the developed primary and super-harmonic resonance cases, the effect of different key parameters, such as thermal variations, electromagnetic fields, and the piezoelectric potential, on the vibration behavior of SiNW was studied. The main concluding remarks based on the presented perturbation analysis are as follows:

- It is shown that the SiNW resonator is capable of detecting tiny masses even in the order of zeptogram. As the mass of added particle increases, the frequency of SiNW resonator reduces.

- Increasing temperature and piezoelectric voltage reduces the frequency of SiNW resonator. It means that when the SiNW resonator is used for tiny mass sensing applications, temperature and piezoelectric potential should be monitored.

- It is observed that increasing electromagnetic field enhances the stiffness and also frequency of SiNW resonators. This is also another important factor that should be taken into account for designing nanowire resonators in sensing applications.

In order to have more refined results regarding the frequency analysis of SiNW resonators, we used the Finite Difference Method. Obtained numerical results confirmed the qualitative outcomes of perturbation analysis regarding the frequency behavior of SiNW resonators with respect to different parameters and the added tiny mass.

Moreover, we have used MD simulations to consider interatomic interactions of SiNW in the targeted nanosystem. Using MD simulations enables investigating not only the frequency behavior of nanowire resonators under different cases, but also providing a set of results to explore potency of nonlocal Euler-Bernoulli beam theory for the prediction of dynamic behavior of SiNW resonators. To show the application of SiNW resonators in detecting of tiny masses such as biological objects, we have modelled the SiNW resonator with a molecule of HIV located in the middle, considering clamped-clamped boundary conditions. The following are the main highlights of the MD simulations:

- It is shown that increasing temperature increases the amplitude of oscillations of SiNW resonators. A similar conclusion we have obtained by using the analytical technique. However, interestingly, when it comes to the analysis of thermal variations, the MD simulations do not confirm the results obtained by both numerical and

analytical approaches where the frequency of SiNW resonator reduces with thermal variations. Based on MD simulations, the variations of temperature has no effect on the frequency of SiNW oscillations, and its effect can only be seen in SiNW resonator amplitudes of oscillations.

- The effects of SiNW cross section and length on the nanowire frequency response were also studied by MD simulations. It is observed that the frequency of SiNW resonator drastically increases by enhancing the area of nanowire cross section. On the other hand, an increase in the length of SiNW reduces its frequency of oscillations.

- Our results show that adding an HIV virus to the SiNW resonator reduces its frequency of oscillations. This result confirms our postulation regarding the shift of frequency after adding a tiny particle to the nanowire resonator. In addition, it shows a similar trend predicted by the continuum theory. However, the obtained frequency shift using MD simulations is higher than the predicted value by analytical and numerical simulations. The main reason of this difference is attributed to the deficiency of continuum methods in modelling atomic interactions of nanowire resonators.

As future directions of the presented work, we note the following. The continuum model described in this thesis can be extended using other beam theories. In addition, the flexoelectric effect can be combined with the developed model to analyze the effect of flexoelectricty on the vibration of nanowire resonators. MD simulations can be applied to analyze the sensitivity of SiNW resonators for detection of other types of bio-particles. The effect of electromagnetic field can also be considered as another avenue of research for the vibration analysis of SiNW by using MD simulations. Moreover, other types of force fields for simulating the HIV molecule and other biological object can be utilized. Finally, an exciting future work can be based on experimental results and analysis of SiNW resonators for biological object detection.

Appendix A

Physical Units

Table A.1 Non-SI units and their conversion

Symbol	Unit	SI Unit Conversion
g	gram	10^{-3} kg
fg	femtogram	10^{-18} kg
ag	attogram	10^{-21} kg
zg	zeptogram	10^{-24} kg
yg	yoctogram	10^{-27} kg
nm	nanometer	10^{-9} m
Å	angstrom	10^{-10} m
pm	picometer	10^{-12} m
Hz	Hertz	s^{-1}
GHz	gigahertz	10^{9} s^{-1}
THz	terahertz	10^{12} s^{-1}
ps	picosecond	10^{-12} s
fs	femtosecond	10^{-15} s
nM	nanomoles	10^{-9} mol
kcal	kilocalorie	4184 $kg.m^{2}.s^{-2}$
GPa	giga-Pascal	10^{9} $kg.m^{-1}.s^{-2}$

Appendix B

Material Parameters

Following are the values of the material properties of a silicon nanowire used in the presented thesis (based on ref. [86]):

Table B.1 Material and piezoelectric properties of silicon nanowire

Parameter	**Value**
E	210 GPa
ρ	2700 kgm^{-3}
E^s	10.6543 $N.m^{-1}$
τ_0	0.6048 $N.m^{-1}$
ρ_0	3.17×10^{-7} kgm^{-3}
e_{31}	-10 $C.m^{-2}$
λ_{33}	1.0275×10^{-8} $F.m^{-1}$

Appendix C

Derivation of the Piezoelectric Potential

Substituting Eq. (2.48) into Eq. (2.50) yields the following partial differential equation:

$$\frac{\partial(e_{31}\varepsilon_{xx})}{\partial z}+\lambda_{33}\frac{\partial E_z}{\partial z}=0. \tag{C.1}$$

Using Eq. (2.47) we will have:

$$e_{31}\frac{\partial \varepsilon_{xx}}{\partial z}-\lambda_{33}\frac{\partial^2\psi}{\partial z^2}=0. \tag{C.2}$$

Implementing Eq. (2.2) to Eq. (C.2) results in a relationship as below:

$$e_{31}\Big[\frac{\partial}{\partial z}\Big(\frac{\partial u}{\partial x}-z\frac{\partial^2 w}{\partial x^2}+\frac{1}{2}(\frac{\partial w}{\partial x})^2\Big)\Big]-\lambda_{33}\frac{\partial^2\psi}{\partial z^2}=0. \tag{C.3}$$

In Eq. (C.3), the $\frac{\partial u}{\partial x}$ and $\frac{1}{2}(\frac{\partial w}{\partial x})^2$ terms will be omitted. Therefore, this equation (Eq. (C.3)) can be rearranged as the following form:

$$\frac{\partial^2\psi}{\partial z^2}=-\frac{e_{31}}{\lambda_{33}}\frac{\partial^2 w}{\partial x^2}. \tag{C.4}$$

In order to solve the above-mentioned partial differential equation, we take the integral from both sides of it, which results in the following:

$$\psi(x,z) - \frac{e_{31}}{2\lambda_{33}} z^2 \frac{\partial^2 w}{\partial x^2} + C_1 z + C_2, \tag{C.5}$$

where C_1 and C_2 are the constants of integration. For the purpose of obtaining C_1 and C_2, we apply the boundary conditions as provided in Eq. (2.51). Thus, we will have the following form of equations:

$$-\frac{e_{31}}{2\lambda_{33}} \frac{\partial^2 w}{\partial x^2} (-h)^2 + C_1(-h) + C_2 = 0, \tag{C.6}$$

and

$$-\frac{e_{31}}{2\lambda_{33}} \frac{\partial^2 w}{\partial x^2} (h)^2 + C_1(h) + C_2 = 2V_e. \tag{C.7}$$

Based on Eq. (C.6) we have:

$$C_2 = \frac{e_{31}}{2\lambda_{33}} \frac{\partial^2 w}{\partial x^2} h^2 + C_1 h. \tag{C.8}$$

By substituting Eq. (C.8) into Eq. (C.7) we obtain the following relationship for C_1:

$$C_1 = \frac{V_e}{h}. \tag{C.9}$$

Now, we plug C_1 and C_2, obtained in Eq. (C.8) and Eq. (C.9), in Eq. (C.5) which results in a relationship for the piezoelectric potential as follows:

$$\psi(x,z) = -\frac{e_{31}}{\lambda_{33}} \left(\frac{z^2 - h^2}{2} \right) \frac{\partial^2 w}{\partial x^2} + \left(1 + \frac{z}{h} \right) v. \tag{C.10}$$

Appendix D

Potential Parameters

The functional forms of force field represented in Eqs. (5.4-5.7) are used for HIV MD calculations in the presented study. The considered HIV virus consists of 405 atoms. This includes four different types of atoms such as: Carbon (C), Hydrogen (H), Nitrogen (N) and Oxygen (O). The potential parameters for these specific atoms in our MD simulations are provided in the following tables which are obtained by DREIDING force field [122]:

Table D.1 Potential parameters used for bond stretch interactions

Bond stretch interaction	Parameters
C : C	$K_{bs} = 350.0\ kcal/mol,\ r_0 = 1.53$ Å
C : H	$K_{bs} = 350.0\ kcal/mol,\ r_0 = 1.09$ Å
N : C	$K_{bs} = 350.0\ kcal/mol,\ r_0 = 1.462$ Å
N : H	$K_{bs} = 350.0\ kcal/mol,\ r_0 = 1.022$ Å
O : C	$K_{bs} = 350.0\ kcal/mol,\ r_0 = 1.42$ Å
O : H	$K_{bs} = 350.0\ kcal/mol,\ r_0 = 0.98$ Å

Table D.2 Potential parameters used for bond angle interactions

Bond angle interaction	Parameters
C : C : C	$K_{ba} = 50.0\ (kcal/mol)/rad^2,\ \theta_0 = 109.471^\circ$
C : C : H	$K_{ba} = 50.0\ (kcal/mol)/rad^2,\ \theta_0 = 109.471^\circ$
C : N : C	$K_{ba} = 50.0\ (kcal/mol)/rad^2,\ \theta_0 = 106.7^\circ$
C : N : H	$K_{ba} = 50.0\ (kcal/mol)/rad^2,\ \theta_0 = 106.7^\circ$
C : O : H	$K_{ba} = 50.0\ (kcal/mol)/rad^2,\ \theta_0 = 104.51^\circ$
H : C : H	$K_{ba} = 50.0\ (kcal/mol)/rad^2,\ \theta_0 = 109.471^\circ$
H : N : H	$K_{ba} = 50.0\ (kcal/mol)/rad^2,\ \theta_0 = 106.70^\circ$
N : C : C	$K_{ba} = 50.0\ (kcal/mol)/rad^2,\ \theta_0 = 109.471^\circ$
N : C : H	$K_{ba} = 50.0\ (kcal/mol)/rad^2,\ \theta_0 = 109.471^\circ$
N : C : N	$K_{ba} = 50.0\ (kcal/mol)/rad^2,\ \theta_0 = 109.471^\circ$
O : C : C	$K_{ba} = 50.0\ (kcal/mol)/rad^2,\ \theta_0 = 109.471^\circ$
O : C : H	$K_{ba} = 50.0\ (kcal/mol)/rad^2,\ \theta_0 = 109.471^\circ$
O : C : N	$K_{ba} = 50.0\ (kcal/mol)/rad^2,\ \theta_0 = 109.471^\circ$
O : C : O	$K_{ba} = 50.0\ (kcal/mol)/rad^2,\ \theta_0 = 109.471^\circ$

Table D.3 Potential parameters used for the Lennard-Jones potential

Non-bonded interaction	Parameters
C : C	$\varepsilon_{LJ} = 0.077\ kcal/mol,\ \sigma_{LJ} = 4.18$ Å
H : H	$\varepsilon_{LJ} = 0.0025\ kcal/mol,\ \sigma_{LJ} = 3.2$ Å
N : N	$\varepsilon_{LJ} = 0.104\ kcal/mol,\ \sigma_{LJ} = 3.995$ Å
O : O	$\varepsilon_{LJ} = 0.104\ kcal/mol,\ \sigma_{LJ} = 3.71$ Å
C : H	$\varepsilon_{LJ} = 0.014\ kcal/mol,\ \sigma_{LJ} = 3.65$ Å
C : N	$\varepsilon_{LJ} = 0.089\ kcal/mol,\ \sigma_{LJ} = 4.08$ Å
C : O	$\varepsilon_{LJ} = 0.089\ kcal/mol,\ \sigma_{LJ} = 3.93$ Å
C : Si	$\varepsilon_{LJ} = 0.043\ kcal/mol,\ \sigma_{LJ} = 4.30$ Å
H : N	$\varepsilon_{LJ} = 0.016\ kcal/mol,\ \sigma_{LJ} = 3.57$ Å
H : O	$\varepsilon_{LJ} = 0.016\ kcal/mol,\ \sigma_{LJ} = 3.44$ Å
H : Si	$\varepsilon_{LJ} = 0.008\ kcal/mol,\ \sigma_{LJ} = 3.76$ Å
N : O	$\varepsilon_{LJ} = 0.104\ kcal/mol,\ \sigma_{LJ} = 3.84$ Å
N : Si	$\varepsilon_{LJ} = 0.05\ kcal/mol,\ \sigma_{LJ} = 4.2$ Å
O : Si	$\varepsilon_{LJ} = 0.05\ kcal/mol,\ \sigma_{LJ} = 4.05$ Å

Appendix E

Linear Frequency of the NW without Added Mass

The linear frequency of the nanowire resonator without added mass, ω_0, can be obtained by using the following relationship:

$$\omega_0 = \sqrt{\frac{\alpha_2}{\alpha'}}, \tag{E.1}$$

where α_2 can be found by Eq. (3.5), and α' is as follows:

$$\alpha' = \Pi(\int_0^1 \phi^2(\xi)d\xi - \Upsilon \int_0^1 \phi''(\xi)\phi(\xi)d\xi). \tag{E.2}$$

References

[1] H Cho, MF Yu, AF Vakakis, LA Bergman, and DM McFarland. Tunable, broadband nonlinear nanomechanical resonator. *Nano Letters*, 10(5):1793–1798, 2010.

[2] E Asadi, H Askari, MB Khamesee, and A Khajepour. High frequency nano electromagnetic self-powered sensor: Concept, modelling and analysis. *Measurement*, 107:31–40, 2017.

[3] XL Feng, R He, P Yang, and ML Roukes. Very high frequency silicon nanowire electromechanical resonators. *Nano Letters*, 7(7):1953–1959, 2007.

[4] K Eom, DS Park, HS Yoon, and T Kwon. Nanomechanical resonators and their applications in biological/chemical detection: nanomechanics principles. *Physics Reports*, 503(4-5):115–163, 2011.

[5] D Ramos, M Arroyo-Hernandez, E Gil-Santos, HD Tong, C Van Rijn, M Calleja, and J Tamayo. Arrays of dual nanomechanical resonators for selective biological detection. *Analytical Chemistry*, 81(6):2274–2279, 2009.

[6] M Dilena, M Fedele Dell'Oste, J Fernández-Sáez, A Morassi, and R Zaera. Mass detection in nanobeams from bending resonant frequency shifts. *Mechanical Systems and Signal Processing*, 116:261–276, 2019.

[7] M A Roudbari and R Ansari. Single-walled boron nitride nanotube as nano-sensor. *Continuum Mechanics and Thermodynamics*, pages 1–20, 2018.

[8] HR Ali-Akbari, S Ceballes, and A Abdelkefi. Nonlinear performance analysis of forced carbon nanotube-based bio-mass sensors. *International Journal of Mechanics and Materials in Design*, pages 1–25, 2018.

[9] H Farokhi, M P Païdoussis, and A K Misra. Nonlinear behaviour and mass detection sensitivity of geometrically imperfect cantilevered carbon nanotube resonators. *Communications in Nonlinear Science and Numerical Simulation*, 65:272–298, 2018.

[10] Q Wan, QH Li, YJ Chen, TH Wang, XL He, JP Li, and CL Lin. Fabrication and ethanol sensing characteristics of zno nanowire gas sensors. *Applied Physics Letters*, 84(18):3654–3656, 2004.

[11] A Norouzzadeh, R Ansari, and H Rouhi. Nonlinear wave propagation analysis in Timoshenko nano-beams considering nonlocal and strain gradient effects. *Meccanica*, 53(13):3415–3435, 2018.

[12] R Barretta, R Luciano, F M de Sciarra, and G Ruta. Stress-driven nonlocal integral model for timoshenko elastic nano-beams. *European Journal of Mechanics-A/Solids*, 72:275–286, 2018.

[13] A Farajpour, H Farokhi, M H Ghayesh, and S Hussain. Nonlinear mechanics of nanotubes conveying fluid. *International Journal of Engineering Science*, 133:132–143, 2018.

[14] H Jamshidifar, H Askari, and B Fidan. Parameter identification and adaptive control of carbon nanotube resonators. *Asian Journal of Control*, 20(4):1329–1338, 2018.

[15] MA Eltaher, AE Alshorbagy, and FF Mahmoud. Vibration analysis of Euler-Bernoulli nanobeams by using finite element method. *Applied Mathematical Modelling*, 37(7):4787–4797, 2013.

[16] H Roostai and M Haghpanahi. Vibration of nanobeams of different boundary conditions with multiple cracks based on nonlocal elasticity theory. *Applied Mathematical Modelling*, 38(3):1159–1169, 2014.

[17] J Zhou, Z Wang, A Grots, and X He. Electric field drives the nonlinear resonance of a piezoelectric nanowire. *Solid State Communications*, 144(3-4):118–123, 2007.

[18] GY Su, YX Li, XY Li, and R Müller. Free and forced vibrations of nanowires on elastic substrates. *International Journal of Mechanical Sciences*, 138-139:62 – 73, 2018.

[19] GF Wang and XQ Feng. Effect of surface stresses on the vibration and buckling of piezoelectric nanowires. *EPL (Europhysics Letters)*, 91(5):56007, 2010.

[20] J He and CM Lilley. Surface stress effect on bending resonance of nanowires with different boundary conditions. *Applied Physics Letters*, 93(26):263108, 2008.

[21] J Fritz, MK Baller, HP Lang, H Rothuizen, P Vettiger, E Meyer, HJ Güntherodt, C Gerber, and JK Gimzewski. Translating biomolecular recognition into nanomechanics. *Science*, 288(5464):316–318, 2000.

[22] W Pang, L Yan, H Zhang, H Yu, ES Kim, and WC Tang. Femtogram mass sensing platform based on lateral extensional mode piezoelectric resonator. *Applied Physics Letters*, 88(24):243503, 2006.

[23] H Askari, H Jamshidifar, and B Fidan. High resolution mass identification using nonlinear vibrations of nanoplates. *Measurement*, 101:166 – 174, 2017.

[24] K Kiani and B Ghaffari, H Mehri. Application of elastically supported single-walled carbon nanotubes for sensing arbitrarily attached nano-objects. *Current Applied Physics*, 13(1):107–120, 2013.

[25] DE Segall, S Ismail-Beigi, and TA Arias. Elasticity of nanometer-sized objects. *Physical Review B*, 65(21):214109, 2002.

[26] H Üstünel, D Roundy, and TA Arias. Modeling a suspended nanotube oscillator. *Nano Letters*, 5(3):523–526, 2005.

[27] P Vincent, S Perisanu, A Ayari, M Choueib, V Gouttenoire, M Bechelany, A Brioude, D Cornu, and ST Purcell. Driving self-sustained vibrations of nanowires with a constant electron beam. *Physical Review B*, 76(8):085435, 2007.

[28] K Kiani. Free longitudinal vibration of tapered nanowires in the context of nonlocal continuum theory via a perturbation technique. *Physica E: Low-Dimensional Systems and Nanostructures*, 43(1):387–397, 2010.

[29] SM Hasheminejad and B Gheshlaghi. Dissipative surface stress effects on free vibrations of nanowires. *Applied Physics Letters*, 97(25):253103, 2010.

[30] YM Fu, HQ Zhou, and P Zhang. Nonlinear free vibration of nanowires including size effects. *Micro & Nano Letters*, 7(4):348–352, 2012.

[31] H Askari, E Esmailzadeh, and D Zhang. Nonlinear vibration analysis of nonlocal nanowires. *Composites Part B: Engineering*, 67:607–613, 2014.

[32] H Askari, D Zhang, and E Esmailzadeh. Periodic solutions for nonlinear oscillations of nanowires using variational iteration method. In *Nanotechnology (IEEE-NANO), 2013 13th IEEE Conference on*, pages 566–569. IEEE, 2013.

[33] Q He and CM Lilley. The vibration model and quality factor analysis of Timoshenko nanowires with surface stress. In *Nanotechnology (IEEE-NANO), 2012 12th IEEE Conference on*, pages 1–6. IEEE, 2012.

[34] AT Samaei, B Gheshlaghi, and GF Wang. Frequency analysis of piezoelectric nanowires with surface effects. *Current Applied Physics*, 13(9):2098–2102, 2013.

[35] K Kiani. Forced vibrations of a current-carrying nanowire in a longitudinal magnetic field accounting for both surface energy and size effects. *Physica E: Low-dimensional Systems and Nanostructures*, 63:27–35, 2014.

[36] K Kiani. Vibrations and instability of double-nanowire-systems as electric current carriers. *Modern Physics Letters B*, 29(25):1550144, 2015.

[37] K Kiani. Stability and vibrations of doubly parallel current-carrying nanowires immersed in a longitudinal magnetic field. *Physics Letters A*, 379(4):348 – 360, 2015.

[38] K Kiani. Vibrations and instability of pretensioned current-carrying nanowires acted upon by a suddenly applied three-dimensional magnetic field. *Materials Chemistry and Physics*, 162:531 – 541, 2015.

[39] JX Wu, XF Li, AY Tang, and KY Lee. Free and forced transverse vibration of nanowires with surface effects. *Journal of Vibration and Control*, 23(13):2064–2077, 2017.

[40] YQ Zhang, M Pang, and WQ Chen. Transverse vibrations of embedded nanowires under axial compression with high-order surface stress effects. *Physica E: Low-dimensional Systems and Nanostructures*, 66:238 – 244, 2015.

[41] L Jin and L Li. Nonlinear dynamics of silicon nanowire resonator considering nonlocal effect. *Nanoscale Research Letters*, 12(1):331, 2017.

[42] HM Sedighi and A Bozorgmehri. Nonlinear vibration and adhesion instability of casimir-induced nonlocal nanowires with the consideration of surface energy. *Journal of the Brazilian Society of Mechanical Sciences and Engineering*, 39(2):427–442, 2017.

[43] YT Yang, C Callegari, XL Feng, KL Ekinci, and ML Roukes. Zeptogram-scale nanomechanical mass sensing. *Nano Letters*, 6(4):583–586, 2006.

[44] AY Joshi, SC Sharma, and SP Harsha. Zeptogram scale mass sensing using single walled carbon nanotube based biosensors. *Sensors and Actuators A: Physical*, 168(2):275 – 280, 2011.

[45] S. Adhikari and R. Chowdhury. Zeptogram sensing from gigahertz vibration: graphene based nanosensor. *Physica E: Low-dimensional Systems and Nanostructures*, 44(7):1528 – 1534, 2012.

[46] F Patolsky, G Zheng, and CM Lieber. Nanowire sensors for medicine and the life sciences. *Nanomedicine*, 1(1):51–65, 2006.

[47] G Abadal, Z J Davis, B Helbo, X Borrisé, R Ruiz, A Boisen, F Campabadal, J Esteve, E Figueras, F Pérez-Murano, and N Barniol. Electromechanical model of a resonating nano-cantilever-based sensor for high-resolution and high-sensitivity mass detection. *Nanotechnology*, 12(2):100, 2001.

[48] M Su, S Li, and VP Dravid. Microcantilever resonance-based dna detection with nanoparticle probes. *Applied Physics Letters*, 82(20):3562–3564, 2003.

[49] A Volodin, D Buntinx, M Ahlskog, A Fonseca, JB. Nagy, and C Van Haesendonck. Coiled carbon nanotubes as self-sensing mechanical resonators. *Nano Letters*, 4(9):1775–1779, 2004.

[50] H Sone, A Ikeuchi, T Izumi, H Okano, and S Hosaka. Femtogram mass biosensor using self-sensing cantilever for allergy check. *Japanese Journal of Applied Physics*, 45(3S):2301, 2006.

[51] RA Barton, B Ilic, SS Verbridge, BR Cipriany, JM Parpia, and HG Craighead. Fabrication of a nanomechanical mass sensor containing a nanofluidic channel. *Nano Letters*, 10(6):2058–2063, 2010.

[52] D K Kang, H I Yang, and C W Kim. Geometrically nonlinear dynamic behavior on detection sensitivity of carbon nanotube-based mass sensor using finite element method. *Finite Elements in Analysis and Design*, 126:39–49, 2017.

[53] HY Chiu, P Hung, HWC Postma, and M Bockrath. Atomic-scale mass sensing using carbon nanotube resonators. *Nano Letters*, 8(12):4342–4346, 2008.

[54] O K Kwon, K S Kim, J Park, and J W Kang. Molecular dynamics modeling and simulations of graphene-nanoribbon-resonator-based nanobalance as yoctogram resolution detector. *Computational Materials Science*, 67:329–333, 2013.

[55] K Duan, L Li, Y Hu, and X Wang. Pillared graphene as an ultra-high sensitivity mass sensor. *Scientific reports*, 7(1):14012, 2017.

[56] K Duan, Y Li, L Li, Y Hu, and X Wang. Diamond nanothread based resonators: ultra-high sensitivity and low dissipation. *Nanoscale*, 10(17):8058–8065, 2018.

[57] HS Wasisto, S Merzsch, A Stranz, A Waag, E Uhde, T Salthammer, and E Peiner. Silicon nanowire resonators: Aerosol nanoparticle mass sensing in the workplace. *IEEE Nanotechnology Magazine*, 7(2):18–23, 2013.

[58] Z Li, B Rajendran, TI Kamins, X Li, Y Chen, and RS Williams. Silicon nanowires for sequence-specific dna sensing: device fabrication and simulation. *Applied Physics A*, 80(6):1257–1263, Mar 2005.

[59] A San Paulo, M Calleja, and J Tamayo. Nanomechanical mass sensing and stiffness spectrometry based on two-dimensional vibrations of resonant nanowires. *Nature Nanotechnology*, 5(9):641, 2010.

[60] SJ Kim, T Ono, and M Esashi. Study on the noise of silicon capacitive resonant mass sensors in ambient atmosphere. *Journal of Applied Physics*, 102(10):104304, 2007.

[61] B Lassagne, D Garcia-Sanchez, A Aguasca, and A Bachtold. Ultra-sensitive mass sensing with a nanotube electromechanical resonator. *Nano Letters*, 8(11):3735–3738, 2008.

[62] LB Biedermann, RC Tung, A Raman, RG Reifenberger, MM Yazdanpanah, and RW Cohn. Characterization of silver–gallium nanowires for force and mass sensing applications. *Nanotechnology*, 21(30):305701, 2010.

[63] J Ren, S Shen, D Wang, Z Xi, L Guo, Z Pang, Y Qian, X Sun, and X Jiang. The targeted delivery of anticancer drugs to brain glioma by pegylated oxidized multi-walled carbon nanotubes modified with angiopep-2. *Biomaterials*, 33(11):3324–3333, 2012.

[64] X Zhang, L Meng, Q Lu, Z Fei, and P J Dyson. Targeted delivery and controlled release of doxorubicin to cancer cells using modified single wall carbon nanotubes. *Biomaterials*, 30(30):6041–6047, 2009.

[65] A Bianco, K Kostarelos, and M Prato. Applications of carbon nanotubes in drug delivery. *Current Opinion in Chemical Biology*, 9(6):674–679, 2005.

[66] L Meng, X Zhang, Q Lu, Z Fei, and PJ Dyson. Single walled carbon nanotubes as drug delivery vehicles: targeting doxorubicin to tumors. *Biomaterials*, 33(6):1689–1698, 2012.

[67] KE Fischer, BJ Alemán, SL Tao, RH Daniels, EM Li, MD Bunger, G Nagaraj, P Singh, A Zettl, and TA Desai. Biomimetic nanowire coatings for next generation adhesive drug delivery systems. *Nano Letters*, 9(2):716–720, 2009.

[68] KM Pondman, ND Bunt, AW Maijenburg, Richard JA van Wezel, U Kishore, L Abelmann, E Johan, and B ten Haken. Magnetic drug delivery with fepd nanowires. *Journal of Magnetism and Magnetic Materials*, 380:299–306, 2015.

[69] SS Rao. *Vibration of continuous systems*. John Wiley & Sons, 2007.

[70] JN Reddy. Nonlocal nonlinear formulations for bending of classical and shear deformation theories of beams and plates. *International Journal of Engineering Science*, 48(11):1507–1518, 2010.

[71] A D Kerr. Elastic and viscoelastic foundation models. *Journal of Applied Mechanics*, 31(3):491–498, 1964.

[72] SC Wang, XG Liang, and XH Xu. Thermal conductivity of silicon nanowire by nonequilibrium molecular dynamics simulations. In *ASME 2008 First International Conference on Micro/Nanoscale Heat Transfer*, pages 1155–1161. American Society of Mechanical Engineers, 2008.

[73] OA Bauchau and JI Craig. *Euler-Bernoulli beam theory*, pages 173–221. Springer Netherlands, Dordrecht, 2009.

[74] JN Reddy. Nonlocal nonlinear formulations for bending of classical and shear deformation theories of beams and plates. *International Journal of Engineering Science*, 48(11):1507 – 1518, 2010.

[75] LJ Sudak. Column buckling of multiwalled carbon nanotubes using nonlocal continuum mechanics. *Journal of Applied Physics*, 94(11):7281–7287, 2003.

[76] J Peddieson, GR Buchanan, and RP McNitt. Application of nonlocal continuum models to nanotechnology. *International Journal of Engineering Science*, 41(3-5):305–312, 2003.

[77] AC Eringen and DGB Edelen. On nonlocal elasticity. *International Journal of Engineering Science*, 10(3):233 – 248, 1972.

[78] AC Eringen. Nonlocal polar elastic continua. *International Journal of Engineering Science*, 10(1):1 – 16, 1972.

[79] J N Reddy. *An introduction to continuum mechanics*. Cambridge university press, 2013.

[80] J Peddieson, GR Buchanan, and RP McNitt. Application of nonlocal continuum models to nanotechnology. *International Journal of Engineering Science*, 41(3):305 – 312, 2003.

[81] ZG Zhou, LZ Wu, and SY Du. Non-local theory solution for a mode i crack in piezoelectric materials. *European Journal of Mechanics-A/Solids*, 25(5):793–807, 2006.

[82] MA Eltaher, FA Omar, WS Abdalla, and EH Gad. Bending and vibrational behaviors of piezoelectric nonlocal nanobeam including surface elasticity. *Waves in Random and Complex Media*, pages 1–17, 2018.

[83] R Ansari and S Sahmani. Bending behavior and buckling of nanobeams including surface stress effects corresponding to different beam theories. *International Journal of Engineering Science*, 49(11):1244 – 1255, 2011.

[84] GF Wang and XQ Feng. Timoshenko beam model for buckling and vibration of nanowires with surface effects. *Journal of Physics D: Applied Physics*, 42(15):155411, 2009.

[85] T Chen, M S Chiu, and C N Weng. Derivation of the generalized Young-Laplace equation of curved interfaces in nanoscaled solids. *Journal of Applied Physics*, 100(7):074308, 2006.

[86] S Hosseini-Hashemi, I Nahas, M Fakher, and R Nazemnezhad. Nonlinear free vibration of piezoelectric nanobeams incorporating surface effects. *Smart Materials and Structures*, 23(3):035012, 2014.

[87] P Soltani and A Farshidianfar. Periodic solution for nonlinear vibration of a fluid-conveying carbon nanotube, based on the nonlocal continuum theory by energy balance method. *Applied Mathematical Modelling*, 36(8):3712–3724, 2012.

[88] S Narendar, SS Gupta, and S Gopalakrishnan. Wave propagation in single-walled carbon nanotube under longitudinal magnetic field using nonlocal Euler-Bernoulli beam theory. *Applied Mathematical Modelling*, 36(9):4529–4538, 2012.

[89] J Kraus. Electromagnetics. *McGrawHill, USA*, 1984.

[90] B Gheshlaghi and SM Hasheminejad. Vibration analysis of piezoelectric nanowires with surface and small scale effects. *Current Applied Physics*, 12(4):1096–1099, 2012.

[91] H Jiang, C Wang, and Y Luo. Vibration of piezoelectric nanobeams with an internal residual stress and a nonlinear strain. *Physics Letters A*, 379(40):2631 – 2636, 2015.

[92] DH Hodges and GA Pierce. *Introduction to structural dynamics and aeroelasticity*, volume 15. Cambridge University Press, 2011.

[93] AH Nayfeh and DT Mook. *Nonlinear oscillations*. John Wiley and Sons, 2008.

[94] NE Sanchez. The method of multiple scales: Asymptotic solutions and normal forms for nonlinear oscillatory problems. *Journal of Symbolic Computation*, 21(2):245 – 252, 1996.

[95] AH Nayfeh. *Introduction to perturbation techniques*. John Wiley and Sons, 2011.

[96] J Wang. Effect of temperature on elasticity of silicon nanowires. In *Key Engineering Materials*, volume 483, pages 526–531. Trans Tech Publ, 2011.

[97] R Ansari, K Hosseini, A Darvizeh, and B Daneshian. A sixth-order compact finite difference method for non-classical vibration analysis of nanobeams including surface stress effects. *Applied Mathematics and Computation*, 219(10):4977–4991, 2013.

[98] M Karimi, MH Shokrani, and AR Shahidi. Size-dependent free vibration analysis of rectangular nanoplates with the consideration of surface effects using finite difference method. *Journal of Applied and Computational Mechanics*, 1(3):122–133, 2015.

[99] GD Smith. *Numerical solution of partial differential equations: finite difference methods*. Oxford University Press, 1985.

[100] A Krishnan, G George, and P Malathi. Use of finite difference method in the study of stepped beams. *International Journal of Mechanical Engineering Education*, 26(1):11–24, 1998.

[101] A Mohebbi and M Dehghan. High-order solution of one-dimensional sine–gordon equation using compact finite difference and dirkn methods. *Mathematical and Computer Modelling*, 51(5-6):537–549, 2010.

[102] R De Borst, M A Crisfield, J J Remmers, and C V Verhoosel. *Nonlinear finite element analysis of solids and structures*. John Wiley & Sons, 2012.

[103] Ch Shu and B E Richards. Application of generalized differential quadrature to solve two-dimensional incompressible navier-stokes equations. *International Journal for Numerical Methods in Fluids*, 15(7):791–798, 1992.

[104] M Faghih Shojaei and R Ansari. Variational differential quadrature: a technique to simplify numerical analysis of structures. *Applied Mathematical Modelling*, 49:705–738, 2017.

[105] AI Aria and MI Friswell. A nonlocal finite element model for buckling and vibration of functionally graded nanobeams. *Composites Part B: Engineering*, 166:233–246, 2019.

[106] JK Phadikar and SC Pradhan. Variational formulation and finite element analysis for nonlocal elastic nanobeams and nanoplates. *Computational materials science*, 49(3):492–499, 2010.

[107] R Ansari, V Mohammadi, M Faghih Shojaei, R Gholami, and S Sahmani. On the forced vibration analysis of timoshenko nanobeams based on the surface stress elasticity theory. *Composites Part B: Engineering*, 60:158–166, 2014.

[108] A Shahabodini, R Ansari, and M Darvizeh. Atomistic-continuum modeling of vibrational behavior of carbon nanotubes using the variational differential quadrature method. *Composite Structures*, 185:728–747, 2018.

[109] B Arash. *Molecular dynamics studies on application of carbon nanotubes and graphene sheets as nano-resonator sensors*. PhD thesis, University of Manitoba, 2013.

[110] J W Kang, J J Seo, and H J Hwang. A study on silicon nanotubes based on the Tersoff potential. *arXiv preprint cond-mat/0210038*, 2002.

[111] D Georgakaki, OG Ziogos, and HM Polatoglou. Vibrational and mechanical properties of si/ge nanowires as resonators: A molecular dynamics study. *Physica Status Solidi (a)*, 211(2):267–276, 2014.

[112] J W Kang, H W Kim, K S Kim, and J H Lee. Molecular dynamics modeling and simulation of a graphene-based nanoelectromechanical resonator. *Current Applied Physics*, 13(4):789–794, 2013.

[113] BJ Alder and T Wainwright. Phase transition for a hard sphere system. *The Journal of Chemical Physics*, 27(5):1208–1209, 1957.

[114] A Hospital, JR Goñi, M Orozco, and JL Gelpí. Molecular dynamics simulations: advances and applications. *Advances and Applications in Bioinformatics and Chemistry: AABC*, 8:37, 2015.

[115] WK Liu, S Jun, and D Qian. Computational nanomechanics of materials. *Journal of Computational and Theoretical Nanoscience*, 5(5):970–996, 2008.

[116] JW Yoon and HJ Hwang. Molecular dynamics modeling and simulations of a single-walled carbon-nanotube-resonator encapsulating a finite nanoparticle. *Computational Materials Science*, 50(9):2741–2744, 2011.

[117] MP Allen et al. Introduction to molecular dynamics simulation. *Computational Soft Matter: from Synthetic Polymers to Proteins*, 23:1–28, 2004.

[118] MP Allen and DJ Tildesley. *Computer simulation of liquids*. Oxford university press, 2017.

[119] N A Marks and M Robinson. Variable timestep algorithm for molecular dynamics simulation of non-equilibrium processes. *Nuclear Instruments and Methods in Physics Research Section B: Beam Interactions with Materials and Atoms*, 352:3–8, 2015.

[120] J Liu, Y Wu, J Shen, Y Gao, L Zhang, and D Cao. Polymer–nanoparticle interfacial behavior revisited: A molecular dynamics study. *Physical Chemistry Chemical Physics*, 13(28):13058–13069, 2011.

[121] A R. Alian and S A. Meguid. *Multiscale Modeling of Nanoreinforced Composites*, pages 1–39. Springer International Publishing, 2016.

[122] SL Mayo, BD Olafson, and WA Goddard. Dreiding: a generic force field for molecular simulations. *Journal of Physical Chemistry*, 94(26):8897–8909, 1990.

[123] AK Rappé, CJ Casewit, KS Colwell, WA Goddard, and WM Skiff. Uff, a full periodic table force field for molecular mechanics and molecular dynamics simulations. *Journal of the American Chemical Society*, 114(25):10024–10035, 1992.

[124] G Pawar. *Modeling and simulation of the pore-scale*. PhD thesis, The University of Utah, 2016.

[125] D Hossain, MA Tschopp, DK Ward, JL Bouvard, P Wang, and MF Horstemeyer. Molecular dynamics simulations of deformation mechanisms of amorphous polyethylene. *Polymer*, 51(25):6071–6083, 2010.

[126] J L Tsai, S H Tzeng, and Y T Chiu. Characterizing elastic properties of carbon nanotubes/polyimide nanocomposites using multi-scale simulation. *Composites Part B: Engineering*, 41(1):106–115, 2010.

[127] M S Lavine, N Waheed, and G C Rutledge. Molecular dynamics simulation of orientation and crystallization of polyethylene during uniaxial extension. *Polymer*, 44(5):1771–1779, 2003.

[128] J Tersoff. New empirical approach for the structure and energy of covalent systems. *Physical Review B*, 37(12):6991, 1988.

[129] S F Hwang, Y H Li, and Z H Hong. Molecular dynamic simulation for cu cluster deposition on si substrate. *Computational Materials Science*, 56:85–94, 2012.

[130] T Kumagai, S Izumi, S Hara, and S Sakai. Development of bond-order potentials that can reproduce the elastic constants and melting point of silicon for classical molecular dynamics simulation. *Computational materials science*, 39(2):457–464, 2007.

[131] C S Moura and L Amaral. Molecular dynamics simulation of silicon nanostructures. *Nuclear Instruments and Methods in Physics Research Section B: Beam Interactions with Materials and Atoms*, 228(1-4):37–40, 2005.

[132] E Bichoutskaia, A M Popov, Y E Lozovik, O V Ershova, I V Lebedeva, and A A Knizhnik. Nanoresonator based on relative vibrations of the walls of carbon nanotubes. *Fullerenes, Nanotubes, and Carbon Nanostructures*, 18(4-6):523–530, 2010.

[133] J H Zhang, Q A Huang, H Yu, and J Wang. The influence of surface effects on size-dependent mechanical properties of silicon nanobeams at finite temperature. *Journal of Physics D: Applied Physics*, 42(4):045409, 2009.

[134] D Donadio and G Galli. Temperature dependence of the thermal conductivity of thin silicon nanowires. *Nano letters*, 10(3):847–851, 2010.

[135] A K Naik, M S Hanay, W K Hiebert, X L Feng, and M L Roukes. Towards single-molecule nanomechanical mass spectrometry. *Nature nanotechnology*, 4(7):445, 2009.

[136] O Malvar, E Gil-Santos, JJ Ruz, D Ramos, V Pini, M Fernández-Regúlez, M Calleja, J Tamayo, and A San Paulo. Tapered silicon nanowires for enhanced nanomechanical sensing. *Applied Physics Letters*, 103(3):033101, 2013.